NORSAR

NORSAR Scientific Report No. 2-2009

Semiannual Technical Summary

1 January - 30 June 2009

Frode Ringdal (ed.)

Kjeller, August 2009

REPORT DOCUMENTATION PAGE

Form Approved
OMB No. 0704-0188

PLEASE DO NOT RETURN YOUR FORM TO THE ABOVE ADDRESS.

1. REPORT DATE *(DD-MM-YYYY)*	2. REPORT TYPE	3. DATES COVERED *(From - To)*
15-08-2009	Semiannual Technical Summary	1 January - 30 June 2009

4. TITLE AND SUBTITLE

Semiannual Technical Summary, 1 January - 30 June 2009

5a. CONTRACT NUMBER

FA2521-06-C-8003

5b. GRANT NUMBER

5c. PROGRAM ELEMENT NUMBER

NDC Support / R&D

6. AUTHOR(S)

Frode Ringdal (Ed.)

5d. PROJECT NUMBER

T/6110

5e. TASK NUMBER

SOW Task 4.2 & 4.3

5f. WORK UNIT NUMBER

CDRL sequence nos. A001-A004

7. PERFORMING ORGANIZATION NAME(S) AND ADDRESS(ES)

Stiftelsen NORSAR
Post Box 53
NO-2027 Kjeller
Norway

8. PERFORMING ORGANIZATION REPORT NUMBER

Scientific Report No. 2-2009

9. SPONSORING/MONITORING AGENCY NAME(S) AND ADDRESS(ES)

AFTAC/TTS, 1030 South Highway A1A MS 1000, Patrick AFB, FL 32925-3002

Army Space and Missile Defense Command , 1515 Wilson Blvd., Suite 720
Arlington, VA 22209

10. SPONSOR/MONITOR'S ACRONYM(S)

AFTAC/TTS & USASMDC

11. SPONSOR/MONITOR'S REPORT NUMBER(S)

12. DISTRIBUTION/AVAILABILITY STATEMENT

Approved for public release; distribution unlimited

13. SUPPLEMENTARY NOTES

14. ABSTRACT

This report describes activities carried out at NORSAR under Contract No. FA2521-06-C-8003 (T/6110) for the period 1 January - 30 June 2009. In addition, it provides summary information on operation and maintenance (O&M) activities at the Norwegian National Data Center (NDC) during the same period. The O&M activities, including operation of transmission links within Norway and to Vienna, Austria, are being funded jointly by the CTBTO/PTS and the Norwegian Government, with the understanding that the funding of O&M activities for primary stations in the International Monitoring System (IMS) will gradually be transferred to the CTBTO/PTS. The O&M statistics presented in this report are included for the purpose of completeness, and in order to maintain consistency with earlier reporting practice. Some of the research activities described in this report are funded by the United States (cont.)

15. SUBJECT TERMS

NORSAR, Norwegian Seismic Array

16. SECURITY CLASSIFICATION OF:			17. LIMITATION OF ABSTRACT	18. NUMBER OF PAGES	19a. NAME OF RESPONSIBLE PERSON
a. REPORT	b. ABSTRACT	c. THIS PAGE			Mr. Kyle S. Roberts, AFTAC/TTX
U	U	U	SAR	76	19b. TELEPHONE NUMBER *(Include area code)* (321) 494-9472

Reset

Standard Form 298 (Rev. 8/98)
Prescribed by ANSI Std. Z39.18

Government, and the United States also covers the cost of transmission of selected data from the Norwegian NDC to the United States NDC.

The seismic arrays operated by NOR-NDC comprise the Norwegian Seismic Array (NOA), the Arctic Regional Seismic Array (ARCES) and the Spitsbergen Regional Array (SPITS). This report presents statistics for these three arrays as well as for additional seismic stations which through cooperative agreements with institutions in the host countries provide continuous data to NOR-NDC. These additional stations include the Finnish Regional Seismic Array (FINES) and the Hagfors array in Sweden (HFS).

The NOA Detection Processing system has been operated throughout the period with an uptime of 100%. A total of 2,036 seismic events have been reported in the NOA monthly seismic bulletin during the reporting period. On-line detection processing and data recording at the NDC of data from ARCES, FINES, SPITS and HFS data have been conducted throughout the period. Processing statistics for the arrays for the reporting period are given.

A summary of the activities at the NOR-NDC and relating to field installations during the reporting period is provided in Section 4. Norway is now contributing primary station data from two seismic arrays: NOA (PS27) and ARCES (PS28), one auxiliary seismic array SPITS (AS72), and one auxiliary three-component station JMIC (AS73). These data are being provided to the IDC via the global communications infrastructure (GCI). Continuous data from the three arrays are in addition being transmitted to the US NDC. The performance of the data transmission to the US NDC has been satisfactory during the reporting period.

So far among the Norwegian stations, the NOA and the ARCES array (PS27 and PS28 respectively), the radionuclide station at Spitsbergen (RN49) and the auxiliary seismic stations on Spitsbergen (AS72) and Jan Mayen (AS73) have been certified. Provided that adequate funding continues to be made available (from the CTBTO/PTS and the Norwegian Ministry of Foreign Affairs), we envisage continuing the provision of data from these and other Norwegian IMS-designated stations in accordance with current procedures. As part of NORSAR's obsolescence management, a recapitalization plan for PS27 and PS28 has been submitted to CTBTO/PTS in order to prevent severe degradation of the stations due to lack of spare parts.

The IMS infrasound station originally planned to be located near Karasjok (IS37) may need to be moved to another site, since the local authorities have not granted the permissions required for the establishment of the station. Alternative locations outside Karasjok are currently being pursued.

Summaries of three scientific and technical contributions presented in Chapter 6 of this report are provided below:

Section 6.1 is entitled: "A climatology of infrasound observations at the experimental ARCI array in Norway". ARCI is a temporary, experimental three-element infrasound array which was established at ARCES in March 2008. The purpose of the installation is to gain experience with simultaneous recording of seismometer and microbarometer data using minimal wind noise reduction equipment. The aim of the present study is to identify the sources of infrasound signals recorded at the array and to build up a climatology of station specific detections. Infrasound data from ARCI has been processed by evaluating the Fisher ratio over the period from March 2008 until May 2009. Two frequency bands have been processed. A large number of events are detected in both the low and high frequency band. With a detection threshold at an SNR of one, 1.8 million events are detected between 0.1 and 1.0 Hz and 16,475 events between 1.0 and 7.0 Hz. Detections in the low frequency band are mostly related to oceanic wave activ-

ity which leads to microbaroms. In the high frequency band, mainly man-made events, related to mining and military activity are detected.

The characteristics of the medium, *i.e.*, wind and temperature structure up to stratospheric altitudes, have been derived from ECMWF models. A clear relation has been shown between upper atmospheric winds and the directionality of the detections for the low frequency band. These seasonal changes are also partly visible in the high frequency band. In winter the sources to the west are detected while preference is given to sources in the east during summer. The state of the boundary layer, or turbulence and low level winds, partly determines the signal coherency. In summer, there is a daily variation caused by the influence of solar radation. A stable boundary layer during nighttime leads to less coherency loss.

In conclusion, the general behavior of ARCI can be understood by evaluating the detectability in relation to atmospheric processes and source activity. The study confirms that upper atmospheric winds and the state of the boundary layer play an important role in the detectability of infrasound.

Section 6.2 is a study of a large aftershock sequence following the M 5.9 Spitsbergen earthquake on 21 February 2008. The study focuses on evaluating the performance of a detector based on the frequency-dependent Multi-Channel Wiener Filter (MCWF), as compared to the standard detection processing applied at the NORSAR data center.
The MCWF technique is applied to ARCES array data (ARCES is at an epicentral distance of 850 km), using the detections by the much closer SPITS array (distance 150 km) as a reference. ARCES detections are considered reliable when an SNR threshold is exceeded and the estimated back-azimuth and apparent velocity are consistent with signals originating in the epicentral area. The conventional beamforming, when applied to ARCES, detects 513 aftershocks during 2008, with 181 false alarms. In comparison, the MCWF technique detects 577 aftershocks with 165 false alarms. Thus there is a clear improvement in this particular application of the MCWF technique.

Section 6.3 is a study of the detection capability of IMS primary and auxiliary seismic stations. We have investigated the IDC Reviewed Event Bulletin (REB) for the time period 1 January 2000 to 31 March 2009 to quantify the event detection capability of individual seismic stations of the International Monitoring System (IMS). For a specific target area, we can obtain estimates of the detection threshold of a given station by considering the ensemble of REB reported events in the area, and simply downscaling each event magnitude with the observed SNR at the station. However, there are some factors that must be considered, such as:

- Correcting for possible biases in the REB magnitudes caused by non-detections (by using maximum likelihood estimates)
- Correcting for skewness in the distribution of threshold estimates, also caused by non-detections
- Considering the validity of using the signal-to-noise ratio for downscaling the event magnitude

We address these issues by dividing the events into a binned global grid system and introduce a data censoring procedure to reduce these effects. A major result of this study is a quantification and ranking of the IMS primary and auxiliary seismic stations based on their capability to detect events within regional, teleseismic and core phase distance ranges. For each station, source regions with noticeable signal amplitude focusing effects (bright spots) and defocusing

effects are conveniently identified and quantified. We also present results from applying maximum likelihood magnitude estimation techniques for validation of the censoring procedure.

Frode Ringdal

AFTAC Project Authorization	:	T/6110
Purchase Request No.	:	F3KTK85290A1
Name of Contractor	:	Stiftelsen NORSAR
Effective Date of Contract	:	1 March 2006
Contract Expiration Date	:	30 September 2011
Amount of Contract	:	$ 1,003,494.00
Project Manager	:	Frode Ringdal +47 63 80 59 00
Title of Work	:	The Norwegian Seismic Array (NORSAR) Phase 3
Period Covered by Report	:	1 January - 30 June 2009

The views and conclusions contained in this document are those of the authors and should not be interpreted as necessarily representing the official policies, either expressed or implied, of the U.S. Government.

Part of the research presented in this report was supported by the Army Space and Missile Defense Command, under contract no. W9113M-05-C-0224. Other activities were supported and monitored by AFTAC, Patrick AFB, FL32925, under contract no. FA2521-06-C-8003. Other sponsors are acknowledged where appropriate.

The operational activities of the seismic field systems and the Norwegian National Data Center (NDC) are currently jointly funded by the Norwegian Government and the CTBTO/PTS, with the understanding that the funding of appropriate IMS-related activities will gradually be transferred to the CTBTO/PTS.

Table of Contents

Page

1 Summary

This report describes activities carried out at NORSAR under Contract No. FA2521-06-C-8003 for the period 1 January - 30 June 2009. In addition, it provides summary information on operation and maintenance (O&M) activities at the Norwegian National Data Center (NOR-NDC) during the same period. The O&M activities, including operation of transmission links within Norway and to Vienna, Austria are being funded jointly by the CTBTO/PTS and the Norwegian Government, with the understanding that the funding of O&M activities for primary stations in the International Monitoring System (IMS) will gradually be transferred to the CTBTO/PTS. The O&M statistics presented in this report are included for the purpose of completeness, and in order to maintain consistency with earlier reporting practice. Some of the research activities described in this report are funded by the United States Government, and the United States also covers the cost of transmission of selected data from the Norwegian NDC to the United States NDC.

The seismic arrays operated by NOR-NDC comprise the Norwegian Seismic Array (NOA), the Arctic Regional Seismic Array (ARCES) and the Spitsbergen Regional Array (SPITS). This report presents statistics for these three arrays as well as for additional seismic stations which through cooperative agreements with institutions in the host countries provide continuous data to NOR-NDC. These additional stations include the Finnish Regional Seismic Array (FINES) and the Hagfors array in Sweden (HFS).

The NOA Detection Processing system has been operated throughout the period with an uptime of 100%. A total of 2,036 seismic events have been reported in the NOA monthly seismic bulletin during the reporting period. On-line detection processing and data recording at the NDC of data from ARCES, FINES, SPITS and HFS data have been conducted throughout the period. Processing statistics for the arrays for the reporting period are given.

A summary of the activities at the NOR-NDC and relating to field installations during the reporting period is provided in Section 4. Norway is now contributing primary station data from two seismic arrays: NOA (PS27) and ARCES (PS28), one auxiliary seismic array SPITS (AS72), and one auxiliary three-component station JMIC (AS73). These data are being provided to the IDC via the global communications infrastructure (GCI). Continuous data from the three arrays are in addition being transmitted to the US NDC. The performance of the data transmission to the US NDC has been satisfactory during the reporting period.

So far among the Norwegian stations, the NOA and the ARCES array (PS27 and PS28 respectively), the radionuclide station at Spitsbergen (RN49) and the auxiliary seismic stations on Spitsbergen (AS72) and Jan Mayen (AS73) have been certified. Provided that adequate funding continues to be made available (from the CTBTO/PTS and the Norwegian Ministry of Foreign Affairs), we envisage continuing the provision of data from these and other Norwegian IMS-designated stations in accordance with current procedures. As part of NORSAR's obsolescence management, a recapitalization plan for PS27 and PS28 has been submitted to CTBTO/PTS in order to prevent severe degradation of the stations due to lack of spare parts.

The IMS infrasound station originally planned to be located near Karasjok (IS37) may need to be moved to another site, since the local authorities have not granted the permissions required for the establishment of the station. Alternative locations outside Karasjok are currently being pursued.

Summaries of three scientific and technical contributions presented in Chapter 6 of this report are provided below:

Section 6.1 is entitled: "A climatology of infrasound observations at the experimental ARCI array in Norway". ARCI is a temporary, experimental three-element infrasound array which was established at ARCES in March 2008. The purpose of the installation is to gain experience with simultaneous recording of seismometer and microbarometer data using minimal wind noise reduction equipment. The aim of the present study is to identify the sources of infrasound signals recorded at the array and to build up a climatology of station specific detections. Infrasound data from ARCI has been processed by evaluating the Fisher ratio over the period from March 2008 until May 2009. Two frequency bands have been processed. A large number of events are detected in both the low and high frequency band. With a detection threshold at an SNR of one, 1.8 million events are detected between 0.1 and 1.0 Hz and 16,475 events between 1.0 and 7.0 Hz. Detections in the low frequency band are mostly related to oceanic wave activity which leads to microbaroms. In the high frequency band, mainly man-made events, related to mining and military activity are detected.

The characteristics of the medium, *i.e.*, wind and temperature structure up to stratospheric altitudes, have been derived from ECMWF models. A clear relation has been shown between upper atmospheric winds and the directionality of the detections for the low frequency band. These seasonal changes are also partly visible in the high frequency band. In winter the sources to the west are detected while preference is given to sources in the east during summer. The state of the boundary layer, or turbulence and low level winds, partly determines the signal coherency. In summer, there is a daily variation caused by the influence of solar radation. A stable boundary layer during nighttime leads to less coherency loss.

In conclusion, the general behavior of ARCI can be understood by evaluating the detectability in relation to atmospheric processes and source activity. The study confirms that upper atmospheric winds and the state of the boundary layer play an important role in the detectability of infrasound.

Section 6.2 is a study of a large aftershock sequence following the M 5.9 Spitsbergen earthquake on 21 February 2008. The study focuses on evaluating the performance of a detector based on the frequency-dependent Multi-Channel Wiener Filter (MCWF), as compared to the standard detection processing applied at the NORSAR data center.
The MCWF technique is applied to ARCES array data (ARCES is at an epicentral distance of 850 km), using the detections by the much closer SPITS array (distance 150 km) as a reference. ARCES detections are considered reliable when an SNR threshold is exceeded and the estimated back-azimuth and apparent velocity are consistent with signals originating in the epicentral area. The conventional beamforming, when applied to ARCES, detects 513 aftershocks during 2008, with 181 false alarms. In comparison, the MCWF technique detects 577 aftershocks with 165 false alarms. Thus there is a clear improvement in this particular application of the MCWF technique.

Section 6.3 is a study of the detection capability of IMS primary and auxiliary seismic stations. We have investigated the IDC Reviewed Event Bulletin (REB) for the time period 1 January 2000 to 31 March 2009 to quantify the event detection capability of individual seismic stations of the International Monitoring System (IMS). For a specific target area, we can obtain estimates of the detection threshold of a given station by considering the ensemble of REB reported events in the area, and simply downscaling each event magnitude with the observed SNR at the station. However, there are some factors that must be considered, such as:

- Correcting for possible biases in the REB magnitudes caused by non-detections (by using maximum likelihood estimates)
- Correcting for skewness in the distribution of threshold estimates, also caused by non-detections
- Considering the validity of using the signal-to-noise ratio for downscaling the event magnitude

We address these issues by dividing the events into a binned global grid system and introduce a data censoring procedure to reduce these effects. A major result of this study is a quantification and ranking of the IMS primary and auxiliary seismic stations based on their capability to detect events within regional, teleseismic and core phase distance ranges. For each station, source regions with noticeable signal amplitude focusing effects (bright spots) and defocusing effects are conveniently identified and quantified. We also present results from applying maximum likelihood magnitude estimation techniques for validation of the censoring procedure.

Frode Ringdal

2 Operation of International Monitoring System (IMS) Stations in Norway

2.1 PS27 — Primary Seismic Station NOA

The mission-capable data statistics were 100%, the same as for the previous reporting period. The net instrument availability was 99.631%.

There were no outages of all subarrays at the same time in the reporting period.

Monthly uptimes for the NORSAR on-line data recording task, taking into account all factors (field installations, transmissions line, data center operation) affecting this task were as follows:

2009		Mission Capable	Net instrument availability
January	:	100%	99.992%
February	:	100%	98.961%
March	:	100%	99.996%
April	:	100%	99.968%
May	:	100%	99.954%
June	:	100%	99.183%

B. Paulsen

NOA Event Detection Operation

In Table 2.1.1 some monthly statistics of the Detection and Event Processor operation are given. The table lists the total number of detections (DPX) triggered by the on-line detector, the total number of detections processed by the automatic event processor (EPX) and the total number of events accepted after analyst review (teleseismic phases, core phases and total).

	Total DPX	**Total EPX**	**Accepted Events**		**Sum**	**Daily**
			P-phases	**Core Phases**		
Jan	13,086	1,077	216	60	276	8.9
Feb	10,179	957	293	70	363	13.0
Mar	11,535	1,015	241	74	315	10.2
Apr	8,597	931	328	68	396	13.2
May	5,894	747	247	78	325	10.5
Jun	6,705	989	284	77	361	12.0
	55,996	5,716	1,609	427	2,036	11.3

Table 2.1.1. *Detection and Event Processor statistics, 1 January - 30 June 2009.*

NOA detections

The number of detections (phases) reported by the NORSAR detector during day 001, 2009, through day 181, 2009, was 55,996, giving an average of 309 detections per processed day (181 days processed).

B. Paulsen
U. Baadshaug

2.2 PS28 — Primary Seismic Station ARCES

The mission-capable data statistics were 100%, as compared to 99.939% for the previous reporting period. The net instrument availability was 99.741%.

There were no outages of all subarrays at the same time in the reporting period.

Monthly uptimes for the ARCES on-line data recording task, taking into account all factors (field installations, transmission lines, data center operation) affecting this task were as follows:

2009		Mission Capable	Net instru-ment avail-ability
January	:	100%	99.069%
February	:	100%	99.717%
March	:	100%	99.914%
April	:	100%	99.772%
May	:	100%	100%
June	:	100%	99.980%

B. Paulsen

Event Detection Operation

ARCES detections

The number of detections (phases) reported during day 001, 2009, through day 181, 2009, was 239,173, giving an average of 1321 detections per processed day (181 days processed).

Events automatically located by ARCES

During days 001, 2009, through 181, 2009, 8,672 local and regional events were located by ARCES, based on automatic association of P- and S-type arrivals. This gives an average of 47.9 events per processed day (181 days processed). 66% of these events are within 300 km, and 89 % of these events are within 1000 km.

U. Baadshaug

2.3 AS72 — Auxiliary Seismic Station Spitsbergen

The mission-capable data for the period were 93.629%, as compared to 95.736% for the previous reporting period. The net instrument availability was 91.108%.

The main outages in the period are presented in Table 2.3.1.

Day	Period
Feb 17	2306-0000
Feb 18	0000-0800
Apr 19	0713-0000
Apr 20	0000-0000
Apr 21	0000-0445
Apr 22	0000-0000
Apr 23	0000-0000
Apr 24	0000-0000
Apr 25	0000-0000
Apr 26	0000-0000
Apr 27	0000-0000
Apr 28	0000-0000
Apr 29	0000-0000
Apr 30	0000-0834
Apr 30	1323-1511

Table 2.31. *The main interruptions in recording of Spitsbergen data at NDPC, 1 January - 30 June 2009.*

Monthly uptimes for the Spitsbergen on-line data recording task, taking into account all factors (field installations, transmissions line, data center operation) affecting this task were as follows:

2009		Mission Capable	Net instrument availability
January	:	99.999%	90.716%
February	:	98.672%	92.843%
March	:	100%	100%
April	:	63.105%	63.090%
May	:	100%	100%
June	:	100%	100%

B. Paulsen

Event Detection Operation

Spitsbergen array detections

The number of detections (phases) reported from day 001, 2009, through day 181, 2009, was 573,033, giving an average of 3,332 detections per processed day (172 days processed).

Events automatically located by the Spitsbergen array

During days 001, 2009 through 181, 2009, 47,088 local and regional events were located by the Spitsbergen array, based on automatic association of P- and S-type arrivals. This gives an average of 273.8 events per processed day (172 days processed). 72% of these events are within 300 km, and 91% of these events are within 1000 km.

U. Baadshaug

2.4 AS73 — Auxiliary Seismic Station at Jan Mayen

The IMS auxiliary seismic network includes a three-component station on the Norwegian island of Jan Mayen. The station location given in the protocol to the Comprehensive Nuclear- Test-Ban Treaty is 70.9°N, 8.7°W.

The University of Bergen has operated a seismic station at this location since 1970. A so-called Parent Network Station Assessment for AS73 was completed in April 2002. A vault at a new location (71.0^{o}N, 8.5^{o}W) was prepared in early 2003, after its location had been approved by the PrepCom. New equipment was installed in this vault in October 2003, as a cooperative effort between NORSAR and the CTBTO/PTS. Continuous data from this station are being transmitted to the NDC at Kjeller via a satellite link installed in April 2000. Data are also made available to the University of Bergen.

The station was certified by the CTBTO/PTS on 12 June 2006.

J. Fyen

2.5 IS37 — Infrasound Station at Karasjok

The IMS infrasound network should, according to the protocol of the CTBT, include a station at Karasjok in northern Norway. The coordinates given for this station are 69.5°N, 25.5°E. These coordinates coincide with those of the primary seismic station PS28.

It has, however, proved very difficult to obtain the necessary permits for use of land for an infrasound station in Karasjok. Various alternatives for locating the station in Karasjok were prepared, but all applications to the local authorities to obtain the permissions needed to establish the station were turned down by the local governing council in June 2007.

In 2008, investigations were initiated to identify an alternative site for IS37 outside Karasjok. Various sites at Bardufoss, at 69.1^{o} N, 18.6^{o} E are currently being pursued to select one of them for possible installation of IS37. The CTBTO PrepCom has approved a corresponding coordinate change for the station.

J. Fyen

2.6 RN49 — Radionuclide Station on Spitsbergen

The IMS radionuclide network includes a station on the island of Spitsbergen. This station has been selected to be among those IMS radionuclide stations that will monitor for the presence of relevant noble gases upon entry into force of the CTBT.

A site survey for this station was carried out in August of 1999 by NORSAR, in cooperation with the Norwegian Radiation Protection Authority. The site survey report to the PTS contained a recommendation to establish this station at Platåberget, near Longyearbyen. The infrastructure for housing the station equipment was established in early 2001, and a noble gas detection system, based on the Swedish “SAUNA” design, was installed at this site in May 2001, as part of PrepCom’s noble gas experiment. A particulate station (“ARAME” design) was installed at the same location in September 2001. A certification visit to the particulate station took place in October 2002, and the particulate station was certified on 10 June 2003. Both systems underwent substantial upgrading in May/June 2006. The equipment at RN49 is being maintained and operated under a contract with the CTBTO/PTS.

S. Mykkeltveit

3 Contributing Regional Seismic Arrays

3.1 NORES

NORES has been out of operation since lightning destroyed the station electronics on 11 June 2002.

B. Paulsen

3.2 Hagfors (IMS Station AS101)

Data from the Hagfors array are made available continuously to NORSAR through a cooperative agreement with Swedish authorities.

The mission-capable data statistics were 99.967%, as compared to 99.979% for the previous reporting period. The net instrument availability was 99.966%.

The main outages in the period are presented in Table 3.2.1.

Day	Period
Jan 15	0227-0230
Jan 22	0847-0850
Jan 26	1247-1250
Feb 17	2027-2030
Feb 19	1147-1150
Feb 25	0907-0911
Mar 10	1547-1551
Mar 12	1507-1510
Mar 21	1308-1311
Mar 21	1748-1751
Mar 26	1628-1631
Apr 01	2208-2211
Apr 07	0928-0931
Apr 23	1908-1911
Apr 27	1028-1031
May 02	1308-1312
May 07	0108-0112
May 10	0728-0732
May 18	2008-2012
May 20	0248-0252
May 23	1338-1341
Jun 28	0409-0413
Jun 28	2009-2013

Day	Period
Jun 28	2209-2213
Jun 29	1849-1853

Table 3.2.1. *The main interruptions in recording of Hagfors data at NDPC, 1 January - 30 June 2009.*

Monthly uptimes for the Hagfors on-line data recording task, taking into account all factors (field installations, transmissions line, data center operation) affecting this task were as follows:

2009		Mission Capable	Net instrument availability
January	:	99.977%	99.976%
February	:	99.976%	99.976%
March	:	99.964%	99.964%
April	:	99.969%	99.969%
May	:	99.948%	99.947%
June	:	99.967%	99.966%

B. Paulsen

Hagfors Event Detection Operation

Hagfors array detections

The number of detections (phases) reported from day 001, 2009, through day 181, 2009, was 188,954, giving an average of 1044 detections per processed day (181 days processed).

Events automatically located by the Hagfors array

During days 001, 2009, through 181, 2009, 5,359 local and regional events were located by the Hagfors array, based on automatic association of P- and S-type arrivals. This gives an average of 19.6 events per processed day (181 days processed). 70% of these events are within 300 km, and 94% of these events are within 1000 km.

U. Baadshaug

3.3 FINES (IMS station PS17)

Data from the FINES array are made available continuously to NORSAR through a cooperative agreement with Finnish authorities.

The mission-capable data statistics were 99.991%, as compared to 99.997% for the previous reporting period. The net instrument availability was 99.408%.

The main outages in the period are presented in Table 3.3.1.

Day	Period
May 25	0928-0931
May 27	1043-1046
May 28	0603-0612
May 28	0702-0709

Table 3.3.1. *The main interruptions in recording of FINES data at NDPC, 1 January - 30 June 2009.*

Monthly uptimes for the FINES on-line data recording task, taking into account all factors (field installations, transmissions line, data center operation) affecting this task were as follows:

2009		Mission Capable	Net instrument availability
January	:	100%	100%
February	:	100%	100%
March	:	100%	100%
April	:	100%	99.046%
May	:	99.949%	97.468%
June	:	100%	100%

B. Paulsen

FINES Event Detection Operation

FINES detections

The number of detections (phases) reported during day 001, 2009, through day 181, 2009, was 51,870, giving an average of 287 detections per processed day (181 days processed).

Events automatically located by FINES

During days 001, 2009, through 181, 2009, 1992 local and regional events were located by FINES, based on automatic association of P- and S-type arrivals. This gives an average of 11.0 events per processed day (181 days processed). 84% of these events are within 300 km, and 93% of these events are within 1000 km.

U. Baadshaug

3.4 Regional Monitoring System Operation and Analysis

The Regional Monitoring System (RMS) was installed at NORSAR in December 1989 and has been operated at NORSAR from 1 January 1990 for automatic processing of data from ARCES and NORES. A second version of RMS that accepts data from an arbitrary number of arrays and single 3-component stations was installed at NORSAR in October 1991, and regular operation of the system comprising analysis of data from the 4 arrays ARCES, NORES, FINES and GERES started on 15 October 1991. As opposed to the first version of RMS, the one in current operation also has the capability of locating events at teleseismic distances.

Data from the Apatity array was included on 14 December 1992, and from the Spitsbergen array on 12 January 1994. Detections from the Hagfors array were available to the analysts and could be added manually during analysis from 6 December 1994. After 2 February 1995, Hagfors detections were also used in the automatic phase association.

Since 24 April 1999, RMS has processed data from all the seven regional arrays ARCES, NORES, FINES, GERES (until January 2000), Apatity, Spitsbergen, and Hagfors. Starting 19 September 1999, waveforms and detections from the NORSAR array have also been available to the analyst.

Phase and event statistics

Table 3.5.1 gives a summary of phase detections and events declared by RMS. From top to bottom the table gives the total number of detections by the RMS, the number of detections that are associated with events automatically declared by the RMS, the number of detections that are not associated with any events, the number of events automatically declared by the RMS, and finally the total number of events worked on interactively (in accordance with criteria that vary over time; see below) and defined by the analyst.

New criteria for interactive event analysis were introduced from 1 January 1994. Since that date, only regional events in areas of special interest (e.g, Spitsbergen, since it is necessary to acquire new knowledge in this region) or other significant events (e.g, felt earthquakes and large industrial explosions) were thoroughly analyzed. Teleseismic events of special interest are also analyzed.

To further reduce the workload on the analysts and to focus on regional events in preparation for Gamma-data submission during GSETT-3, a new processing scheme was introduced on 2 February 1995. The GBF (Generalized Beamforming) program is used as a pre-processor to RMS, and only phases associated with selected events in northern Europe are considered in the automatic RMS phase association. All detections, however, are still available to the analysts and can be added manually during analysis.

	Jan 09	Feb 09	Mar 09	Apr 09	May 09	Jun 09	Total
Phase detections	247,632	230,346	249,580	136,937	149,413	132,819	1,146,727
- Associated phases	11,089	11,714	14,393	8,101	7,392	5,605	58,294
- Unassociated phases	236,543	218,632	235,187	128,836	142,021	127,214	1,088,433
Events automatically declared by RMS	2,619	2,531	3,203	1,725	1,268	1,096	12,442

	Jan 09	Feb 09	Mar 09	Apr 09	May 09	Jun 09	Total
No. of events defined by the analyst	67	61	74	68	110	94	474

Table 3.5.1. RMS phase detections and event summary 1 January - 30 June 2009.

U. Baadshaug

B. Paulsen

4 NDC and Field Activities

4.1 NDC Activitities

NORSAR functions as the Norwegian National Data Center (NDC) for CTBT verification. Six monitoring stations, comprising altogether 132 field sensors plus radionuclide monitoring equipment, will be located on Norwegian territory as part of the future IMS as described elsewhere in this report. The four seismic IMS stations are all in operation today, and all of them are currently providing data to the CTBTO on a regular basis. PS27, PS28, AS73 and RN49 are all certified. The infrasound station in northern Norway is planned to be established within next year. Data recorded by the Norwegian stations is being transmitted in real time to the Norwegian NDC, and provided to the IDC through the Global Communications Infrastructure (GCI). Norway is connected to the GCI with a frame relay link to Vienna.

Operating the Norwegian IMS stations continues to require significant efforts by personnel both at the NDC and in the field. Strictly defined procedures as well as increased emphasis on regularity of data recording and timely data transmission to the IDC in Vienna have led to increased reporting activities and implementation of new procedures for the NDC. The NDC carries out all the technical tasks required in support of Norway's treaty obligations. NORSAR will also carry out assessments of events of special interest, and advise the Norwegian authorities in technical matters relating to treaty compliance. A challenge for the NDC is to carry 40 years' experience over to the next generation of personnel.

Verification functions; information received from the IDC

After the CTBT enters into force, the IDC will provide data for a large number of events each day, but will not assess whether any of them are likely to be nuclear explosions. Such assessments will be the task of the States Parties, and it is important to develop the necessary national expertise in the participating countries. An important task for the Norwegian NDC will thus be to make independent assessments of events of particular interest to Norway, and to communicate the results of these analyses to the Norwegian Ministry of Foreign Affairs.

Monitoring the Arctic region

Norway will have monitoring stations of key importance for covering the Arctic, including Novaya Zemlya, and Norwegian experts have a unique competence in assessing events in this region. On several occasions in the past, seismic events near Novaya Zemlya have caused political concern, and NORSAR specialists have contributed to clarifying these issues.

International cooperation

After entry into force of the treaty, a number of countries are expected to establish national expertise to contribute to the treaty verification on a global basis. Norwegian experts have been in contact with experts from several countries with the aim of establishing bilateral or multilateral cooperation in this field. One interesting possibility for the future is to establish NORSAR as a regional center for European cooperation in the CTBT verification activities.

NORSAR event processing

The automatic routine processing of NORSAR events as described in NORSAR Sci. Rep. No. 2-93/94, has been running satisfactorily. The analyst tools for reviewing and updating the solutions have been continually modified to simplify operations and improve results. NORSAR is currently applying teleseismic detection and event processing using the large-aperture NOA array as well as regional monitoring using the network of small-aperture arrays in Fennoscandia and adjacent areas.

Communication topology

Norway has implemented an independent subnetwork, which connects the IMS stations AS72, AS73, PS28, and RN49 operated by NORSAR to the GCI at NOR_NDC. A contract has been concluded and VSAT antennas have been installed at each station in the network. Under the same contract, VSAT antennas for 6 of the PS27 subarrays have been installed for intra-array communication. The seventh subarray is connected to the central recording facility via a leased land line. The central recording facility for PS27 is connected directly to the GCI (Basic Topology). All the VSAT communication is functioning satisfactorily. As of 10 June 2005, AS72 and RN49 are connected to NOR_NDC through a VPN link.

Jan Fyen

4.2 Status Report: Provision of data from Norwegian seismic IMS stations to the IDC of the CTBTO/PTS

Introduction

This contribution is a report for the period January - June 2009 on activities associated with provision of data from Norwegian seismic IMS stations to the International Data Centre (IDC) in Vienna. This report represents an update of contributions that can be found in previous editions of NORSAR's Semiannual Technical Summary. All four Norwegian seismic stations providing data to the IDC have now been formally certified.

Norwegian IMS stations and communications arrangements

During the reporting interval, Norway has provided data to the IDC from the four seismic stations shown in Fig. 4.2.1. PS27 —NOA is a 60 km aperture teleseismic array, comprised of 7 subarrays, each containing six vertical short period sensors and a three-component broadband instrument. PS28 — ARCES is a 25-element regional array with an aperture of 3 km, whereas AS72 — Spitsbergen array (station code SPITS) has 9 elements within a 1-km aperture. AS73 — JMIC has a single three-component broadband instrument.

The intra-array communication for NOA utilizes a land line for subarray NC6 and VSAT links based on TDMA technology for the other 6 subarrays. The central recording facility for NOA is located at the Norwegian National Data Center (NOR_NDC).

Continuous ARCES data are transmitted from the ARCES site to NOR_NDC using a 64 kbits/s VSAT satellite link, based on BOD technology.

Continuous SPITS data were transmitted to NOR_NDC via a VSAT terminal located at Platåberget in Longyearbyen (which is the site of the IMS radionuclide monitoring station RN49

installed during 2001) up to 10 June 2005. The central recording facility (CRF) for the SPITS array has been moved to the University of Spitsbergen (UNIS). A 512 bps SHDSL link has been established between UNIS and NOR_NDC. Data from the array elements to the CRF are transmitted via a 2.4 Ghz radio link (Wilan VIP-110). Both AS72 and RN49 data are now transmitted to NOR_NDC over this link using VPN technology.

A minimum of seven-day station buffers have been established at the ARCES and SPITS sites and at all NOA subarray sites, as well as at the NOR_NDC for ARCES, SPITS and NOA. In addition, each individual site of the SPITS array has a 14-day buffer.

The NOA and ARCES arrays are primary stations in the IMS network, which implies that data from these stations is transmitted continuously to the receiving international data center. Since October 1999, this data has been transmitted (from NOR_NDC) via the Global Communications Infrastructure (GCI) to the IDC in Vienna. Data from the auxiliary array station SPITS — AS72 have been sent in continuous mode to the IDC during the reporting period. AS73 — JMIC is an auxiliary station in the IMS, and the JMIC data have been available to the IDC throughout the reporting period on a request basis via use of the AutoDRM protocol (Kradolfer, 1993; Kradolfer, 1996). In addition, continuous data from all three arrays is transmitted to the US_NDC.

Uptimes and data availability

Figs. 4.2.2 and 4.2.3 show the monthly uptimes for the Norwegian IMS primary stations ARCES and NOA, respectively, for the reporting period given as the hatched (taller) bars in these figures. These barplots reflect the percentage of the waveform data that is available in the NOR_NDC data archives for these two arrays. The downtimes inferred from these figures thus represent the cumulative effect of field equipment outages, station site to NOR_NDC communication outage, and NOR_NDC data acquisition outages.

Figs. 4.2.2 and 4.2.3 also give the data availability for these two stations as reported by the IDC in the IDC Station Status reports. The main reason for the discrepancies between the NOR_NDC and IDC data availabilities as observed from these figures is the difference in the ways the two data centers report data availability for arrays: Whereas NOR_NDC reports an array station to be up and available if at least one channel produces useful data, the IDC uses weights where the reported availability (capability) is based on the number of actually operating channels.

Use of the AutoDRM protocol

NOR_NDC's AutoDRM has been operational since November 1995 (Mykkeltveit & Baadshaug, 1996). The monthly number of requests by the IDC for JMIC data for the period January - June 2009 is shown in Fig. 4.2.4.

NDC automatic processing and data analysis

These tasks have proceeded in accordance with the descriptions given in Mykkeltveit and Baadshaug (1996). For the reporting period NOR_NDC derived information on 474 supplementary events in northern Europe and submitted this information to the Finnish NDC as the NOR_NDC contribution to the joint Nordic Supplementary (Gamma) Bulletin, which in turn is forwarded to the IDC. These events are plotted in Fig. 4.2.5.

Data access for the station NIL at Nilore, Pakistan

NOR_NDC continued to provide access to the seismic station NIL at Nilore, Pakistan, through a VSAT satellite link between NOR_NDC and Pakistan's NDC in Nilore.

Current developments and future plans

NOR_NDC is continuing the efforts towards improving and hardening all critical data acquisition and data forwarding hardware and software components, so as to meet the requirements related to operation of IMS stations.

The NOA array was formally certified by the PTS on 28 July 2000, and a contract with the PTS in Vienna currently provides partial funding for operation and maintenance of this station. The ARCES array was formally certified by the PTS on 8 November 2001, and a contract with the PTS is in place which also provides for partial funding of the operation and maintenance of this station. The operation of the two IMS auxiliary seismic stations on Norwegian territory (Spitsbergen and Jan Mayen) is funded by the Norwegian Ministry of Foreign Affairs. Provided that adequate funding continues to be made available (from the PTS and the Norwegian Ministry of Foreign Affairs), we envisage continuing the provision of data from all Norwegian seismic IMS stations without interruption to the IDC in Vienna.

The two stations PS27 and PS28 are both suffering from lack of spare parts. The PS27 NOA equipment was acquired in 1995 and it is now impossible to get spare GPS receivers. The PS28 ARCES equipment was acquired in 1999, and it is no longer possible to get spare digitizers. A recapitilization plan for both arrays was submitted to PTS in October 2008, and discussions with the PTS are being held regarding future configuratons of PS27 and PS28.

U. Baadshaug
S. Mykkeltveit
J. Fyen

References

Kradolfer, U. (1993): Automating the exchange of earthquake information. *EOS, Trans., AGU*, 74, 442.

Kradolfer, U. (1996): AutoDRM — The first five years, *Seism. Res. Lett.*, 67, 4, 30-33.

Mykkeltveit, S. & U. Baadshaug (1996): Norway's NDC: Experience from the first eighteen months of the full-scale phase of GSETT-3. *Semiann. Tech. Summ., 1 October 1995 - 31 March 1996*, NORSAR Sci. Rep. No. 2-95/96, Kjeller, Norway.

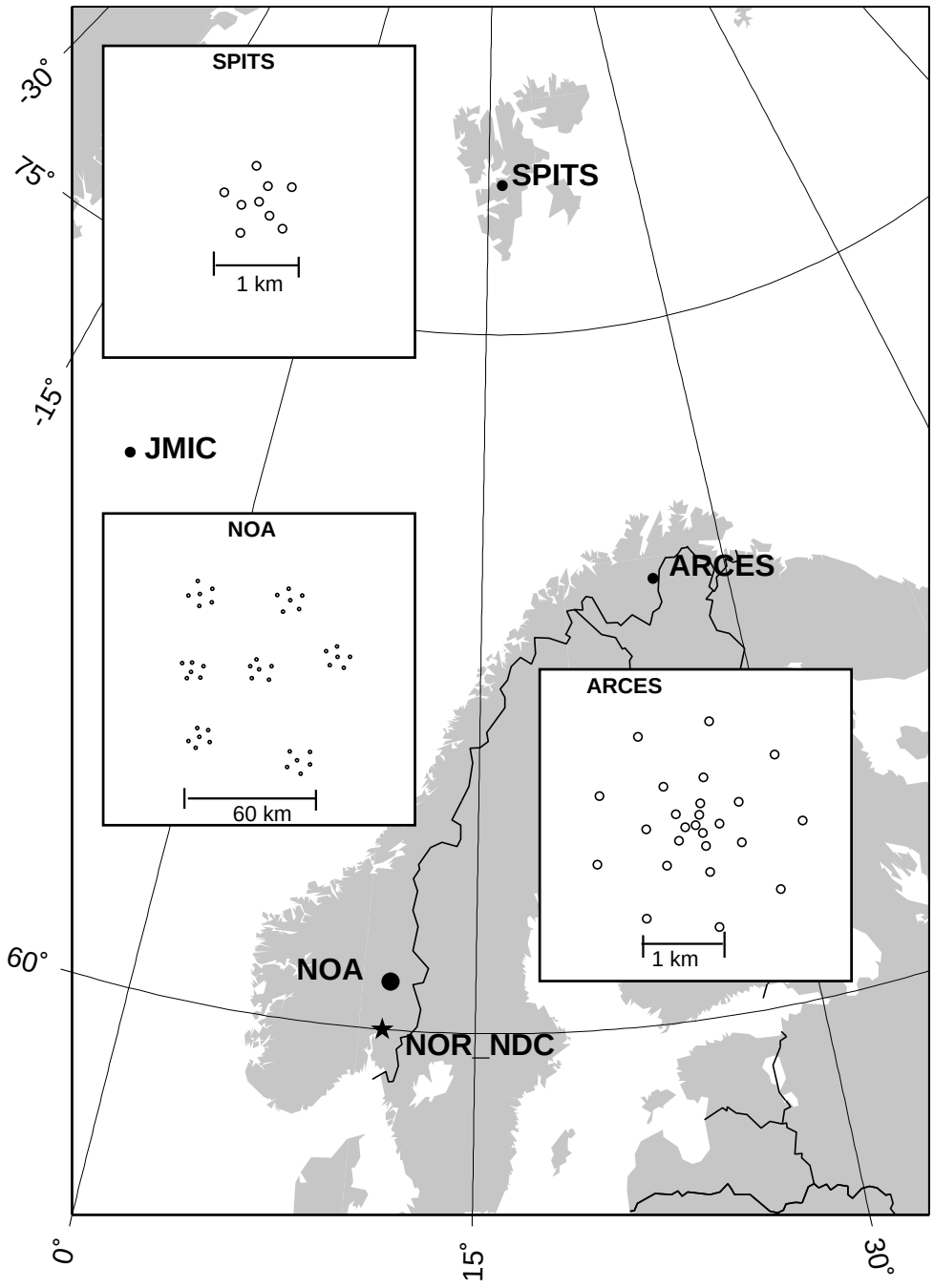

Fig. 4.2.1. The figure shows the locations and configurations of the three Norwegian seismic IMS array stations that provided data to the IDC during the period January - June 2009. The data from these stations and the JMIC three-component station are transmitted continuously and in real time to the Norwegian NDC (NOR_NDC). The stations NOA and ARCES are primary IMS stations, whereas SPITS and JMIC are auxiliary IMS stations.

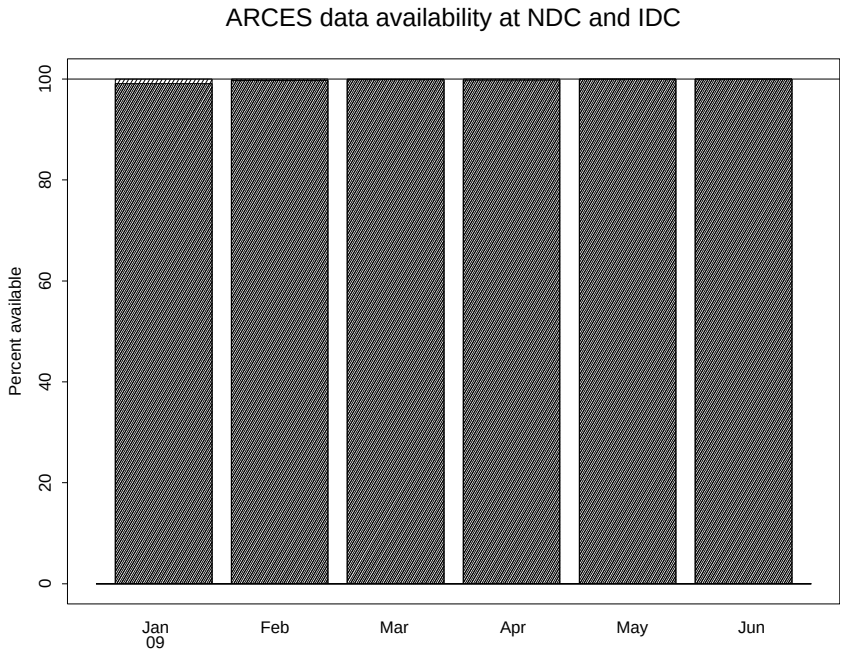

Fig. 4.2.2. The figure shows the monthly availability of ARCES array data for the period January - June 2009 at NOR_NDC and the IDC. See the text for explanation of differences in definition of the term "data availability" between the two centers. The higher values (hatched bars) represent the NOR_NDC data availability.

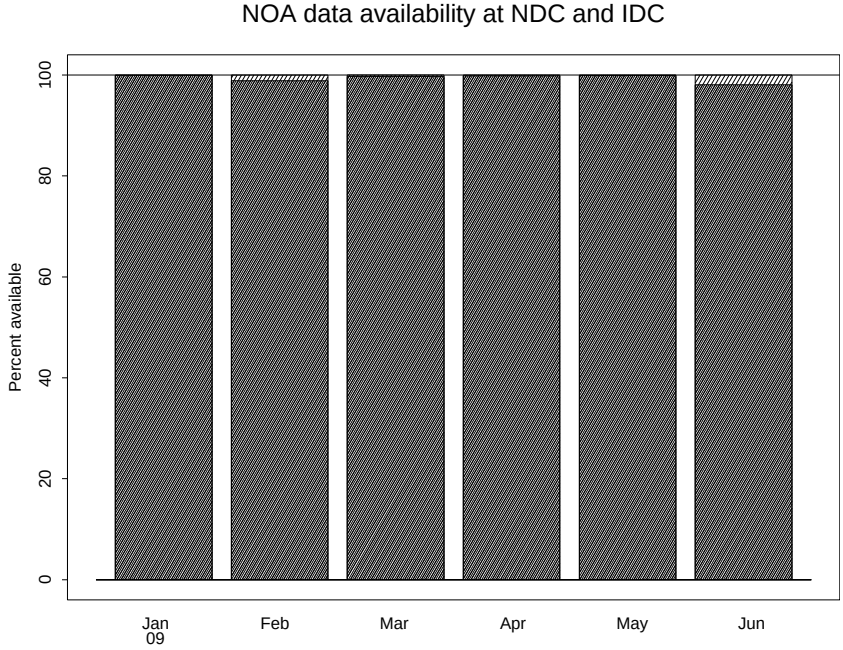

Fig. 4.2.3. The figure shows the monthly availability of NORSAR array data for the period January - June 2009 at NOR_NDC and the IDC. See the text for explanation of differences in definition of the term "data availability" between the two centers. The higher values (hatched bars) represent the NOR_NDC data availability.

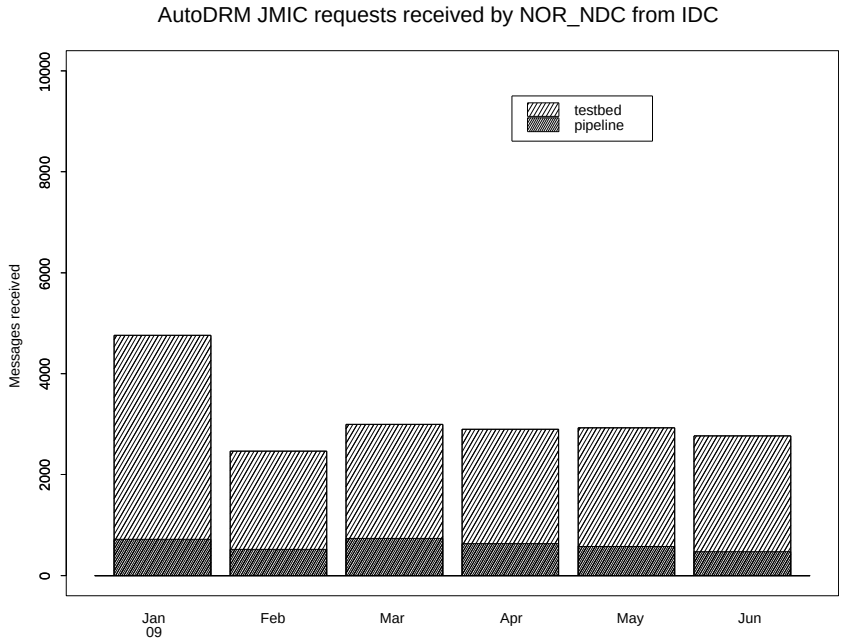

Fig. 4.2.4. The figure shows the monthly number of requests received by NOR_NDC from the IDC for JMIC waveform segments during January - June 2009.

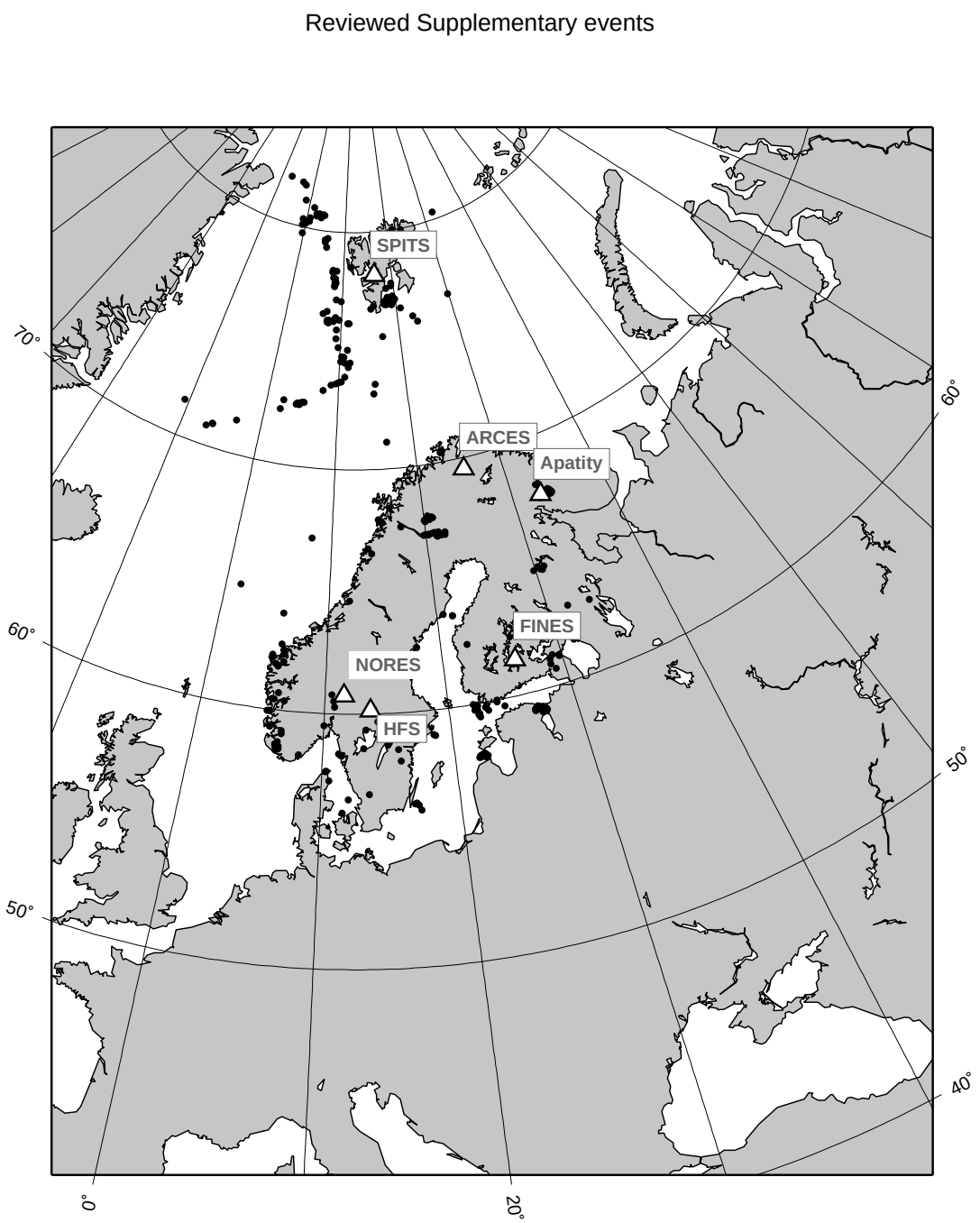

Fig. 4.2.5. The map shows the 474 events in and around Norway contributed by NOR_NDC during January - June 2009 as supplementary (Gamma) events to the IDC, as part of the Nordic supplementary data compiled by the Finnish NDC. The map also shows the main seismic stations used in the data analysis to define these events.

4.3 Field Activities

The activities at the NORSAR Maintenance Center (NMC) at Hamar currently include work related to operation and maintenance of the following IMS seismic stations: the NOA teleseismic array (PS27), the ARCES array (PS28) and the Spitsbergen array (AS72). Some work has also been carried out in connection with the seismic station on Jan Mayen (AS73), the radionuclide station at Spitsbergen (RN49), and preparations for the infrasound station at Karasjok (IS37). NORSAR also acts as a consultant for the operation and maintenance of the Hagfors array in Sweden (AS101).

NORSAR carries out the field activities relating to IMS stations in a manner generally consistent with the requirements specified in the appropriate IMS Operational Manuals, which are currently being developed by Working Group B of the Preparatory Commission. For seismic stations these specifications are contained in the Operational Manual for Seismological Monitoring and the International Exchange of Seismological Data (CTBT/WGB/TL-11/2), currently available in a draft version.

All regular maintenance on the NORSAR field systems is conducted on a one-shift-per-day, five-day-per-week basis. The maintenance tasks include:

- Operating and maintaining the seismic sensors and the associated digitizers, authentication devices and other electronics components.
- Maintaining the power supply to the field sites as well as backup power supplies.
- Operating and maintaining the VSATs, the data acquisition systems and the intra-array data transmission systems.
- Assisting the NDC in evaluating the data quality and making the necessary changes in gain settings, frequency response and other operating characteristics as required.
- Carrying out preventive, routine and emergency maintenance to ensure that all field systems operate properly.
- Maintaining a computerized record of the utilization, status, and maintenance history of all site equipment.
- Providing appropriate security measures to protect against incidents such as intrusion, theft and vandalism at the field installations.

Details of the daily maintenance activities are kept locally. As part of its contract with CTBTO/PTS NORSAR submits, when applicable, problem reports, outage notification reports and equipment status reports. The contents of these reports and the circumstances under which they will be submitted are specified in the draft Operational Manual.

P.W. Larsen
K.A. Løken

5 Documentation Developed

Bungum, H., F. Pettenati, J. Schweitzer, L. Sirovich & J.I. Faleide (2009): The MS 5.4 October 23, 1904, Oslofjord earthquake: Reanalysis based on macroseismic and instrumental data. Bull. Seism. Soc. Am., Vol. 99(5), in press.

Dahlman, O., S. Mykkeltveit & H. Haak (2009): Nuclear Test Ban. Converting Political Visions to Reality, Springer.

Evers, L.G. & J. Schweitzer (2009): A climatology of infrasound observations at the experimental ARC1 array in Norway. In. Semiannual Tech. Sum. 2-2009, 1 January - 30 June 2009, NORSAR, Kjeller, Norway.

Hauser, J., K. Dyer, M.E. Pasyanos, H. Bungum, J.I. Faleide & S.A. Clark (2009): Development and tuning of a 3-D stochastic inversion methodology to the European Arctic. In: Proc., 31st Monitoring Research Review, Tucson, AZ, 21-23 Sep 2009.

Kværna, T. & F. Ringdal (2009): Detection capability of IMS primary and auxiliary seismic stations. In. Semiannual Tech. Sum. 2-2009, 1 January - 30 June 2009, NORSAR, Kjeller, Norway.

Pirli, M. (2009): NORSAR System Responses Manual, Kjeller, Norway, 131 pp.

Sharma, M.L., J. Douglas, H. Bungum & J. Kotadia (2009): Ground-motion prediction equations based on data from the Himalayan and Zagros regions. J. Earthq. Eng., in press.

Wang, J., J. Schweitzer, F. Tilmann & R.S. White (2009): Detection of aftershocks of the February 21, 2008, Spitsbergen M 5.9 event at ARCES. In. Semiannual Tech. Sum. 2-2009, 1 January - 30 June 2009, NORSAR, Kjeller, Norway.

6 Summary of Technical Reports /Papers Published

6.1 A climatology of infrasound observations at the experimental ARCI array in Norway

6.1.1 Introduction

Infrasound was first discovered after the violent eruption of the Krakatoa, Indonesia, in 1883. Low frequency pressure waves were observed at traditional barographs. These appeared to have traveled with the sound speed and up to four passages were noticed at some instruments (Symons, 1888). The first microbarometer recordings date from 1908 when a comet, or asteroid, exploded over Siberia in Russia, the so-called Tunguska event. The societal and scientific interest in infrasound increased during World War I, (*e.g.,* Whipple, 1939), and later in the nuclear testing era (Posey & Pierce, 1971). With the signature of the Limited Test Ban Treaty in 1963, most interest in infrasound promptly came to a stop, since nuclear tests were confined to the underground. Only a few studies could be maintained (Balachandran *et al.*, 1977; Liszka, 1978). In recent years, the study of infrasound gained renewed interest with the signature of the CTBT in 1996, where it is used a verification technique for atmospheric tests (Dahlman *et al.*, 2009).

Sources of infrasound are in general large, since an enormous amount of air has to be displaced to generate such low frequencies (Gossard & Hooke, 1975). Natural sources are: avalanches, lightning, meteors, oceanic waves, severe weather, volcanoes, sprites and earthquakes. Among anthropogenic sources are: explosions, supersonic flights, military activity, rocket launches and nuclear tests. Identifying the sources of infrasound out of this zoo of coherent waves in the atmosphere, is one of the major challenges in infrasound research.

The propagation of infrasound through the highly dynamic atmosphere plays an important role in source identification. Infrasound travels up to thermospheric altitudes of 120 km and experiences refractions due to an increase in wind and/or temperature as a function of altitude. If the gradients in the propagation velocity are strong enough, infrasound will be bended back to the earth's surface (Drob *et al.*, 2003). There are three regions in the atmosphere where such gradients might exist. These are of importance in long range sound propagation, *i.e.*, over distances larger than 150 km. The regions are marked by (1) a strong jet stream at 10 km altitude, near the tropopause, (2) the combined effect of wind and temperature at the stratopause, around 50 km altitude and (3) the temperature increase in the thermosphere from 100 km and upwards.

The aim of this study is to identify the sources around the ARCES infrasound and to build up a climatology of station specific detections. Each infrasound array has its own detection capabilities as the atmospheric conditions and source characteristics are highly variable as function of geographical location and time.

6.1.2 The ARCES infrasound array (ARCI)

A temporary, experimental three-element infrasound array was established at ARCES in March 2008, which will be abbreviated as ARCI (Roth *et al.*, 2008). Purpose of the installation is to gain experience with simultaneous recording of seismometer and microbarometer data using minimal wind noise reduction equipment. Fig. 6.1.1 shows the location and configuration of ARCI. The instruments are microbarometers of type MB2005 which have a flat frequency

response to pressure in the range of 0.02 to 10 Hz. Infrasound measurements are affected by noise due to wind. Therefore, a spatial filter is applied at each instruments which essentially integrates the pressure field. Doing so, pressure fluctuations with a small coherency length, like those of tens of centimeters associated with wind noise, are partly canceled out. The infrasonic waves of interest remain undisturbed because of their much larger coherency length of tens to hundreds of meters. Such analog filters can consist of pipe array with discrete inlets, wind barriers or porous hoses (Hedlin *et al.*, 2003). The latter approach is applied at ARCI with four soaker hoses, each with a length of 12 meters, connected to the MB2005. For one of the three sites, the hoses are additionally held centered inside a 5 cm drainage pipe. Environmental restrictions at the ARCES array prevent installation of larger pipe arrays that require fences.

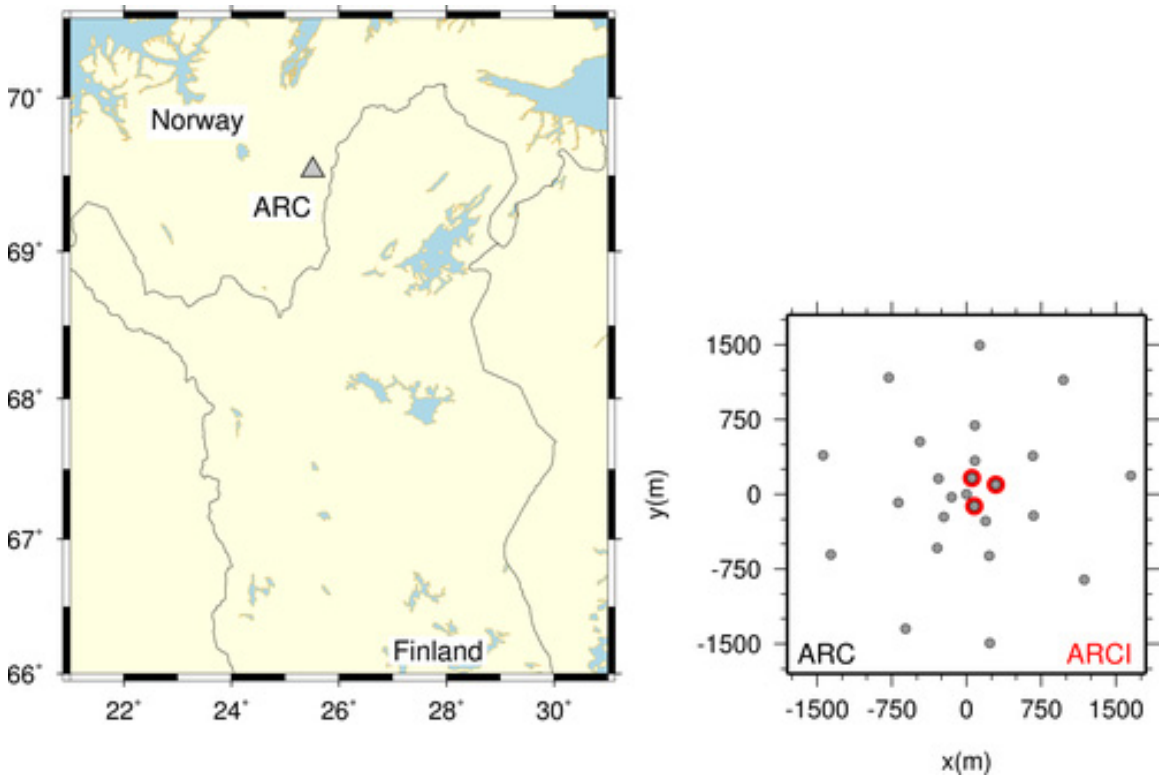

Fig. 6.1.1. The location of the ARCES (ARC) array and positions of the seismometers (gray dots). The temporary array ARCI is configured with three microbarometers (red dots), which are co-located with seismometers in the center of the seismic array.

The temporal resolution of the array is controlled by the sampling rate, leading to a Nyquist frequency which is the highest recoverable frequency given by this digitization in time. Frequencies higher than the Nyquist frequency will be aliased. ARCI is sampled at 80 Hz which means frequencies up to 40 Hz can be resolved. Similarly, the spatial resolution of the array is determined by the configuration and also limited by aliasing. A source cannot uniquely be identified if this so-called spatial aliasing occurs. An infrasound array consists of a limited number of microbarometers in a certain aperture. The reconstruction of the wavefield is affected by this spatial discretization since the atmosphere is not sampled infinitely. In practice, the sensors within an array are placed such that array response approximates a delta function around the desired slowness.

Fig. 6.1.2 shows the array response of ARCI to a monochromatic planar wave of 0.2 and 2.0 Hz, as function of slowness. The main lob is slightly asymmetric which means the array has a

somewhat higher resolution for energy coming from the southwest-northeast direction. Furthermore, side lobs occur at higher frequencies which may lead to spatial aliasing because of the limited sampling of the atmosphere by three microbarometers (Evers, 2008).

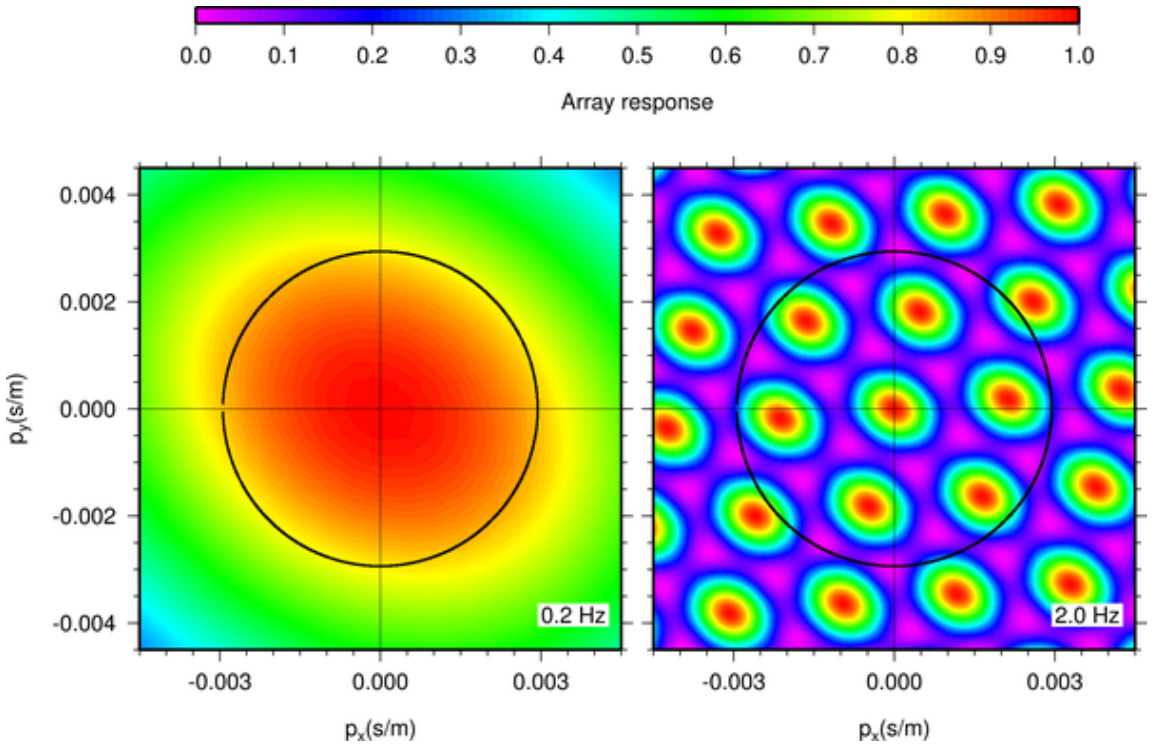

Fig. 6.1.2. The array responses to a monochromatic planar wave of 0.2 Hz (left) and 2.0 Hz (right), as function of slowness. The black circle represents an apparent sound speed of 340 m/s. The broadening of the main lob and occurrence of side lobs is caused by the limited sampling of the atmosphere by three microbarometers. Ideally, the array response would be a delta function which means the atmosphere could be sampled infinitely.

6.1.3 Array processing of infrasound recordings

The detection of coherent infrasonic signals traveling over the array can be achieved by evaluating the Fisher (F) ratio. In essence, a statistical hypothesis is tested. Applying a F-detector is attractive because of its well-known statistical distribution. The hypothesis to be tested is that all recordings made by the microbarometers consist of uncorrelated noise. The alternative hypothesis is valid for the case that not only noise is present but also signal. Evaluated are the variance of the noise and the variance of all recordings, which can not be attributed to the noise since it is common to all signals (Evers, 2008). The F-detector has been described in both the time (Melton & Bailey, 1957) and frequency domain (Smart & Flinn, 1971) and has successfully be applied in infrasound processing to detected, for example, meteors and microbaroms (Evers & Haak, 2001).

The processing sequence applied in this study is as follows:

- Remove the mean of the recordings
- Band-pass filter with a second order Butterworth filter with corner frequencies of 0.1 and 1.0 Hz (the low frequency or microbarom band) and 1.0 and 7.0 (the high frequency band)

- Decimate the data with a factor of 4, to reduce the data volume in order to minimize the computational efforts, from a 80 to 20 Hz sampling rate
- Define a slowness grid of 100x100 point between -0.005 and 0.005 s/m, forming 10,000 beams
- Split the data in segments of 256 samples, which equals a bin of 12.8 seconds
- Evaluate the Fisher ratio for each beam in each bin (with 50% overlapping bins)
- Extract the slowness value, *i.e.*, the back azimuth and apparent sound speed, at the maximum Fisher ratio, for each bin.

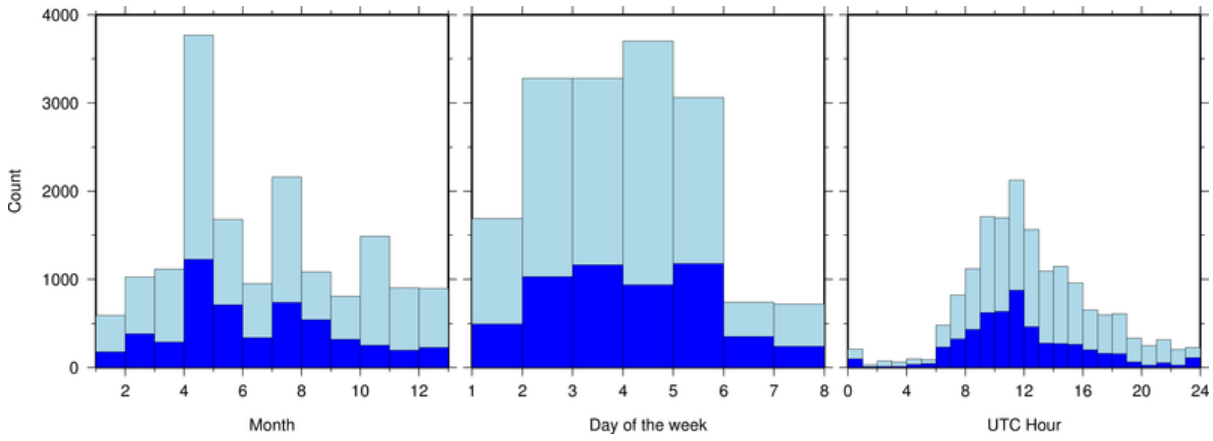

Fig. 6.1.3. Results from the array processing of ARCI data in the high frequency band of 1.0 to 7.0 Hz. The histograms shows the time of occurrence of infrasound events, between 2008, March 13 and 2009, May 14. Light blue colors indicate events with an Signal-to-Noise Ratio (SNR) larger than one (or Fisher ratio of 4 and higher). A total of 16,475 events are detected. Dark blue colors corresponds to SNRs larger than 1.5 of which 5,395 events were detected. The weekday diagram starts with day 1 which is Monday. For the hour histogram, local time in Norway is UTC+2h for summer and UTC+1h for winter.

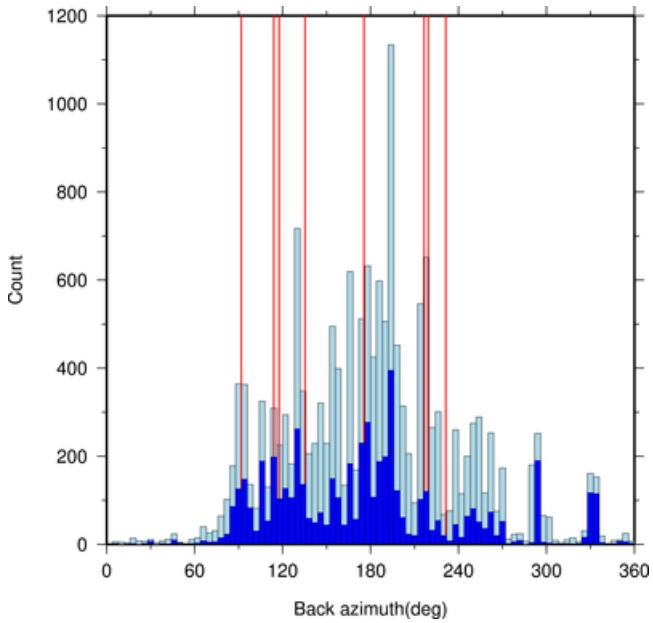

Fig. 6.1.4. The number of events (count) as function of the back azimuth for the high frequency band. Events with a SNR larger than one are denoted by light blue, dark blue is used for and SNR larger than 1.5. The red lines give the back azimuths towards quarries, mines and region of military activity.

Most sources in the high frequency band are man-made. Fig. 6.1.3 shows the time of occurrence of events in this band, for the period of 2008, March 14 up to 2009, May 14. There appear to be less events during the weekends (day 6 and 7) and during nighttime. In other words, most events occur during the working week and at daytime hours, which clearly indicates that the sources are of anthropogenic origin. The resolved back azimuths with respect to ARCI are given in Fig. 6.1.4. Most events occur from a eastern to southwestern direction. Some of these can be explained by quarries, mines and military activity, as indicated by the red lines. Less events find their origin in the the north, although, two distinct peaks, around 290 and 330 degrees, indicate activity to the northwest.

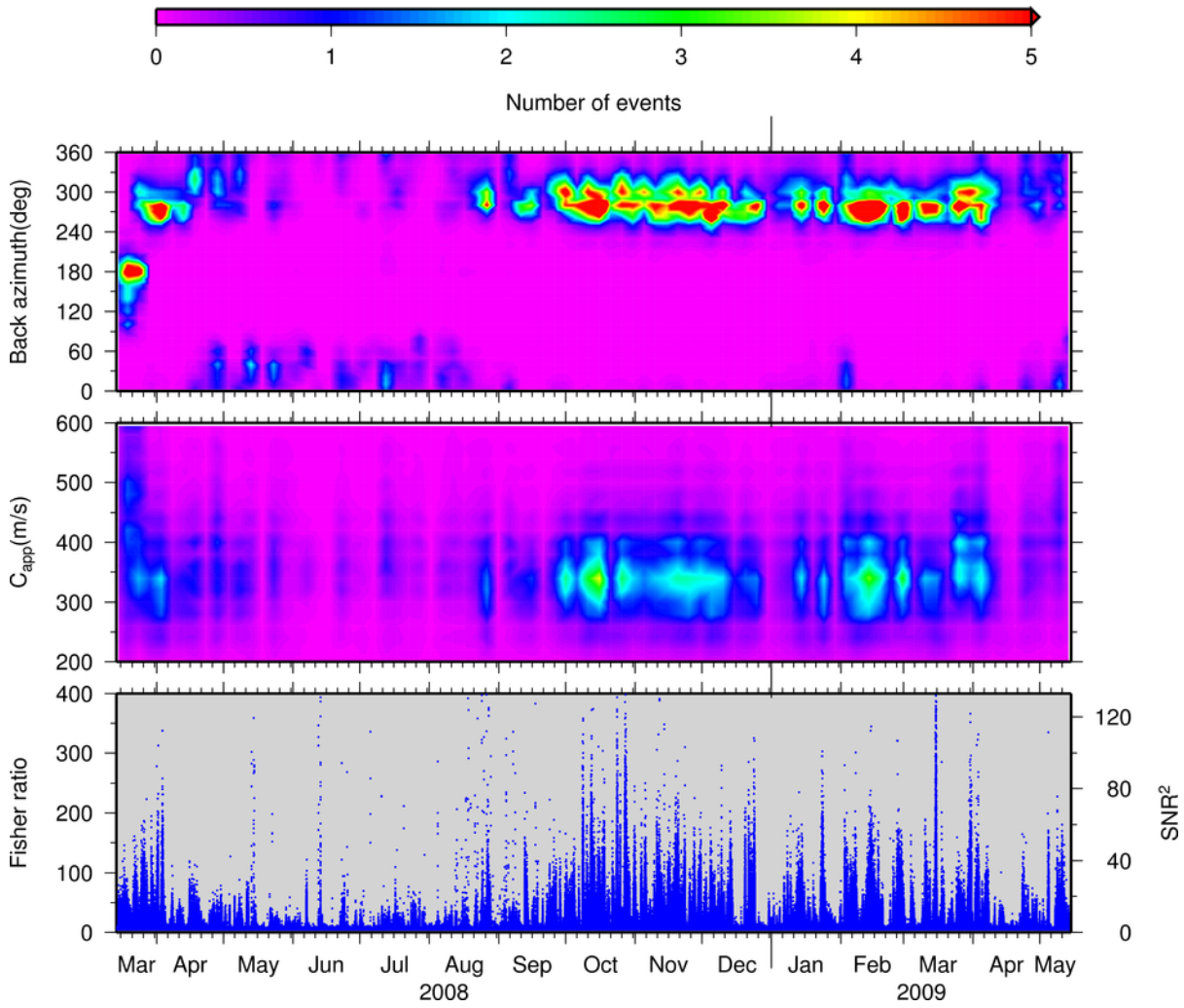

Fig. 6.1.5. Results from the array processing of ARCI data in the low frequency band from 0.1 to 1.0 Hz. The lower frame shows the Fisher ratio as function of time, that is, between 2008, March 13 and 2009, May 14. The Fisher ratio is related to the squared SNR on the traces (see the axis on the right). The top frames gives the resolved apparent sound speed and back azimuth. Color coded are the number events per hour with a SNR larger than one. Five or more events are indicated by red colors. Over the whole timespan, a total of 1.8 million detections were made with a SNR larger than one.

The low frequency band of 0.1 to 1.0 Hz is of utmost importance for the verification of the CTBT as small sized nulcear test (~1 kT TNT) are expected to generate infrasound of 0.1 to 0.2

Hz. It is also this band in which the almost continuous background noise of microbaroms is present, that peak around 0.2 Hz (Posmentier, 1967).

Fig. 6.1.5 shows the results of the above processing approach for ARCI data of 2008, March 14 up to 2009, May 14, for the low frequency band between 0.1 and 1.0 Hz. The lower frame shows the maximum Fisher ratio for each bin. This value is related to the squared Signal-to-Noise Ratio (SNR) on the traces (see axis on the right). The middle and top frame show the resolved apparent sound speed and back azimuth. Color coded are the number of detections within an hour, where five or more detections are denoted by red. Here, only detections with a SNR larger the one are plotted, which equals a Fisher ratio of four and higher. Such a detection will be labeled as an event and are mostly related to microbarom activity.

It follows from the lower frame of Fig. 6.1.5, that signal coherency strongly fluctuates as function of time. Large changes are seen from day to day but there also seems to be a difference between winter and summertime (May to September). These are also reflected in the resolved apparent sound speed and back azimuth. The short time variations in signal coherency show up as gaps, which means no events detected. During summer, less events are detected than in winter and they appear from an eastern directions. In winter, events are detected almost continuously and find their origin to the west of ARCI.

Variations in the detectability of infrasound can have several causes. These could be related to the state of the atmosphere and variations of the source. For the atmosphere, contributions along the source-receiver path will be evaluated in the following and also near receiver effects. The location, time and strength of the source will vary as function of time and will also be analyzed.

6.1.4 The contributions of the atmosphere

Atmospheric causes of the variations in the detectability of infrasound are related to two distinct areas in the atmosphere, the stratosphere and the boundary layer. The boundary layer is approximately the first kilometer of atmosphere, within the lower troposphere. The stratosphere reaches from the tropopause, around 10 km, up to the stratopause near 50 km altitude. The thermosphere, from 100 km and upwards, is not considered here, because thermospheric arrivals are strongly attenuated by the highly rarefied upper atmosphere. These are, therefore, not expected to be observed over ranges of over 1000 km (Sutherland & Bass, 2004).

Stratospheric variability

The wind in the stratosphere, called the polar vortex, varies on a seasonal scale. During winter, winds are directed to the east, around the stratopause, at an altitude of 50 km. These winds can reach values up to 150 m/s. In summer, these winds are directed to the west and somewhat less strong, reaching values of 70 m/s. Fig. 6.1.6 shows the wind and temperature near ARCI, at 69.50N, 25.50E, as function of time. The wind is split in a meridional and zonal component. The meridional wind is the south-north component of the wind and has a positive sign when directed to the north. A positive sign for the zonal wind, which is the west-east component, means it is directed to the east. The change in the zonal wind direction around the equinox should be noted, which causes the anisotropy of the medium. The temperature increase, due to presence of ozone, and strong winds around 50 km altitude may lead the refraction of infrasonic waves back to the earth's surface, due to the increase in effective propagation velocity.

Changes in this so-called stratospheric duct are visible in the surface based microbarometer recordings of ARCI.

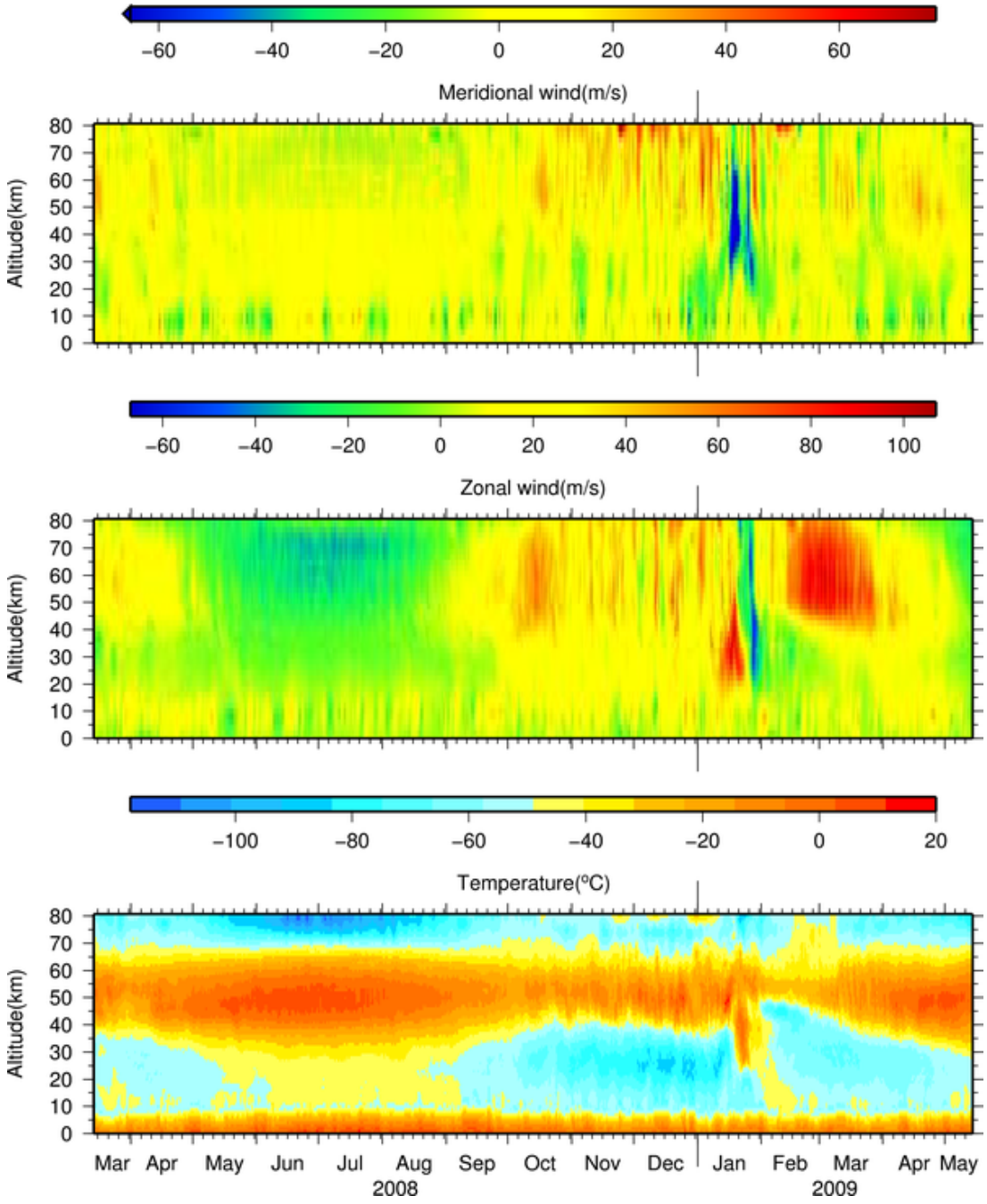

Fig. 6.1.6. The temperature and wind from models provided by the European Centre for Medium-Range Weather Forecasts (ECMWF). These models are available on a 0.5x0.5 deg grid, each six hours per day. The grid node closest to ARCI is chosen, being 69.50N, 25.50E. The wind and temperature is modeled at 91 levels up to approximately 80 km altitude. A positive sign for the zonal wind means it is directed eastwards, i.e., a westerly wind. A positive meridional wind means it is directed to the north. All values for the meridional wind lower than -65 m/s are colored blue, for plotting purposes, the actual lowest value is -140 m/s. An abrupt change in the winds and temperature should be noted in the winter of 2009, between late January and early February. Such changes are related to a major Sudden Stratospheric Warming (SSW).

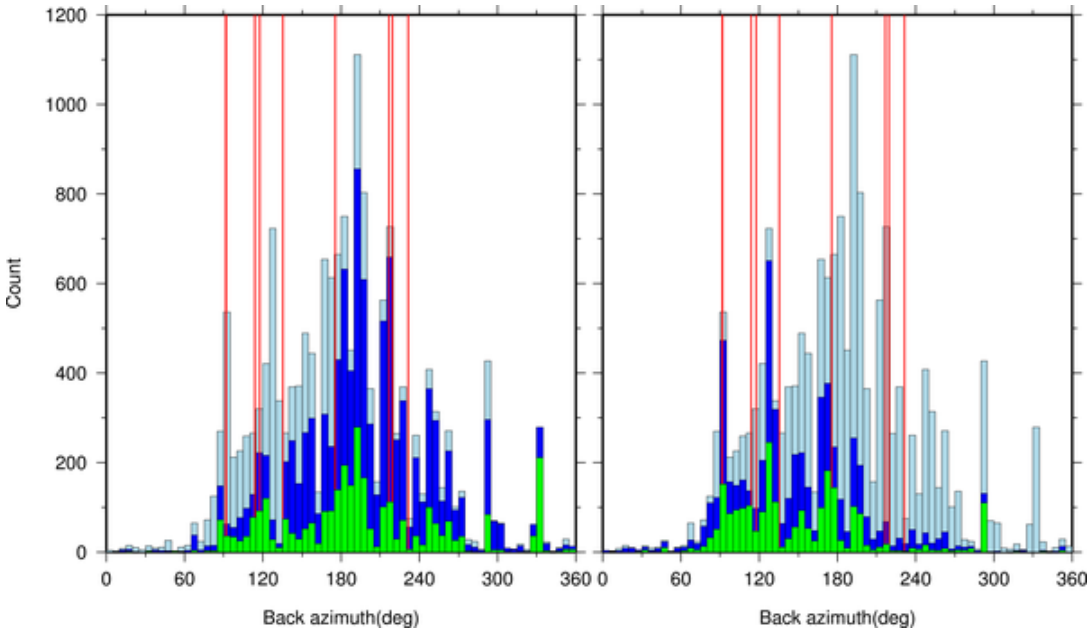

Fig. 6.1.7. The distribution of events in the high frequency band for winter (left) and summer (right). Summer is defined as the period between the equinox in April and September. Light blue colors indicate all detected events, dark blue is used for events in winter and summer with and SNR larger than one, green colors are used for events with and SNR large than 1.5.

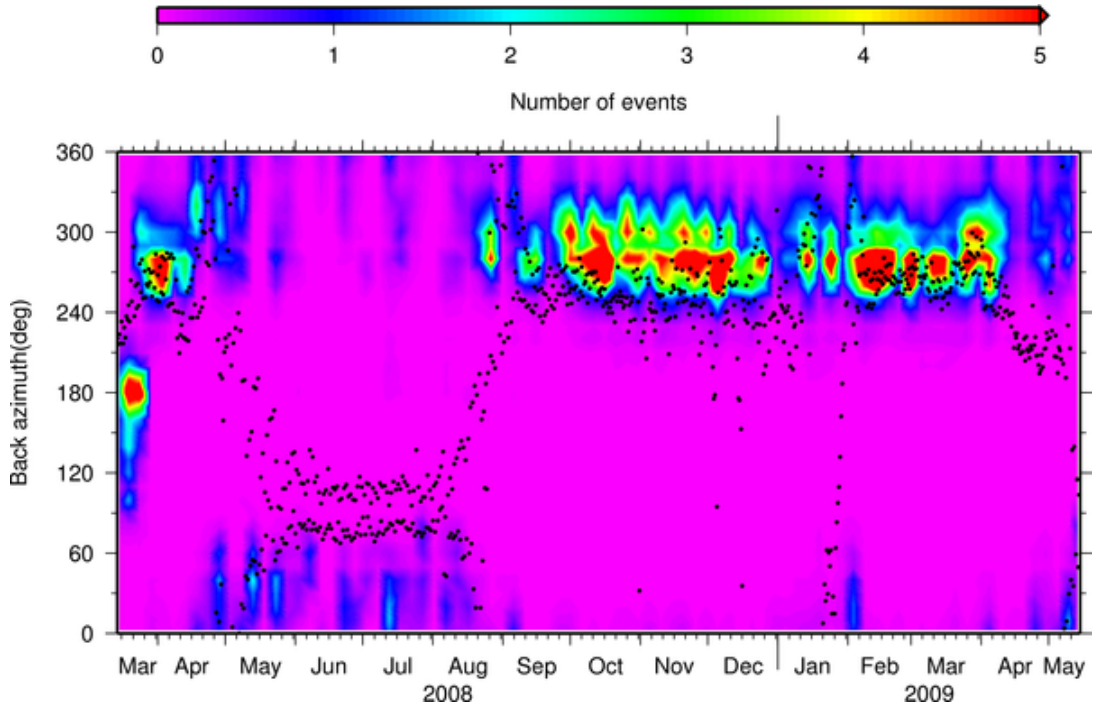

Fig. 6.1.8. The wind direction superimposed on the resolved back azimuths, for the low frequency band. The wind direction is valid for an altitude of 50 km and comes from ECMWF models at 69.50N, 25.5E. The westerly wind in winter changes to an easterly one in summer around the equinox.

For the high frequency band, a distinction is made between summer and winter in Fig. 6.1.7. It follows from this figure, that events from the west are more easily detected in winter as the stratospheric are favorable for such propagation. Events from the east are better detected in summer, but some all show up in wintertime. The detections of sources which are not affected by the direction of the polar vortex probably find their origin close to the array where tropospheric propagation is dominant.

In Fig. 6.1.8, the wind direction at 50 km altitude is superimposed on the resolved back azimuths, for the low frequency band. Clearly, the detection of coherent infrasound is guided by the stratospheric wind. In winter, microbarom energy from the northern Atlantic Ocean is recorded. As the winds turn around the equinox, microbarom energy from the east is being detected.

As can been seen in Fig. 6.1.6, an abrupt change in the winds and temperature occurred in the winter of 2009, between late January and early February. Such changes are related to a major Sudden Stratospheric Warming (SSW). The temperature increases by 50 deg C in the stratosphere, in only a couple of days, and the polar vortex changes direction. The major SSW also had its effect on the infrasound detections (see Fig. 6.1.5). Suddenly, microbaroms from the east are detected because of the change in direction of the polar vortex, which is unusual in winter. To better correlate this observation with the wind, the whole wind field, in three dimensions, should be considered and not just the wind at one grid node.

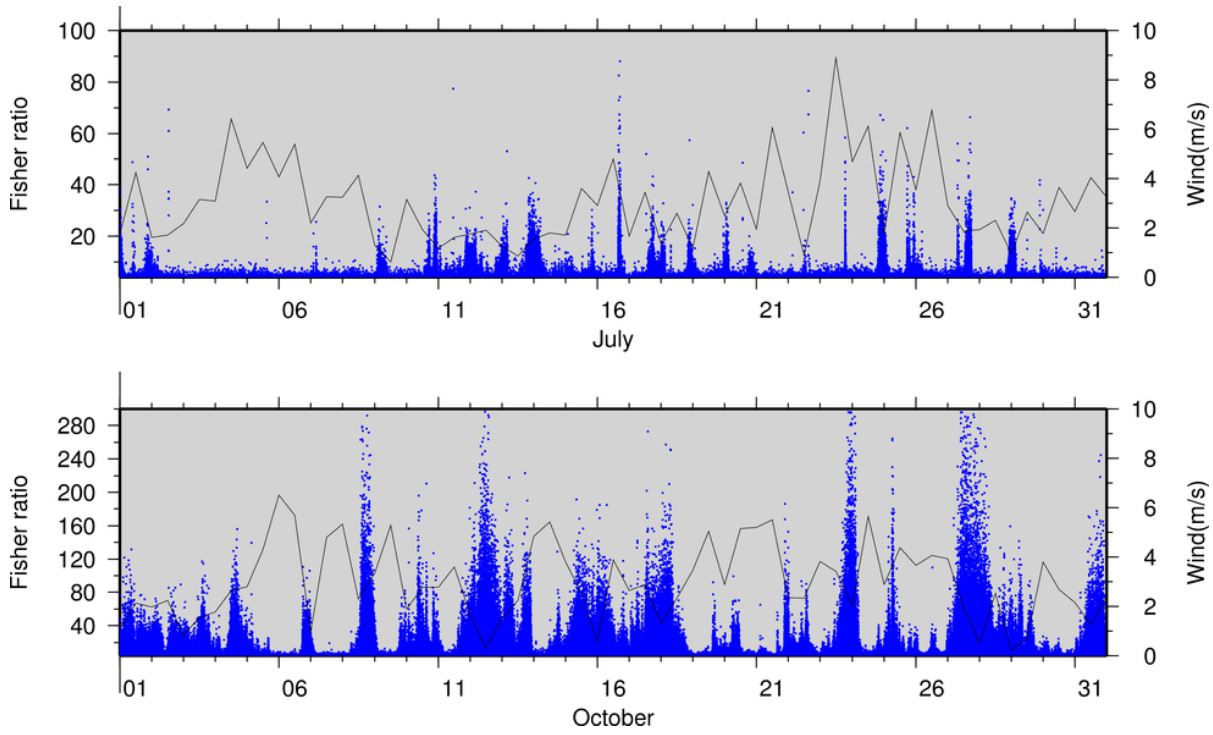

Fig. 6.1.9. The Fisher ratios for 2008, July (top) and October (bottom frame), for the low frequency band. Superimposed are the wind strengths at the first level of the ECMWF models at 69.50N, 25.5E. This first level corresponds to an altitude slightly above the earth's surface.

Variability in the boundary layer

The state of the boundary layer above the array causes de-correlation of the signals. A turbulent atmosphere affects the signal coherency which leads to a decrease of the detection capability. The summer boundary layer is far more turbulent than the winter one. Heating of the boundary layer due to solar radiation generates a high degree of mixing. This effect is also visible on a daily scale where the nighttime boundary layer stabilizes as the influence of solar radiation decreases.

Fig. 6.1.9 shows the signals coherency, by means of the Fisher ratio, for 2008, July and October in the low frequency band. Superimposed are the wind strengths from ECMWF models, at 69.50N, 25.50E, for the first level which is slightly above the earth's surface. It follows from this figure that the wind strength in summer varies on a daily basis. It peaks during daytime and decreases at night when the influence of solar radiation diminishes. The reduction in wind leads to an increase in the detectability of infrasound which is reflected by higher Fisher ratios. Wind variations in winter have longer periods, but also here an increase in wind leads to a decrease in performance of the array.

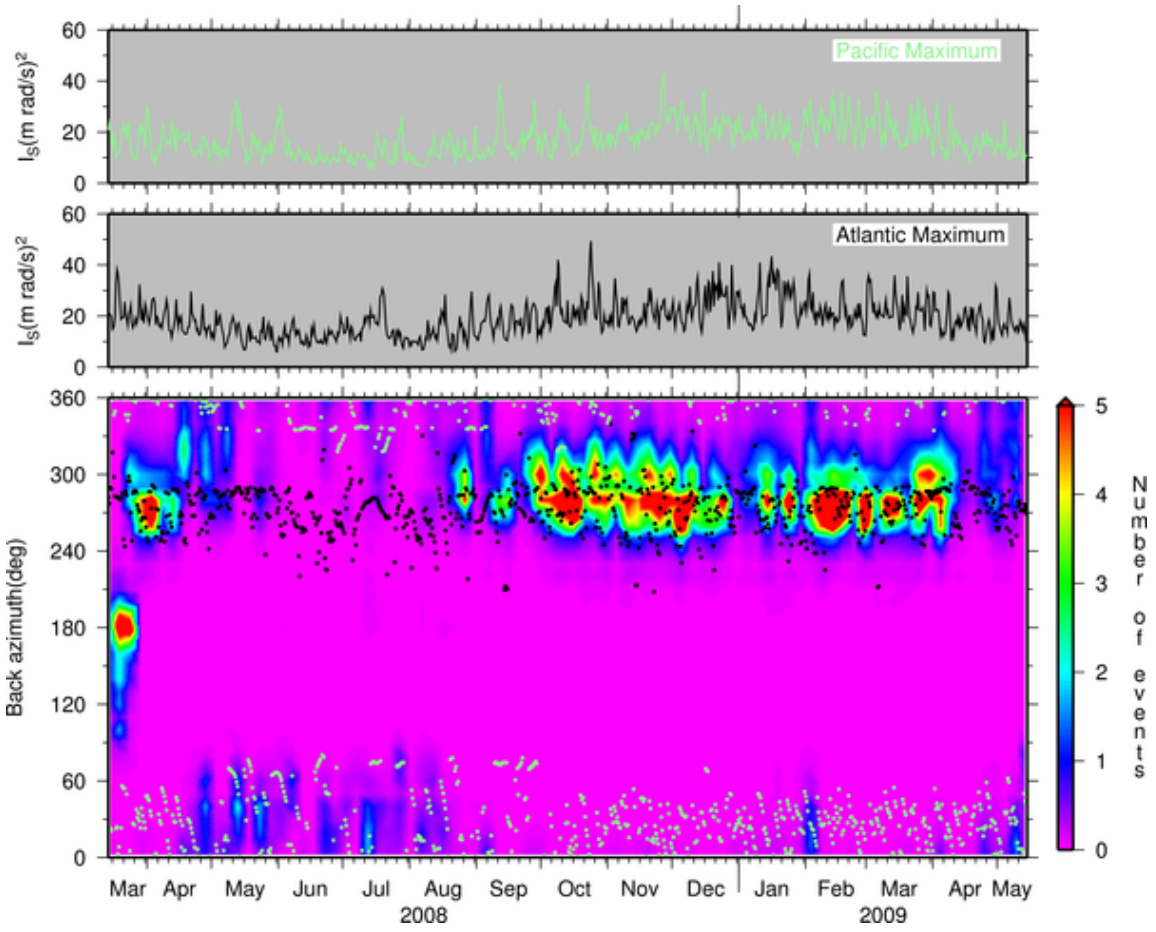

Fig. 6.1.10. An estimate of the microbarom activity in the Atlantic (black) and Pacific Ocean (green dots). The retrieved directions, in the lower frame, and source intensities (I_S, in the upper frames) are calculated from 12-hourly oceanic wave models from ECMWF provided at each 0.5x0.5 deg. As an indicator, the squared multiplication of the wave height and period is taken.

6.1.5 Specifications of the source

The source generating the signals, in the low frequency band, varies in strength over time. The microbaroms are generated by the non-linear interaction of oceanic waves, which often occurs in the vicinity of low pressure systems over the oceans. The interference of almost oppositely traveling waves leads to pressure signals in both the atmosphere and the solid earth, *i.e.* microseism. The signals have a dominant frequency around 0.2 Hz, which is double the frequency of the oceanic waves. The amplitude of induced pressure waves is, in first order, proportional to the squared multiplication of the wave height and frequency. To accurately predict the generation of microbaroms, the directional spectra of oceanic waves should be evaluated to identify the almost oppositely traveling waves and their periods (Kedar *et al.*, 2008). Here, it is assumed that the waves are interacting near the maximum of the squared multiplication of the wave height and frequency. This allows for an efficient calculation, to get an indication of the source activity (Evers & Haak, 2001).

Fig. 6.1.10 shows the back azimuths in the direction of microbarom activity in the Atlantic and Pacific Ocean, from 12-hourly oceanic wave models provided by the ECMWF. The source intensity is also estimated. The observed back azimuths of the infrasound and direction of microbarom activity coincide throughout the seasons The detection of microbaroms is also clearly related to the direction of the stratospheric winds. During the SSW which occurred in the winter of 2009, there is a sudden change in resolved back azimuths. Microbarom energy from the Pacific Ocean is detected, during a short period in early February. This indicates that the low frequency energy detected during summer might also find its origin on the Pacific Ocean.

6.1.6 Discussion and conclusion

Infrasound data from ARCI has been processed by evaluating the Fisher ratio over the period of 2008, March up to 2009, May. Lots of events are detected in both the low and high frequency band. With a detection threshold at a SNR of one, 1.8 million events are detected between 0.1 and 1.0 Hz and 16,475 events between 1.0 and 7.0 Hz. Detections in the low frequency band are mostly related to oceanic wave activity which leads to microbaroms. In the high frequency band, mainly man-made events are detected which are related to mining and military activity.

The characteristics of the medium, *i.e.*, wind and temperature structure up to stratospheric altitudes have been derived from ECMWF models. A clear relation has been shown between upper atmospheric winds and the directionality of the detections for the low frequency band. These seasonal changes are also partly visible in the high frequency band. In winter the sources to the west are detected while preference is given to sources in the east during summer. The state of the boundary layer, or turbulence and low level winds, partly determines the signal coherency. In summer, there is a daily variation caused by the influence of solar radation. A stable boundary layer during nighttime leads to less coherency loss.

In addition, microbarom activity has been estimated by evaluating the ocean wave height and period. ARCI is sensitive to microbaroms from the Atlantic Ocean in winter. Microbarom energy from the east is detected during summer. This anisotropic behavior was also identified during a period of only a couple of days, related to a SWW. A sudden change was noted from the detection of microbarom energy from the Atlantic Ocean to those from the Pacific Ocean.

The importance of taking into account both the characteristics of the medium and source, is illustrated by comparing Fig. 6.1.8 and Fig. 6.1.10. The detections move from west (270 deg) to northwest (330) during 2008, March and April. It follows from Fig. 6.1.10, that the source, microbaroms in the Atlantic Ocean, are occurring with a more or less stable back azimuth between 270 and 300 deg. The stratospheric wind, on other hand, are varying from southwest to north during this period (see Fig. 6.1.8). Therefore, this change in the resolved back azimuths should be attributed to the wind. Another change is visible, in Fig. 6.1.10, between 2008, October and 2009, April. The resolved back azimuth tend to move somewhat from the northwest to the west. The cause should be related to the source, as the wind shows no evidence for such translation. Whether this change relates to the southward movement of sea ice during winter, remains to be investigated.

In conclusion, the general behavior of ARCI can be understood by evaluating the detectability in relation to atmospheric processes and source activity. Upper atmospheric winds and the state of the boundary layer play an important role in the detectability of infrasound. Understanding such dependencies is important for the identification of small-sized nuclear test which are expected to occur in the low frequency or microbarom band.

Läslo G. Evers, KNMI, DeBilt and Delft University of Technology , Delft
Johannes Schweitzer, NORSAR

Acknowledgements

The research visit of Läslo G. Evers at NORSAR was financed by the EC project NERIES (EC Contract Number 026130). Figures in this article were made with the Generic Mapping Tools (Wessel & Smith, 1991).

References

Balachandran, N.K., W.L. Donn & D. Rind (1977). Concorde sonic booms as an atmospheric probe. Science **197**, 47-49.

Dahlman, O., S. Mykkeltveit & H. Haak (2009). Nuclear Test Ban. Springer, Dordrecht.

Drob, D.P., J.M. Picone & M.A. Garcés (2003). The global morphology of infrasound propagation. J. Geophys. Res. **108**, 4680.

Evers, L.G. (2008). The inaudible symphony: on the detection and source identification of atmospheric infrasound. PhD thesis, Delft University of Technology, available at: www.knmi.nl/~evers

Evers, L.G. & H.W. Haak (2001). Listening to sounds from an exploding meteor and oceanic waves. Geoph. Res. Lett. **28**, 41-44.

Gossard, E.E. & W.H. Hooke (1975). Waves in the atmosphere. Elsevier Scientific Publishing Company, Amsterdam.

Hedlin, M.A.H., B. Alcoverro & G. D'Spain (2003). Evaluation of rosette infrasonic noise-reducing spatial filters. J. Acoust. Soc. Am. **114**, 1807-1820.

Kedar, S., M. Longuet-Higgins, F. Webb, N. Graham, R. Clayton & C. Jones (2008). The origin of deep ocean microseisms in the North Atlantic Ocean. Proc. R. Soc. Lond. **A 464**, 777-793.

Liszka, L. (1978). Long-distance focusing of Concorde sonic boom. J. Acoust. Soc. Am. **64**, 631-635.

Melton, B.S. & L.F. Bailey (1957). Multiple signal correlators. Geophysics **XXII**, 565-588.

Posey, J.W. & A.D. Pierce, (1971). Estimation of nuclear explosion energies from micro-barograph records. Nature **232**, 253.

Posmentier, E. (1967). A theory of microbaroms. Geoph. J. R. astr. Soc. **13**, 487-501.

Roth, M., J. Fyen & P.W. LArsen (2008). Setup of an experimental infrasound deployment within the ARCES array. NORSAR Sci. Rep. **2-2008**, 52-59.

Smart, E. & E.A. Flinn (1971). Fast frequency-wavenumber analysis and Fisher signal detection in real-time infrasonic array data processing. Geoph. J. R. astr. Soc. **26**, 279-284.

Sutherland, L.C. & H.E. Bass (2004). Atmospheric absorption in the atmosphere up to 160 km. J. Acoust. Soc. Am. **115**, 1012-1032.

Symons, G.J. (1888). The eruption of Krakatoa and subsequent phenomena. Trübner & Co., London.

Wessel, P. & W.H.F. Smith (1991). Free software helps map and display data. EOS Trans. AGU **72**, 441.

Whipple, F.J.W. (1939). The upper atmosphere, density and temperature, direct measurements and sound evidence. Q. J. R. Meteo. Soc. **65**, 319-323.

6.2 Detection of aftershocks of the Feb 21, 2008 Spitsbergen M 5.9 event at ARCES

6.2.1 Introduction

An earthquake with magnitude 5.9 occurred on Feb, 21, 2008 (052:02.46.17.6) at Storfjorden-Heerland Svalbard region (77.01° N, 19.01° E, depth 15.4 km, (Pirli *et al.*, 2009)). In the following few months, a great number of aftershocks kept happening. This area still showed increased seismicity a year later. Most aftershocks have magnitudes below 3. They are small regional events with regard to the ARCES array in Norway (Mykkeltveit *et al.*, 1987) at a distance of about 850 km. In this study, we apply the frequency-dependent Multi-Channel Wiener Filter (MCWF) to the ARCES array data.

The conventional array process method is delay-and-sum, also known as beamforming. This method maximizes the array response for the assumed direction and slowness of the coherent signal, but is not optimal because the coherent part of the seismic noise at each frequency usually will be concentrated at particular wavenumbers (Douglas, 1998). The MCWF optimizes the conventional beamforming by removing coherent noise from each trace before stacking. The principle of the MCWF is to use the noise on a number of reference traces to predict the noise on the primary channel, and then to subtract the predicted noise from the actual data. It is an adaptive process in which the frequency-dependent filters are determined by the data. It is thus suitable for use with passive seismic monitoring arrays in which the ambient noise might not be stationary. A complete procedure of the MCWF and the discussion about the algorithm can be found in Wang *et al.* (2009).

The ARCES array data is filtered by the MCWF. The SPITS array (Mykkeltveit *et al.*, 1992) at a distance of about 150 km provides reliable reference information on the true number of detectable aftershocks. This study aims to see how does the MCWF techniques help on the event detection by comparing with other methods, such as beamforming combined with band-pass filtering, the method employed by NORSAR.

When one attempts to detect small earthquakes from a large distance, the benefit of an array close to the source region is not always available. Therefore, an independent scheme is developed to apply the MCWF to the continuous data at ARCES during the period from Julian day 053 – 055, a period with a great number of aftershocks without too much overlap between events. The number of detected events from the MCWF filtered data are compared with that from the band-pass filtered data, both in the continuous mode.

6.2.2 Data Example

Geometry

NORSAR arrays: SPITS (at epicentral distance ~150 km) and ARCES (at epicentral distance ~850 km), and aftershocks from Storfjorden-Heerland Svalbard region are used for this study (see Fig. 6.2.1).

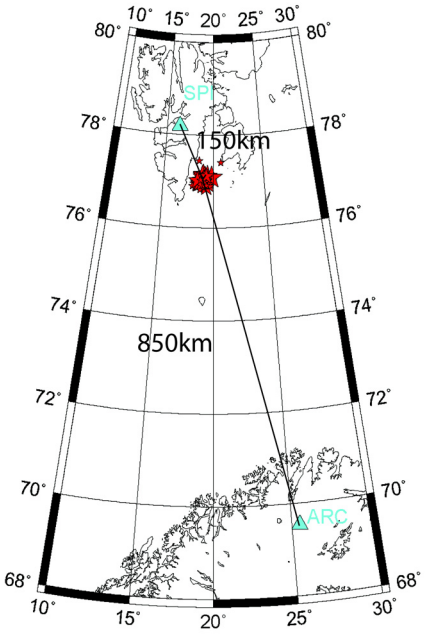

Fig. 6.2.1. Geometry of the source region (red stars) and the arrays SPITS and ARCES (blue triangles).

Data

An aftershock with the origin time 2008.055:18.59.02 is used to demonstrate the improvement of the Signal-to-Noise-Ratio (SNR) by the application of MCWF. The Pg phase is detected by SPITS on 2008.055:18.59.26 with SNR = 290.8 (calculated as ratio between the Short-Term and Long-Term Averaged amplitudes, STA/LTA). Based on the theoretical travel time difference between the source and arrays, SPITS and ARCES, the rough onset time of Pn arriving at ARCES is evaluated to be about 2008.055:19.00.58. Sixty seconds of ARCES array data (055:18:59:42 – 055:19:00:42), preceding the event, is taken as the noise reference data. The next 180 s during 055:19:00:42 – 055:19:03:42 is filtered by the MCWF. The window length of 5 s and the damping factor of 0.01 are used for the MCWF for the optimal results. Fig. 6.2.2 displays the band-pass filtered raw and individually filtered traces of the 25 vertical elements of the ARCES array. The band-pass filter always refers to a Butterworth filter at 3 – 8 Hz, with order 3, unless specifically indicated. Due to the weakness of the signals, it is difficult to tell the exact onset of the signals. But Pn and Sn are still visible and their arrival times match the expected aftershock signals for the ARCES array. The arrival of Pn and Sn are marked by arrows. By comparison, both events show stronger energy of the individually filtered traces than the band-passed raw traces. In fact, the NORSAR event detection program does not report this aftershock at the ARCES array as the NORSAR program uses an SNR threshold of 4.

F-K analysis

The f-k analysis is an important tool for locating the direction from which the signal comes and its apparent velocity. However, weak signals would be easily misled by the high ambient noise in the f-k analysis. The Sn phase of the event at the origin time 2008.055:18.59.02 is used to demonstrate the improvement of the MCWF. Fig. 6.2.3 shows the enlarged Sn and the corresponding f-k analysis from the 25 vertical band-passed elements. Fig. 6.2.4 shows the enlarged Sn and the f-k analysis from 25 individually MCWF filtered traces. The f-k analysis of the individually MCWF filtered traces shows the expected signals, but the f-k analysis from the only band-passed data is smeared out by the noise.

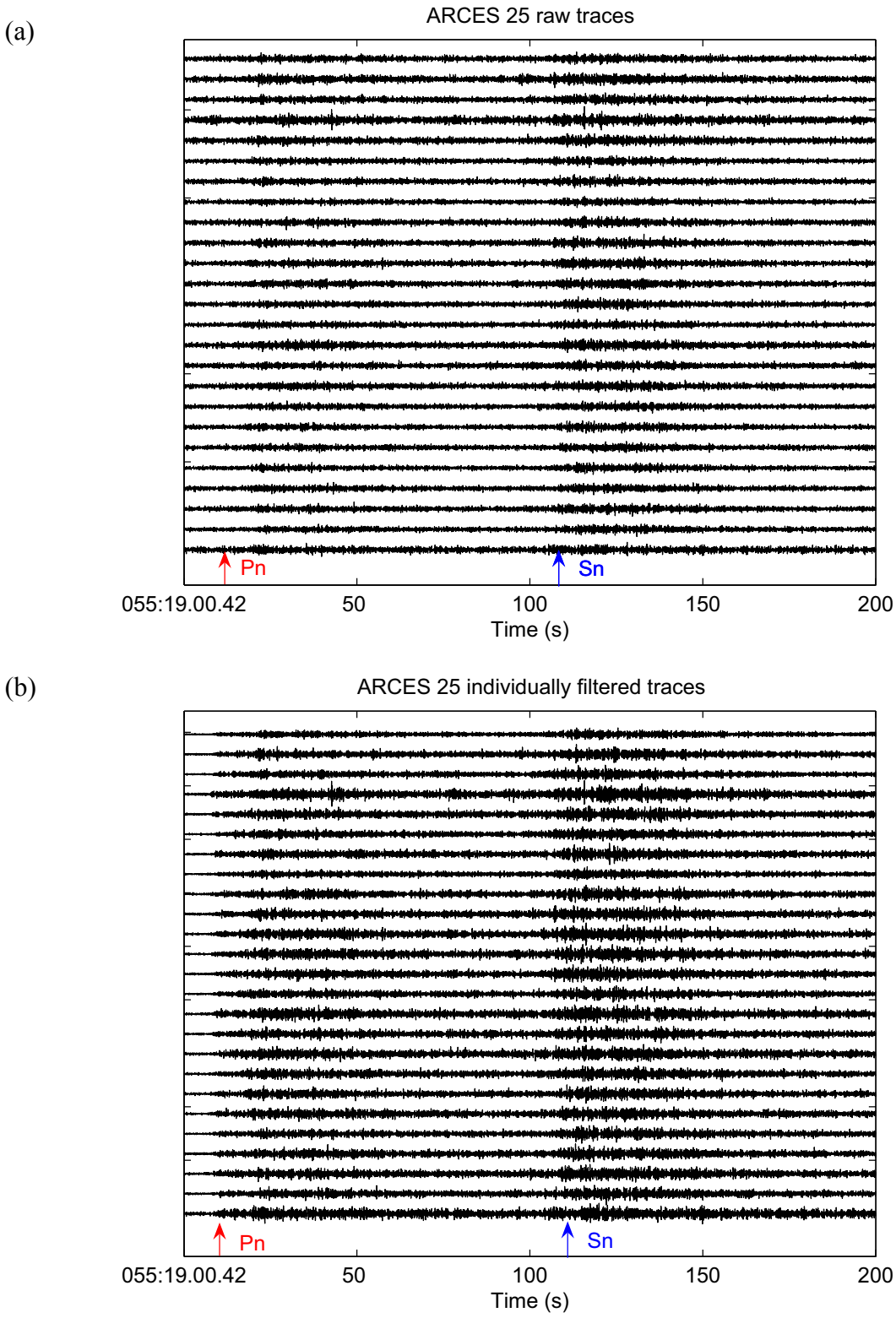

Fig. 6.2.2. Event with the origin time 2008.055:18.59.02. (a) Waveforms of the 25 vertical elements band-passed recordings at ARCES. (b) The band-passed waveform after individually MCWF filtered traces of the ARCES array. The arrival times are marked by red (Pn) and blue (Sn) arrows.

(a)

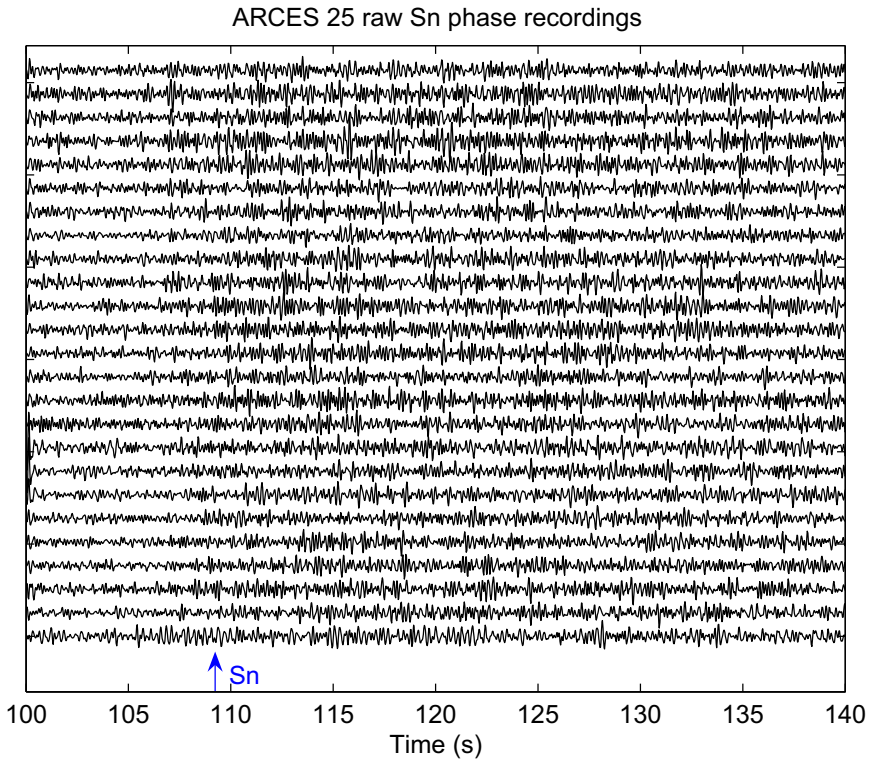

(b)

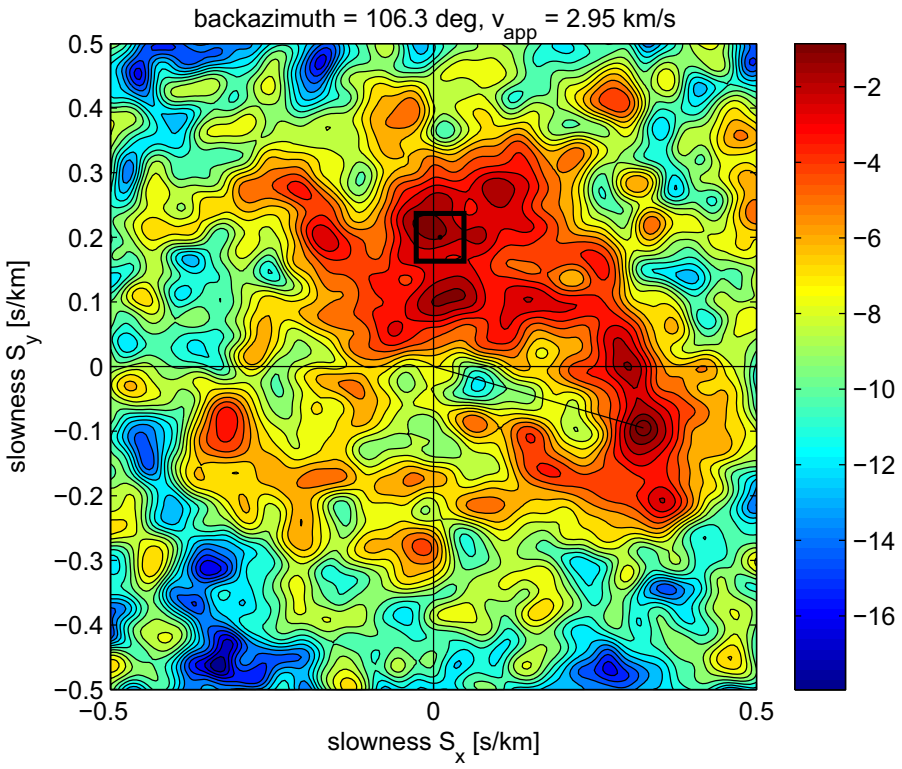

Fig. 6.2.3. Event with the origin time 2008.055:18.59.02. (a) Band-passed raw waveforms of Sn phases recorded by the ARCES array. The arrival is marked by the blue arrow. The start time is consistent with Fig. 6.2.2. (b) F-k analysis of individually filtered S waves over 109 – 111 s. The signal energy peak is expected in the black frame.

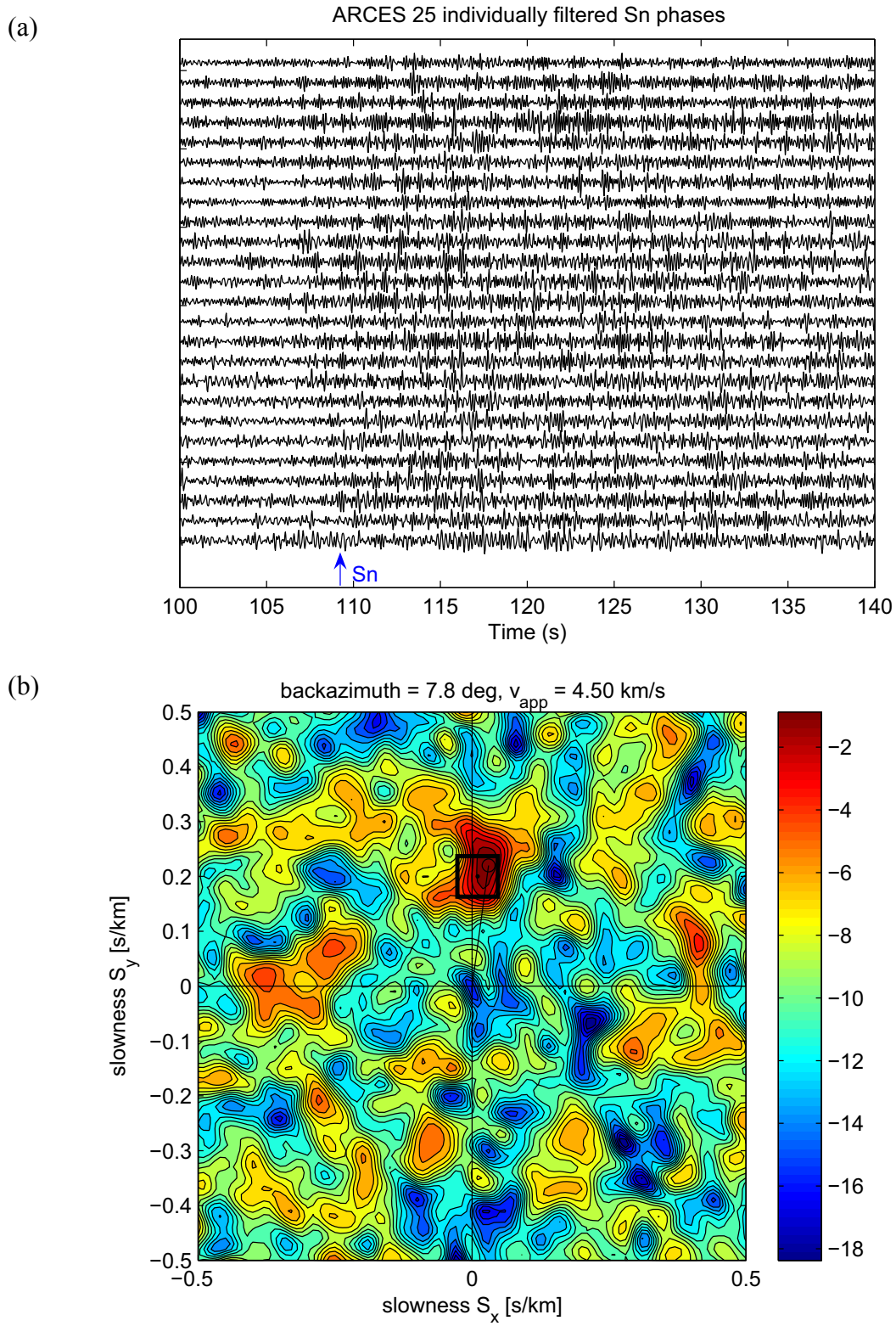

Fig. 6.2.4. Event with the origin time 2008.055:18.59.02. (a) Individually MCWF filtered waveforms combined with the band-pass filter, of Sn phases recorded by ARCES. The arrival is marked by the blue arrow. The start time is consistent with Fig. 6.2.2. (b) F-k analysis of individually filtered S waves over 109 – 111 s. The signal energy peak is expected in the black frame.

6.2.3 Event time indicated MCWF procedure

This section aims to detect aftershocks of the Spitsbergen main shock in the whole year of 2008. Detections by the SPITS array are used to define the possible windows in which aftershocks might be detected at ARCES.

Work flow

As the SPITS array is much closer to the seismic source region than the ARCES array, aftershocks with high SNR detected by ARCES will also be detected by SPITS. On the other hand, the weaker aftershocks could be detected by the SPITS array, but might not necessarily be detected by the ARCES array due to the much smaller signal amplitudes at ARCES. Therefore, the detections by the closer SPITS array provide reliable reference time of aftershocks. The procedure of the MCWF application is summarized in four steps, some of them will be explained in detail later:

- Step I, select SPITS detections
- Step II, MCWF filters the ARCES array data within the analysis time window defined by the SPITS detections and the Pn wave averaged travel time difference between ARCES and SPITS
- Step III, do f-k analysis on each filtered candidate and select signals with the SNR above 3, and the back azimuth and apparent velocity falling into the expected range of the detected aftershocks reported by NORSAR's automatic regional bulletin (http://www.norsardata.no/NDC/bulletins/gbf/2008.html).
- Step IV, double check by eye

Step I and Step II

Fig. 6.2.5 shows the back azimuth and the apparent velocity of some aftershocks detected by both SPITS and ARCES arrays as reported in the bulletin. These detections are made by the Generalized Beam Forming (GBF) method, the routine automatic NORSAR event location program (Ringdal & Kværna, 1989). This plot gives the upper and lower limit of the detectable parameters of the potential aftershocks detected by both arrays. It is important to obtain these event parameters from the real observations rather than the theoretical calculation based on the location of the source and receiver, because of systematic slowness errors (Schweitzer, 2001). We use the back azimuth and apparent velocity range of 54 Pg phases detected by the SPITS array to set a search range of the SPITS detections for the whole year 2008. The back azimuth and apparent velocity of 46 Pn and Sn phase pairs detected by the ARCES array are then used in step III to judge whether those declared candidates are aftershocks or not. The back azimuth searching range for Pg phase at SPITS is 130 – 170° and the apparent velocity range is 4 – 8 km/s according to Fig. 6.2.5. However, the initial searching ranges should be somewhat wider than that Fig. 6.2.5 suggests to ensure that no potential aftershocks are filtered out in the very beginning. This is because SPITS is much closer to the source region than ARCES so that SPITS is more sensitive to the back azimuth of aftershocks than ARCES. When more constraints are added in, the candidate events become clearer.

In total, there are 49857 detections claimed by the SPITS array during step I. The distribution of the SPITS detections with respect to the Julian day in 2008 is shown in Fig. 6.2.6. Among these detections, only those whose SNR at SPITS exceed 30 are assumed to be detectable by ARCES.

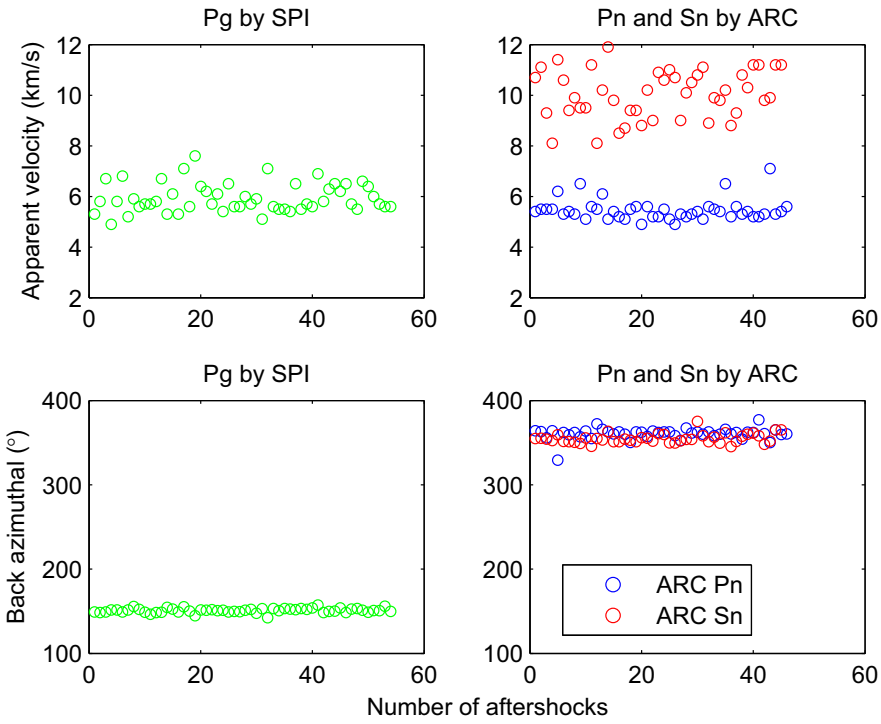

Fig. 6.2.5. Apparent velocity and back azimuth of the Pg phases (green) detected by the SPITS array and the Pn (red) and Sn (blue) phases detected by the ARCES array.

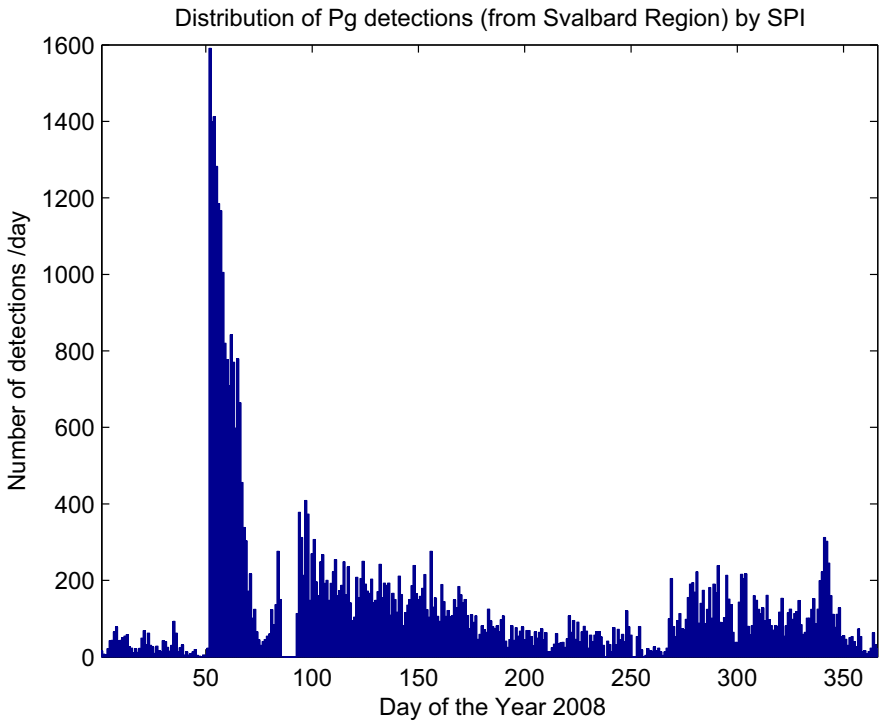

Fig. 6.2.6. Number of Pg detections by the SPITS array. The gap between Julian day 085 and 093 is due to an outage of the array.

5050 detections with SNR above 30 are found, about 10% of the total detections. An analysis time window for each detection is defined by the arrival time at SPITS and the average travel time difference to ARCES and SPITS. The ARCES array data in the analysis time window is filtered by the MCWF. A 60 s noise reference window is used to filter the next 180 s of data. A window length of 5 s and a damping factor of 0.01 are used.

The threshold of the SNR should not be so low that it includes a lot of noise, nor should it be so high as to reject many potentially detectable candidates. A SNR = 30 has proven to be a good threshold in this study. If the threshold of SNR is set to the lower value of 20, 2014 additional detections are made at SPITS, which will include many more candidates to be filtered (about 40%). A few of these additional events were checked and none of them were visible after the ARCES data is filtered by the MCWF.

Theoretically, the threshold of the SNR should not be the only parameter to select possible events candidates, because of the effect of the radiation pattern. If the SPITS array were to be near the nodal plane of a seismic event, the SNR will be much lower, but it could still be detected by the ARCES array. Therefore, using only the threshold of SNR runs the risk of missing some events. Fortunately, this case is not very likely and most of the potential candidates still fall into the selected range.

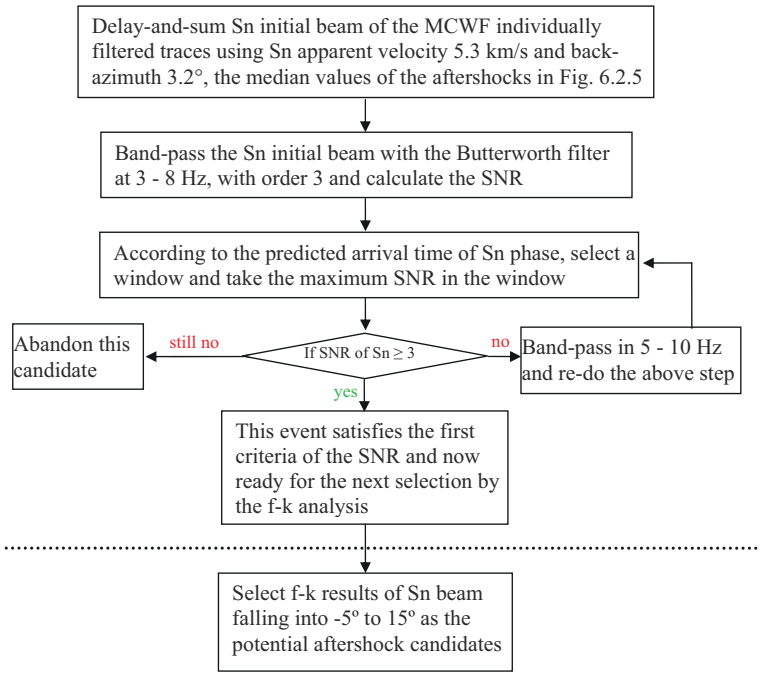

Fig. 6.2.7. The work flow for filtering and selecting aftershocks at ARCES.

Step III and Step IV

Two criteria are used in this step to select potential aftershocks: (1) the SNR of the MCWF filtered Sn beam is above 3; (2) the f-k analysis results of back azimuth and apparent velocity that fall into the acceptable range. The detailed work flow is described in Fig. 6.2.7, where the two steps of selection are separated by a dashed line.

In this example, the SNR threshold, an empirical value, is based on the MCWF filtered Sn beam, rather than MCWF filtered Pn beam, because the energy of Sn is usually stronger than

Pn. There are quite a few cases where Pn is buried in the high ambient noise, but Sn still can be observed. In these cases, the SNR of Pn will be below the threshold and they are thus missed. The averaged back azimuth of 355° and apparent velocity of 10 km/s are used for delay-and-sum beamforming Pn and 3.2° and 5.3 km/s are used for delay-and-sum beamforming of Sn signals. The back azimuth difference between Pn and Sn is due to lateral heterogeneities along the travel path (Schweitzer, 2001).

After the candidates matching the first criterion are selected, the f-k analysis follows to further select the events. The choice of the appropriate window for f-k analysis is a tricky issue when the signal is weak. To overcome the uncertainty resulting from a single f-k analysis window, we ran a few windows around the predicted arrival time of the signals. For example, around the predicted arrival time of the Sn phase, we consider 20 s of individually MCWF filtered data. The f-k analysis is made in each moving 2 s window, with 50% overlap between neighbouring windows. For each f-k analysis, if the apparent velocity and back azimuth falls into the range of 3 – 7 km/s and -5 to 15° the event is marked as a "true alarm", otherwise as a "false alarm". The search range of the apparent velocity and back azimuth is based on the statistical information of the well located aftershocks reported by the bulletin (see Fig. 6.2.5). The same procedure can also be applied to the Pn beam, except that the window length for f-k analysis is 1 s due to the higher frequency content of the Pn waves. Events with apparent velocity and back azimuth of f-k analysis of Pn falling into the 8 – 13 km/s and -10 to 10° ranges, respectively, are marked as "true alarms", otherwise as "false alarms". The criterion of Pn will be used later in the automatic MCWF procedure. The more "true alarms" the candidate has, the more likely it is an aftershock event.

We found by inspection that the Sn beam on its own is a firm and stable constraint to judge whether a candidate detection is an event or not. The Sn beam should be used when the event is so weak that the f-k analysis of the Pn signal is scattered by the ambient noise and does not report the correct signal back azimuth and apparent velocity. It has also been found that the back azimuth is a more important factor than the apparent velocity as a criterion when the ambient noise degrades the f-k analysis. It means that when the back azimuth of the energy peak in the f-k analysis falls into -5 to 15°, the apparent velocity would be within 3 – 7 km/s in most of cases. On the other hand, when the apparent velocity energy peak in the f-k analysis falls into the range 3 – 7 km/s, the back azimuth could be from all possible directions. Therefore, the actual criterion is set by the back azimuth only in the f-k analysis and it is shown to be a feasible and suitable criterion in practice. Finally, those Sn beams whose back azimuth fall into -5 to 15° are accepted.

To summarize, among 5050 detections claimed by the SPITS array with an SNR above 30, there are 1085 detections with the SNR of Sn beam at ARCES above 3. 742 detections out of 1085 candidates are found whose Sn beam (from individual MCWF traces) satisfies the back azimuth criterion. By comparison, we repeat the same procedure of step III on the Sn beam of the band-passed raw data. Among 5050 detections at the SPITS array with the SNR above 30, we found 1021 detections with the SNR of Sn beam above 3. Only 694 detections out of 1021 candidates are found by the Sn beam (from band-passed raw data), based on the same back azimuth criterion. The candidates determined from the MCWF Sn beam and band-passed raw Sn beam are double-checked by eye in the last step. Both methods lose some candidate events off the thresholds in different stages. When the events are too weak, both methods will miss them.

Finally, 631 aftershocks are detected at ARCES in 2008. The Sn beam from the band-passed raw data detects 513 aftershocks with 181 false alarms. By comparison, the Sn beam from the individually MCWF filtered data found 577 aftershocks with 165 false alarms. The MCWF procedure found 10% more events and a 10% lower false alarm rate than the conventional beamforming combined with an appropriate band-pass filter.

These false event alarms occur due to several reasons. One of the main reasons is the disturbance by noise spikes. On some noisy days, a lot of spikes can be observed on the data. The MCWF cannot remove them because they are not predictable. Those spikes usually have high amplitudes, so that the first criterion (SNR larger or equal than 3) will be definitely satisfied. If the back azimuth of the f-k analysis happens to fall into the range -5 to 15°, it will be accepted as a candidate. This problem can be partly solved by setting a proper apparent velocity criterion. However, a tight apparent velocity range runs the risk of rejecting some potential events when the signal is so weak that the apparent velocity reported by the f-k analysis has a large uncertainty. Another reason is that non-aftershocks from the same direction happen to occur at the same arrival time as aftershocks. This happened in a few cases but is easily excluded by eye. The third reason is due to the high level of ambient noise. In that case, the data usually shows nothing except for the stationary noise without spikes. The dominant ambient noise can come from the same direction as the signals so that it is mistaken as a real event by the f-k analysis.

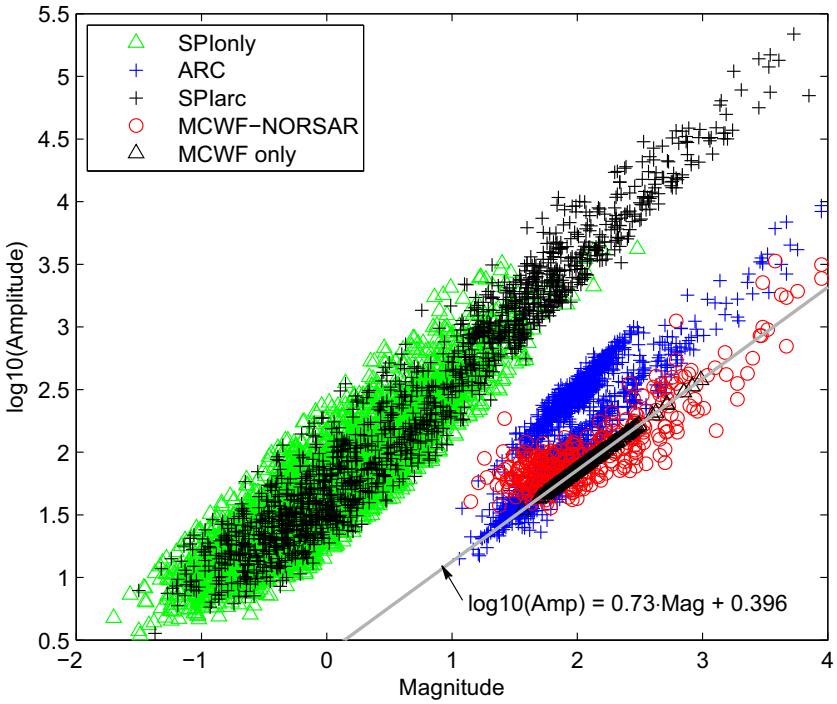

Fig. 6.2.8. The relationship between amplitude vs. magnitude of events. Black crosses are events detected by both SPITS and ARCES with amplitudes from the SPITS array data (NORSAR GBF processing). Green triangles are events detected by SPITS only. Blue crosses are events detected by both SPITS and ARCES with amplitudes from the ARCES array data (NORSAR GBF processing). Red circles are events detected at ARCES by both the MCWF procedure and the NORSAR GBF method with amplitude from the MCWF filtered results. The grey line is the least square line for the red circles, restricted to events with magnitudes larger than 2. Black triangles are events detected by the MCWF procedure only: as no reported magnitudes are available, they are plotted on top of the regression line.

6.2.4 Magnitude of aftershocks

The event identified MCWF procedure detected more events than the conventional beamforming method. Those events are missed by beamforming because of the low SNR. This section investigates the distribution of the magnitude of these missing events.

A list of events from the aftershock region is obtained from the NORSAR bulletins. The aftershock region is defined by longitude 17 to 21.3° E and latitude 76 to 77.6° N. The event location uses the GBF method. GBF automatically groups and locates seismic arrivals based on theoretical travel times for a grid of points covering a target area (Ringdal & Kværna, 1989).

The relationship between log10(amplitude) and the reported magnitude of aftershocks is plotted in Fig. 6.2.8. The amplitude is the value of the beam with the best SNR. The magnitude is defined according to Båth *et al.* (1976). log10(amplitude) and magnitude of both SPITS and ARCES detections follow a linear relationship.

Among 631 claimed aftershocks, there are 365 events reported by the GBF method. They are shown in Fig. 6.2.8 with red circles, with the amplitudes from the MCWF filtered results plotted against GBF defined magnitudes. As the MCWF differs from the GBF method, the amplitudes for the same events could be different. A regression line (see annotation in Fig. 6.2.8) is fit to those red circles (*i.e.*, MCWF amplitudes) with magnitudes larger than 2 because smaller events do not match the linear relationship well. The remaining events, which are detected by the MCWF procedure but not reported by the NORSAR bulletin, are plotted along the line with their log10(amplitude) (black triangles in Fig. 6.2.8) based on the empirical relationship (grey line in Fig. 6.2.8) between log10(amplitude) and magnitude.

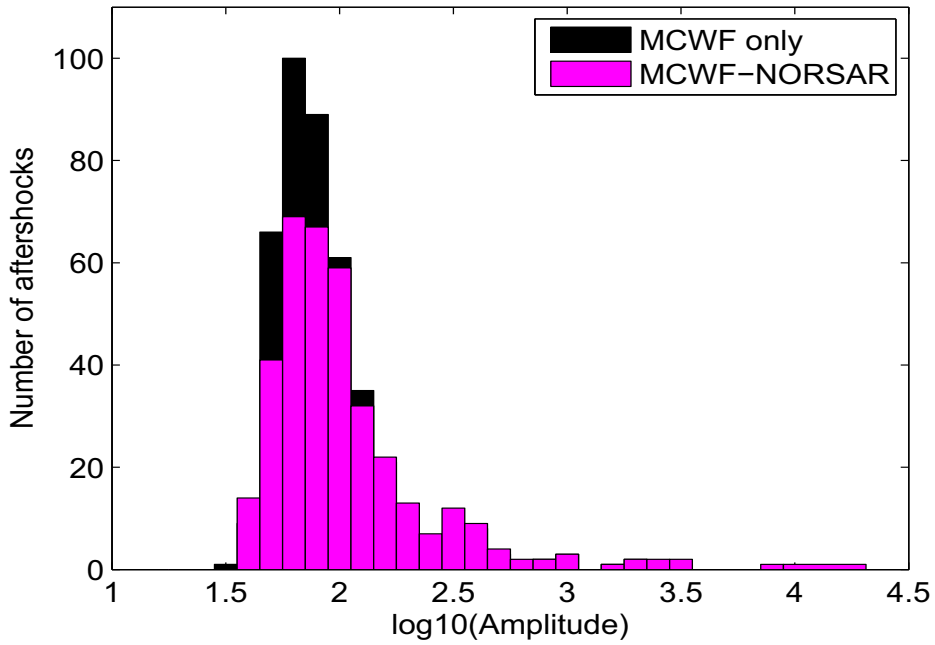

Fig. 6.2.9. Histogram of the number of detections against log10(Amplitude). The purpled bars are events detected by both the MCWF procedure and NORSAR's GBF method. The black bars are events detected by the MCWF procedure only.

Fig. 6.2.9 shows the histogram of the number of event detections by both the NORSAR bulletin and the MCWF procedure (purple). The events detected by the MCWF procedure are plot-

ted in black, and those detected by the GBF method in purple. Therefore, it is clear that the MCWF procedure does not reduce much the magnitude of the smallest detectable event but instead detects additional aftershocks, mainly events whose log10(amplitude) is between 1.7 and 2.

6.2.5 Automatic MCWF Procedure

In practice, event directions are not predictable in many cases. It would thus be required that the algorithm can filter events blindly, i.e., by filtering the continuous data with the MCWF without the benefit of prior information. As a test, the 3x24-hour continuous data on Julian days 053 – 055 are filtered continuously using the automatic MCWF detection procedure. Julian day 053 is one day after the main shock when there are not too many overlaps among aftershocks, but it still remains an active period.

The automatic MCWF procedure is to filter the whole data in a continuous mode and delay-and-sum to form the MCWF Sn beam. The Sn beam is used to select the events, instead of the Pn beam, because the Pn beam does not reliably detect weak aftershocks. The selection of aftershocks is conducted using the methods in Step III of section "Event Time Identified MCWF Procedure", *i.e.*, the SNR and the back azimuth of the Sn beam from the f-k analysis, are used to select the potential aftershocks. The five steps of the automatic MCWF procedure are (also see Fig. 6.2.10):

1. The first 120 s data is taken as the noise reference, which is used to filter the next 120 s of data. The filtered data are multiplied by a triangular window.
2. Take the data filtered in step 1 as the noise reference data for the next 120 s until the end of the continuous data.
3. Repeat these steps, but start the first window at 60 s instead.
4. Sum the results of steps 2 and 3 as individually filtered outputs.
5. The individually filtered outputs are delay-and-summed into the MCWF Sn beam by the back azimuth 3.2° and apparent velocity 5.3 km/s, the average value of aftershocks reported in Bulletin.

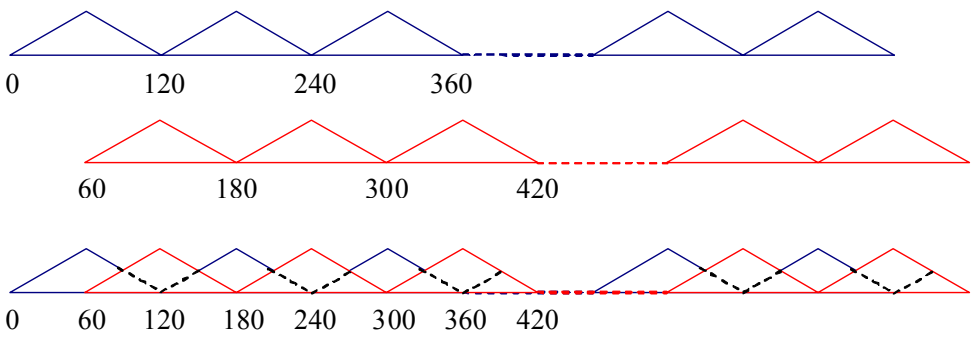

Fig. 6.2.10. The blue trace explains step 1 and 2 of the automatic MCWF procedure. In each window, the data is tapered by a triangular window. The red trace explains step 3, where the whole process is repeated but shifted half a window length. The sum of blue and red traces is the final result.

Theoretically, the SNR is supposed to be improved after being filtered. However, the window is updated by 50% overlap among windows in the automatic filtering process. It is thus possi-

ble that the automatic procedure does not use the proper noise reference data in some cases during filtering. For example, some events might happen to be split into two neighbouring windows, potentially including earthquake signals in the noise reference. This can be compensated in the next window with 50% overlap, but part of the signal is lost in the first round filtering step so that the SNR could be decreased a little. Therefore the SNR threshold to select the candidates should be set lower than 3, which is the value used in "Event Identified MCWF Procedure" Section, where the noise reference preceding the signal is properly chosen with the help of the reliable arrival time indication.

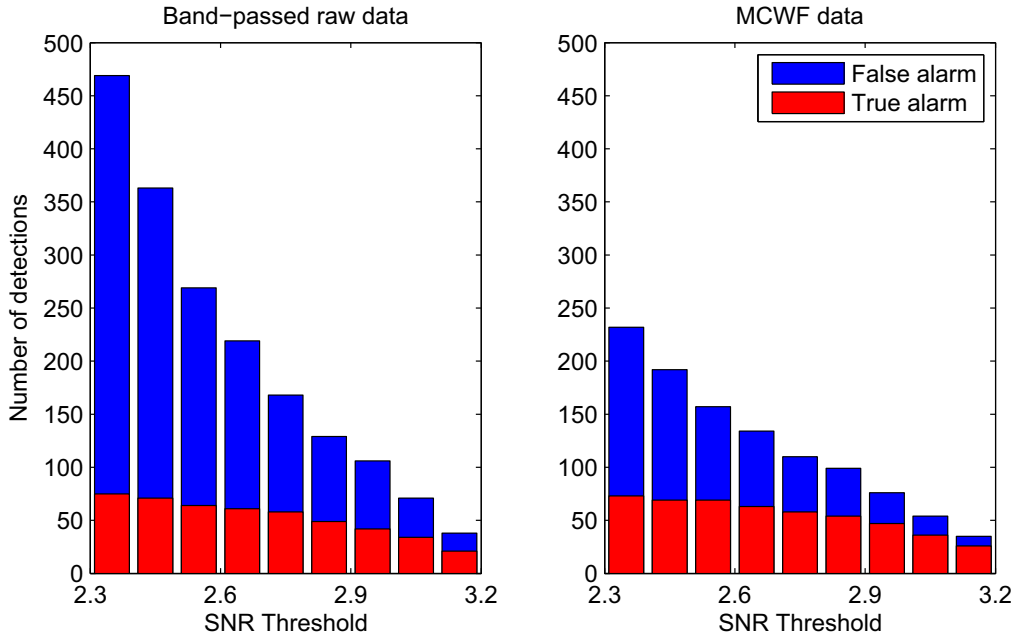

Fig. 6.2.11. The number of true and false detections as function of different STA/LTA thresholds. The number of false alarms is in blue. The number of true alarms is in red. The results detected by the band-passed raw data beamforming is shown in the left panel. The results from the automatic MCWF filtered data is shown in the right panel.

The appropriate threshold is investigated by trying a range between 2.3 and 3.2, with 0.1 increments. The number of detections by setting each threshold are demonstrated in Fig. 6.2.11. There are 78 events detected by band-passed raw data and 79 events detected by the MCWF filtered data when setting a SNR threshold of 2.3, both in automatic mode. The trade-off exists between detecting more events and including more false alarms. By comparison, the number of false alarms from band-passed raw data is significantly increased compared to the MCWF filtered data when the threshold is lower than 2.7. Therefore, a threshold of 2.7 is suggested to detect events as much as possible whilst keeping a moderate number of false alarms.

Fig. 6.2.12 demonstrates the improvement of the SNR of the automatic MCWF procedure. An event with the origin time 2008.054.08.35.51 is detected by the automatic MCWF filtered Sn beam, but missed by the delay-and-sum band-passed raw Sn beam. To keep the results comparable between the MCWF procedure and the NORSAR event detection program, we use the definition of SNR given by Schweitzer *et al.* (2002). A value of 6.0 is used for ζ. The delay time $\varepsilon = 5$ s for updating the LTA as compared to the STA. The STA window length is set to 1 s. The length of the short window is 0.25. A threshold (SNR = 2.7) is set in the SNR curves of both band-passed raw data and individually MCWF filtered results.

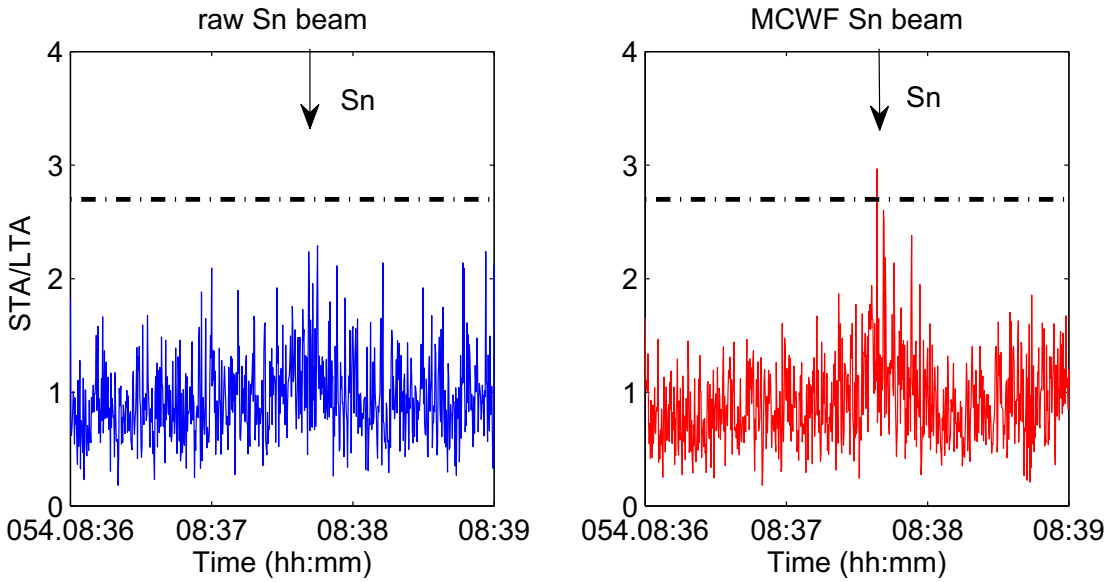

Fig. 6.2.12. Event with origin time 2008.054:08.35.51. Comparison of SNR curves of the band-passed raw Sn beam (blue) and the MCWF Sn beam (red) after the first stage automatic MCWF filtering. A threshold of SNR = 2.7 (black dashed line) in stage 1 is set for both cases. The expected Sn arrival is marked by an arrow.

6.2.6 Conclusion

The NORSAR arrays: SPITS and ARCES, and aftershocks from Storfjorden-Heerland Svalbard region are used to test the improvement of the MCWF on detecting weak regional events. The ARCES array data is filtered by the MCWF according to the time indicated by SPITS detections at a much closer distance than ARCES in 2008. Events are considered reliable when two criteria are satisfied: (1) a SNR threshold value is exceed; (2) the back azimuth and apparent velocity determined from f-k analysis matches that of the average values of aftershocks. For comparison, instead of the MCWF filtered result, the band-passed raw ARCES array data indicated by the SPITS detection is band-passed and analyzed by the f-k method. The events from the band-passed raw data are judged by the same criteria. There are 631 aftershocks detected in the whole year of 2008. The conventional beamforming, detects 513 aftershocks with 181 false alarms; the multi-channel Wiener filtered results found 577 aftershocks with 165 false alarms. The MCWF procedure found 10% more events, whose log10(amplitude) is between 1.7 and 2, and a 10% lower false alarm rate than the conventional beamforming combined with an appropriate band-pass filter.

The automatic MCWF procedure in the continuous mode found that the appropriate threshold of SNR for aftershock detection is 2.7. The MCWF also demonstrates the advantage of reducing the false alarms than the beamforming methods.

Jingbo Wang, Bullard Laboratories, University of Cambridge
Johannes Schweitzer, NORSAR
Frederik Tilmann, Bullard Laboratories, University of Cambridge
Robert S. White, Bullard Laboratories, University of Cambridge

Acknowledgements

The research visit of Jingbo Wang at NORSAR was financed by the EC project NERIES (EC Contract Number 026130). University of Cambridge, Dept. Earth Sciences contribution No. ES1116.

References

Båth, M., O. Kulhanek, T. Eck & R. Wahlström (1976). Lateral inhomogeneities in the upper mantle. Seismol. Inst., Uppsala, Tech. Report **5-76**, 37 pp.

Douglas, A. (1998). Making the most of the recordings from short-period seismometer arrays. Bull. Seism. Soc. Am. **88**, 1155-1170.

Mykkeltveit, S., F. Ringdal, J. Fyen & T. Kværna (1987). Initial results from analysis of data recorded at the new regional array in Finnmark, Norway. NORSAR Sci. Rep. **1-87/88**, 61-82.

Mykkeltveit, S., A. Dahle, J.Fyen, T. Kvrerna, P.W. Larsen, R. Paulsen, F. Ringdal & I. Kuzmin (1992). Extensions of the Northern Europe Regional Array Network - New small-aperture arrays at Apatity, Russia, and on the Arctic island of Spitsbergen. NORSAR Sci. Rep. **1-92/93**, 58-71.

Pirli, M., J. Schweitzer, L. Ottemöller, M. Raeesi, R. Mjelde, K. Atakan, A. Guterch, S.J. Gibbons, B. Paulsen, W Debski, P. Wiejacz & T. Kværna (2009). Preliminary Analysis of the 21 February 2008, Svalbard (Norway), Seismic Sequence. Seism. Res. Lett., submitted.

Ringdal, F. & T. Kværna (1989). A multi-channel processing approach to real time network detection, phase association, and threshold monitoring. Bull. Seism. Soc. Am. **79**, 1927-1940.

Schweitzer, J. (2001). Slowness corrections - one way to improve IDC products. Pure Appl. Geophys. **158**, 375-396.

Schweitzer, J., J. Fyen, S. Mykkeltveit & T. Kværna (2002). Seismic arrays. In: P. Bormann (ed.), New manual of seismologoical observatory practice (NMSOP), Chap. 9, 52 pp.

Wang, J., F. Tilmann, R.S. White & P. Bordoni (2009). Application of frequency-dependent multi-channel Wiener filters to event detection in 2D three-component seismometer arrays. Geophysics, in press.

6.3 Detection Capability of IMS Primary and Auxiliary Seismic Stations

(sponsored by US Army Space and Missile Defence Command, Contract No. W9113M-05-C-0224)

6.3.1 Abstract

We have investigated the Reviewed Event Bulletin (REB) of the International Data Centre (IDC) for the time period 13 June 1999 to 15 July 2009 to quantify the event detection capability of individual seismic stations of the International Monitoring System (IMS). For a specific target area, we can obtain estimates of the detection threshold of a given station by considering the ensemble of REB reported events in the area, and simply downscaling each event magnitude with the observed SNR at the station. However, there are some factors that must be considered, such as:

- Correcting for possible biases in the REB magnitudes caused by non-detections (by using maximum likelihood estimates)
- Correcting for skewness in the distribution of threshold estimates, also caused by non-detections
- Considering the validity of using the signal-to-noise ratio for downscaling the event magnitude

We address these issues by dividing the events into a binned global grid system and introduce a data censoring procedure to reduce these effects. A major result of this study is a quantification and ranking of the IMS primary and auxiliary seismic stations based on their capability to detect events within regional, teleseismic and core phase distance ranges. For each station, source regions with noticeable signal amplitude focusing effects (bright spots) and defocusing effects are conveniently identified and quantified. We also present results from applying maximum likelihood magnitude estimation techniques for validation of the censoring procedure.

6.3.2 Data Processing and Location

Assessments of seismic network detection capabilities are usually based upon assuming statistical models for the noise and signal distributions. Subsequently, a combinational procedure is applied to determine the detection threshold as a function of the number of phase detections required for reliable location (Sykes and Evernden, 1982; Harjes, 1985; Hannon 1985; Ringdal, 1986; Sereno and Bratt, 1989). If available, station corrections for signal attenuation can be included in these computations.

As an example, Figure 6.3.1 shows detection capability of the IMS primary seismic network in late 2007, with 38 stations sending data to the IDC. The capability is represented by the magnitude of the smallest seismic event that would be detected with a 90% probability by three stations or more. Figure 6.3.2 shows the estimated improvement over this capability that could be achieved by bringing the remaining 11 primary seismic stations into operation. No station corrections have been employed in these calculations.

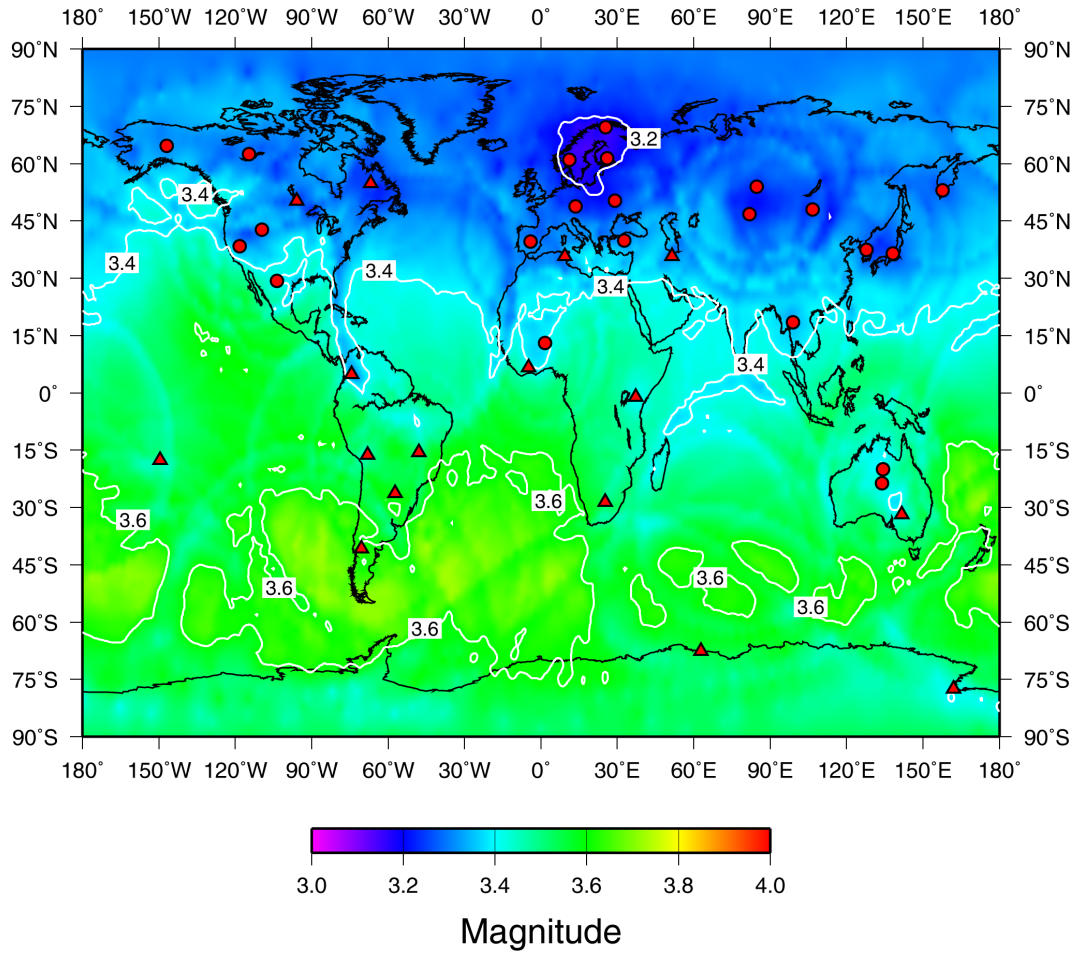

Fig. 6.3.1. Detection capability of the IMS primary seismic network in late 2007, with 38 stations sending data to the IDC. The capability is represented by the magnitude of the smallest seismic event that would be detected with a 90% probability by three stations or more. Array stations are shown as filled circles, whereas filled triangles denote three-component stations. Adopted from Dahlman et al., 2009.

While this type of maps provide a useful overview of global capabilities, they do not give a complete characterization. For example, the noise models used in these capability assessments are not able to accommodate the effect of interfering signals, such as the coda of large earthquakes, which may cause the estimated thresholds to be significantly degraded at times. Furthermore, only a statistical capability assessment is achieved, with no time-dependent evaluation of when the possibility of undetected seismic events is particularly high, for example during unusual background noise conditions or outages of key stations. Therefore, alternative methods, such as the continuous threshold monitoring technique described by Ringdal and Kværna (1989, 1992) and by Kværna and Ringdal (1999), have been showed to be useful supplements to event detection capability analysis.

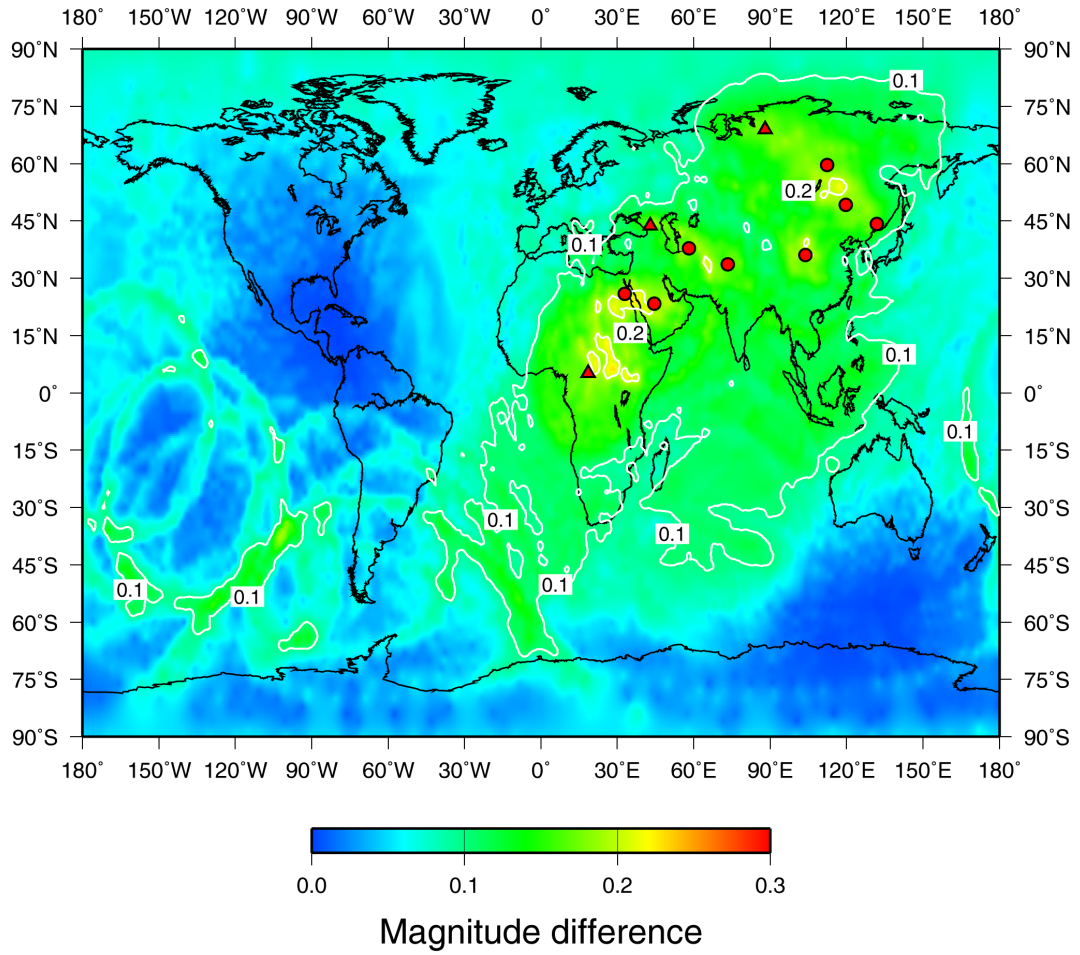

Fig. 6.3.2. Estimated improvement over the IMS capability in late 2007 that could be achieved by bringing the remaining 11 primary seismic stations into operation. Array stations are shown as filled circles, whereas filled triangles denote three-component stations. Adopted from Dahlman et al., 2009.

In this paper we address another aspect that is important for global capability estimation purposes, namely the detection capability of individual IMS stations, both on average within regional and teleseismic distance ranges, and also for specific limited source regions including regions at core phase distance ranges. As is well known, any seismic station has a detection performance that is, compared to its average performance, especially good for some regions and similarly bad for other regions. A well-known example of this is the exceptionally good performance of the NORES seismic array in Norway for detecting nuclear explosions at the former Soviet test site near Semipalatinsk, Kazakhstan (Ringdal, 1990). Additional examples are presented by Kværna et al. (2007) in their analysis of the capability to monitor North Korea's nuclear test site. The topic of the present paper is to carry out a systematic investigation of station capabilities on a regional and global basis, taking advantage of the excellent data base provided by the Reviewed Event Bulletin (REB) of the IDC for the years 1999-2009.

6.3.3 Procedure for estimating station thresholds

The database for our investigation include information about detecting and non-detecting IMS stations for events of the IDC REB. Station m_b estimates of detecting stations and noise magnitude estimates of non-detecting stations were retrieved from the IDC database in Vienna. In order to reduce the variance of the network magnitude estimates we excluded events with less than 5 stations with m_b observations in the estimates of network magnitude. In the context of CTBT monitoring, we are mainly concerned with events at shallow depths, and we therefore only considered events with reported depths less than 50 km.

We will illustrate the procedure for estimating station detection thresholds by presenting an example: As shown in Figure 6.3.3, we consider one station (ARCES) and a specific source area, in this example in China (1.5 degrees within 32°N, 104°E). Our purpose is to estimate the station detection threshold for events from this limited source area. From the REB, we obtain a large number of events, some detected by ARCES, some not detected by this station. Each event has a reference network m_b. Figure 6.3.4 shows the ARCES SNR for the detected events as a function of REB mb. We have used the REB maximum likelihood magnitudes, mbmx, in this paper. For each REB event in this source area detected by ARCES, the procedure is then to scale down the mbmx values by its log(SNR), to arrive at an instantaneous "noise magnitude" (see Figure 6.3.5). We can then add 0.5 m_b units (corresponding to SNR=3) to obtain an estimate of the instantaneous ARCES detection threshold.

Fig. 6.3.3. The source region selected for the case study presented here in centered on 32°N 104°E i China, having a radius of 1.5°, as shown by the open circle. The red curve shows the great circle path to the ARCES array in northern Norway, located at a distance of 56.4° from the center of the source region.

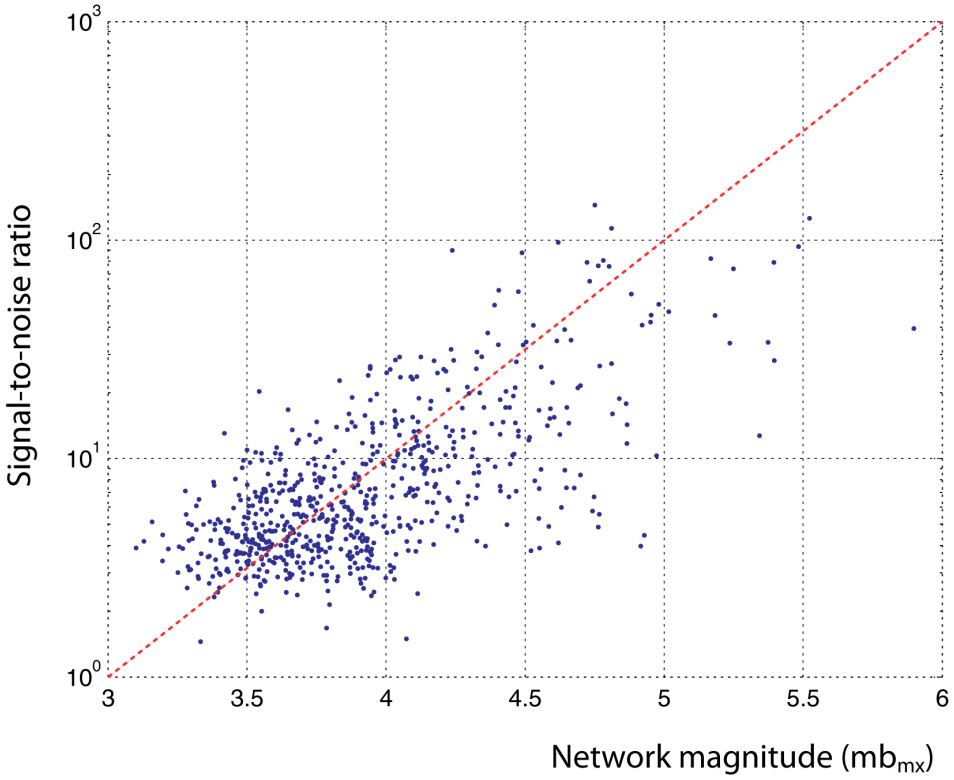

Fig. 6.3.4. Signal-to noise ratios at the ARCES array plotted as a function of REB network magnitude (mbmx) for events in the source region shown in Figure 6.3.3.

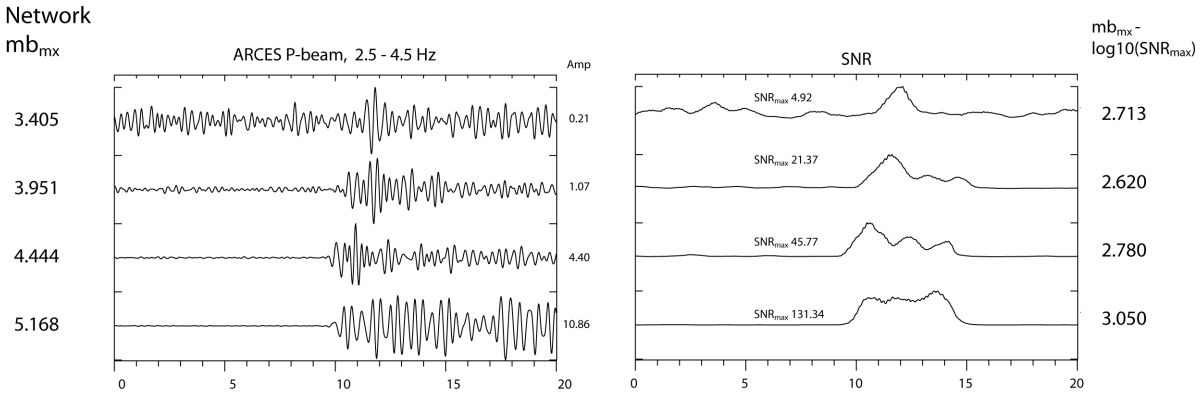

Fig. 6.3.5. Illustration of the procedure of downscaling the network magnitude mbmx by the observed log(SNR) to arrive at an instantaneous "noise magnitude" for a given region. The left-hand panel shows bandpass-filtered ARCES P-beams for 4 different events located in the source region shown in Figure 6.3.3. The corresponding network magnitudes are given to the left of the panel. The right-hand panel shows the corresponding signal-to-noise ratio (SNR) traces, together with the maximum values. The resulting estimates of the instantaneous 'noise magnitudes' of each event are given to the right of the SNR traces.

By carrying out the procedure described above for all the detected events, we obtain a set of instantaneous thresholds that clearly is magnitude dependent (see Figure 6.3.6). For each undetected event we know only that the instantaneous ARCES detection threshold must be higher than the reference network mbmx. This provides us with a classical maximum likelihood estimation framework (Ringdal, 1976). In fact, we have a number of point estimates of the instantaneous ARCES detection threshold (for those events detected by ARCES), and a number of lower bounds (corresponding to the non-detections).

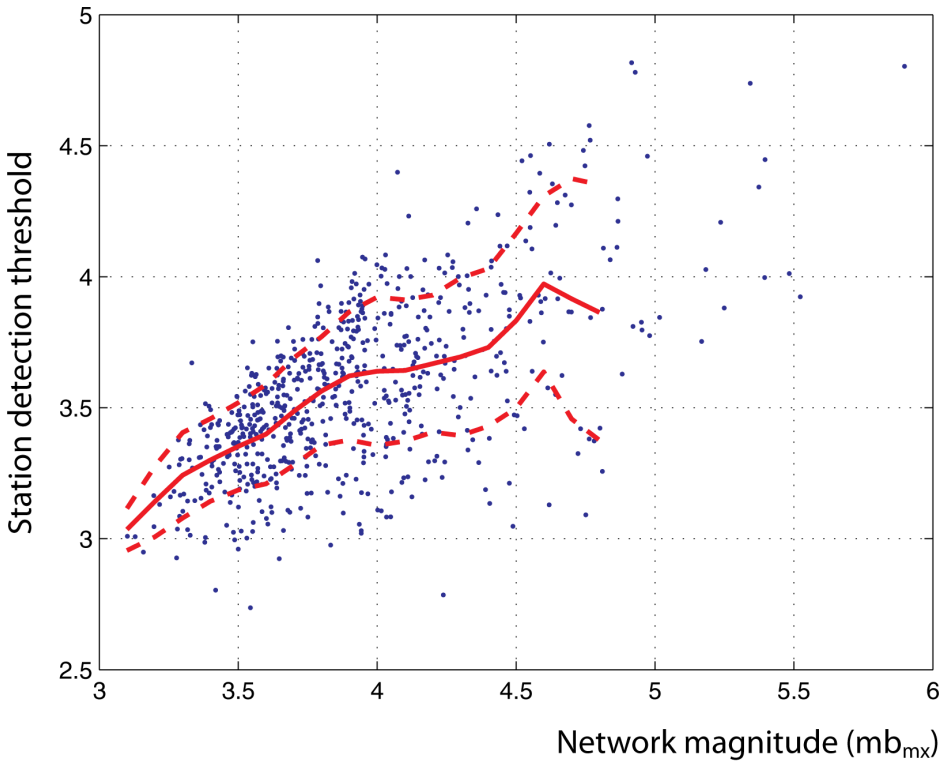

Fig. 6.3.6. The blue symbols show instantaneous detection thresholds at ARCES for events located in the source region in China (see Figure 6.3.3), using the relation of equation (1). The red line shows the running average and the dotted lines show the associated standard deviation. Notice the magnitude dependency.

The instantaneous ARCES detection threshold a_i for the *i'th* detected event is:

$$a_i = \mathrm{mbmx}_i - \log(\mathrm{SNR}_i) + 0.5 \tag{1}$$

Denoting by D the ensemble of REB events in this region detected by ARCES, we obtain the following likelihood function:

$$L(m_t) = \prod_{i \in D} \left(\frac{1}{\sigma}\right) \phi \left[\frac{(a_i - m_t)}{\sigma}\right] \prod_{i \notin D} \left\{1 - \Phi \left[\frac{\mathrm{mbmx}_i - m_t}{\sigma}\right]\right\} \tag{2}$$

Here, ϕ is the density function of the standard normal distribution and Φ is the corresponding cumulative distribution function. The symbol m_t is the ARCES detection threshold which will be estimated as the value which maximizes the likelihood function (2). We choose to keep σ constant (at a value of 0.35) although this parameter could alternatively be estimated directly from the data simultaneously with m_t.

We note in passing that the likelihood function (2) is similar to the one developed by Ringdal (1976), with the important difference that the non-detections here provide *lower bounds* rather than the *upper bounds* presented in that paper.

An illustration of the importance of taking into account non-detected events as well as the detected events is given in Figure 6.3.7. This figure shows that the fraction of non-detections increases dramatically below magnitude 4.0. As a consequence, only those events with particularly favorable path focusing effects or unusually low noise levels at the time of the event would be detected, and thus estimating the thresholds solely on the basis of these events would cause a significant bias.

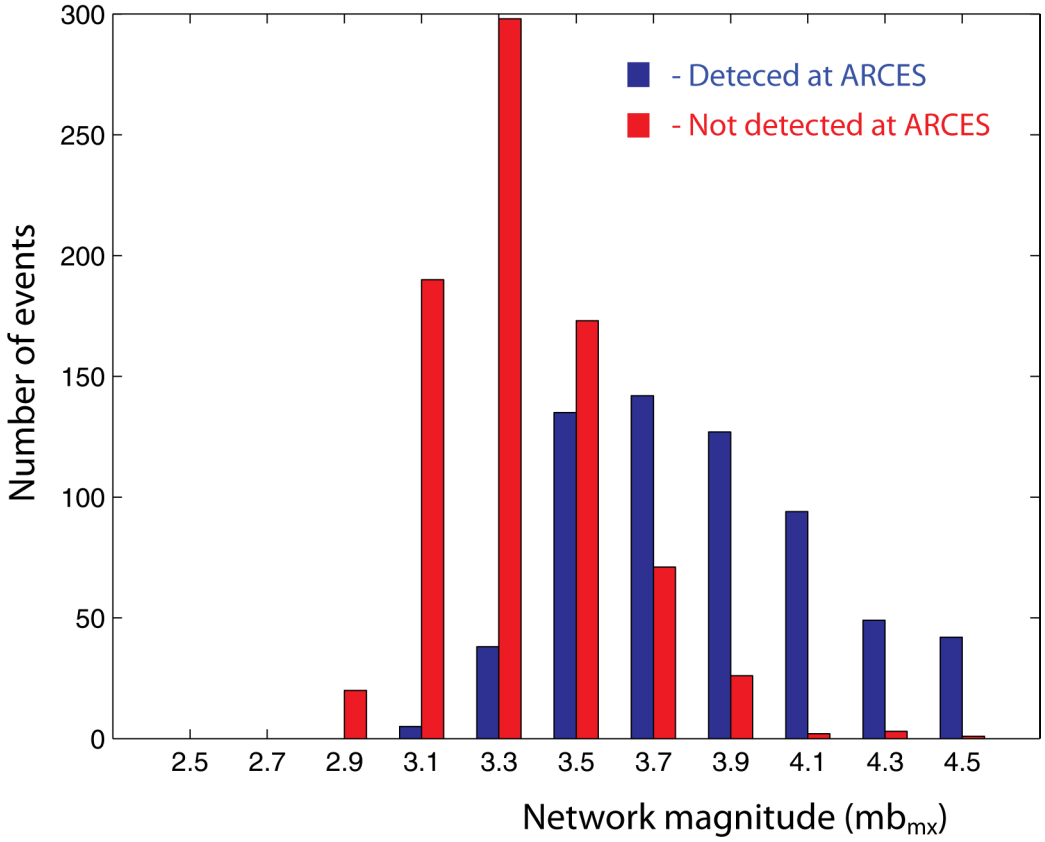

Fig. 6.3.7. Histogram of detected and non-detected P-phases at ARCES for events in the source region in China (see Figure 6.3.3).

It is now a straightforward matter to estimate the overall ARCES detection threshold for the particular site in question, using equation (2) which takes into account detections as well as non-detections. We obtain a threshold of 3.67 (Figure 6.3.8). We can verify that this computation is indeed not depending on event magnitude by computing the threshold as a function of reference magnitude (green line), where we use magnitude bins of 0.3 units. We see from Fig-

ure 6.3.8 that the threshold is essentially independent of the size of reference events in the m_b range 3.5-4.5. Below 3.5 and above 4.5 there are fewer events and the estimates are not as reliable. Censoring the data as illustrated in the figure gives an approximate threshold estimate, and we have used such censoring for most of the estimations done in this paper. As an indication of the consistency between the two approaches, Figure 6.3.9 shows the correspondence between the GERES detection thresholds for different regions as estimated by the maximum likelihood and the censoring algorithm.

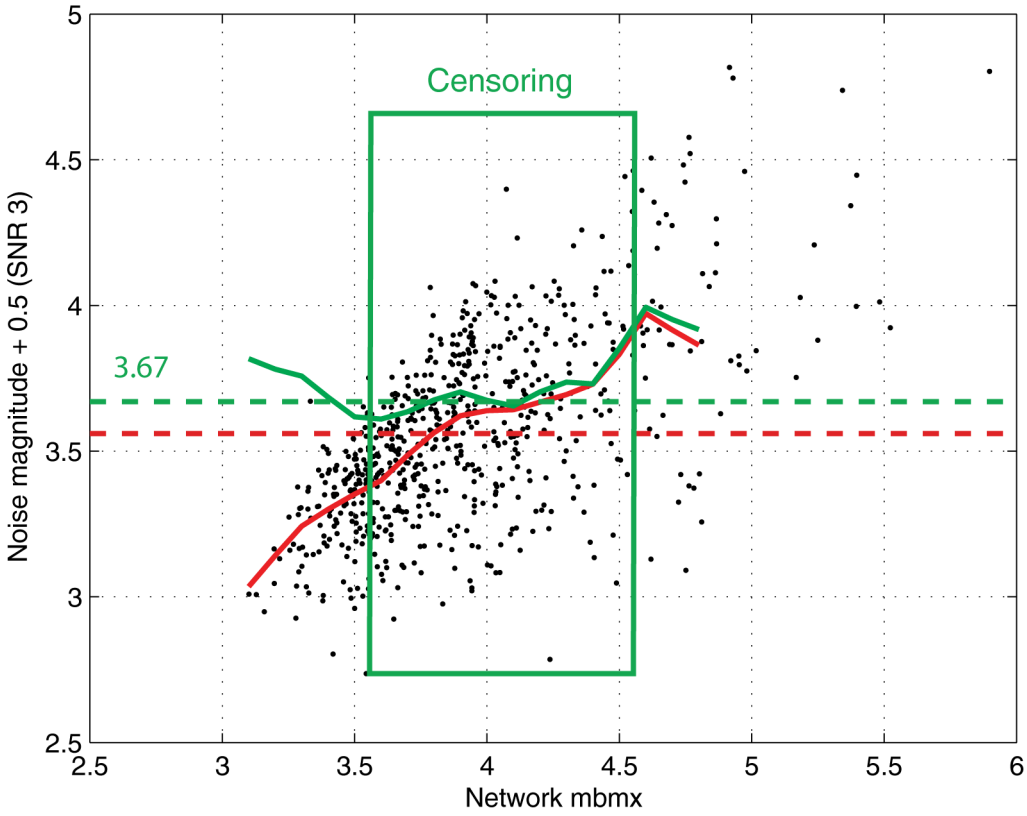

Fig. 6.3.8. The black symbols show instantaneous detection thresholds at ARCES for events located in the source region in China, and the solid red line shows the corresponding running average (similar to Figure 6.3.6). The average value for all events is 3.55 as shown by the red dashed line. The green solid line shows the maximum likelihood estimates of the detection threshold, now taking into account non-detected events, calculated in bins of 0.3 magnitude units. The green dashed line shows the maximum likelihood estimate (3.67) calculated using all events. An alternative to the maximum likelihood estimate is to censor the events used for averaging. The iterative procedure is as follows:
An initial estimate of the detection threshold is calculated from all data (the red dotted line). The average detection threshold is recalculated using only events having network magnitudes in a predefined interval around the initial estimate. In this way the smallest and the largest events, which often appear to be biased, are not included in the averaging process.

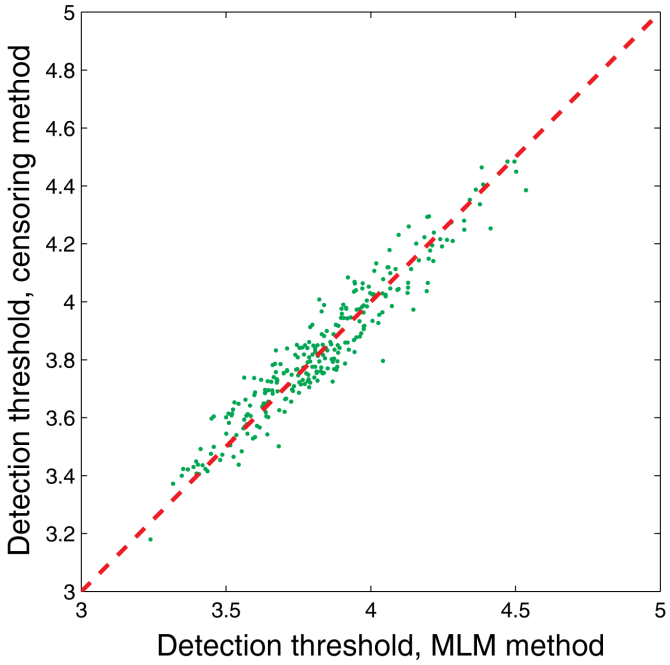

Fig. 6.3.9. The green symbols show the correspondence between the GERES detection thresholds for different regions at teleseismic distance ranges as estimated by the maximum likelihood and the censoring algorithm.

We should note here that we have not been able to apply the maximum likelihood procedure to all source-station combinations for this data set. For example, for auxiliary stations, non-detections are not reported in the REB, and thus it is not appropriate to apply the maximum likelihood procedure. Also for the primary stations, in some cases we find that the REB does not contain noise estimates for non-detections. This makes it in practice impossible for us to distinguish between cases when the lack of detection is due to station outage or to the signal being below the station threshold. In the first case, the event must be deleted in order not to skew the estimate, whereas in the second case the event must definitely be included as a genuine non-detection. In cases where maximum likelihood is not applicable, we must use the censoring approach in order to obtain threshold estimates.

6.3.4 Estimating regionalized detection threshold for a given station on a global basis

Still using the ARCES station as an example, we show in Figures 6.3.10 through 6.3.12 the ARCES regionalized detection thresholds inferred from the REB database during 1999-2009. Figure 6.3.10 indicates the number of events detected by ARCES in each 2^{o}x2^{o} bin, whereas Figures 6.3.11 and 6.3.12 show the regionalized threshold estimates in two different projections, using the censoring method. Notice that we in the following figures show the thresholds calculated without taking into account the SNR of 3.0 required for the detection. The absolute levels thus correspond to what we call the noise thresholds, i.e. SNR = 1.0. Only bins with 5 or more events remaining after applying the censoring procedure are plotted. The scale goes from better than 1.5 (violet) to worse than 4.5 (red). Not surprisingly, the capability is best at local

and regional distances (this applies of course to all stations in the network), but there are in addition significant bright spots in parts of Central Asia and the Middle East as well as indications of excellent detection of core phases southeast of Australia.

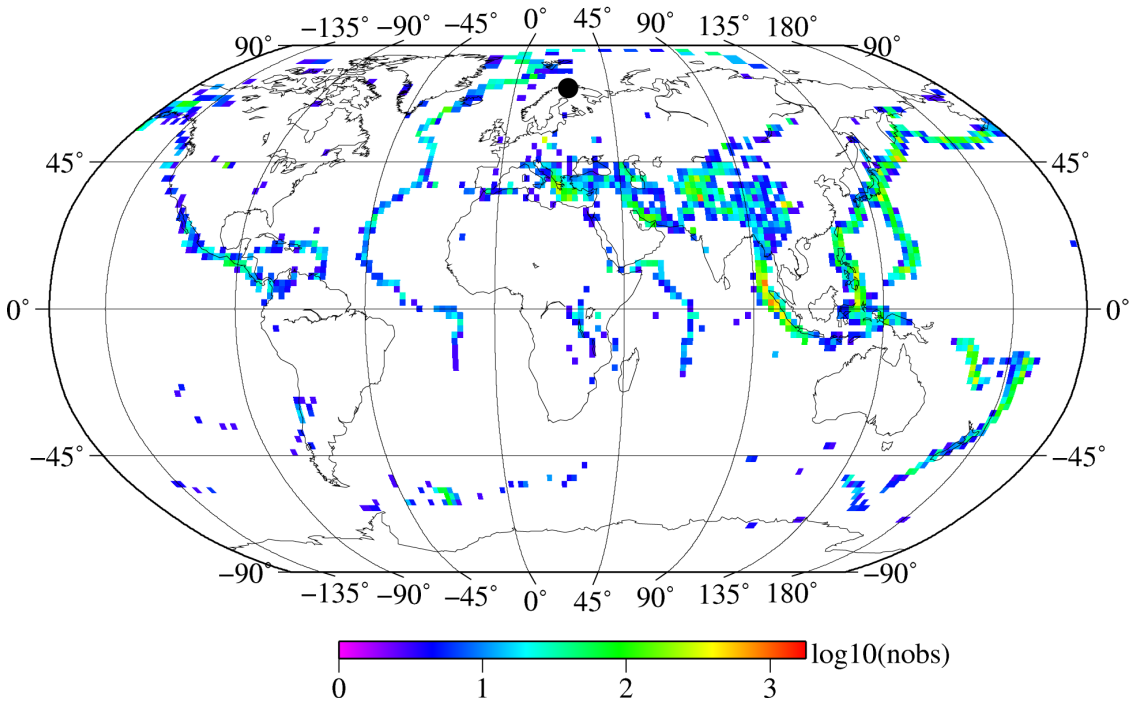

Fig. 6.3.10. The color of each $2^o x 2^o$ bin corresponds to the number of events in the REB with P-phases reported at ARCES.

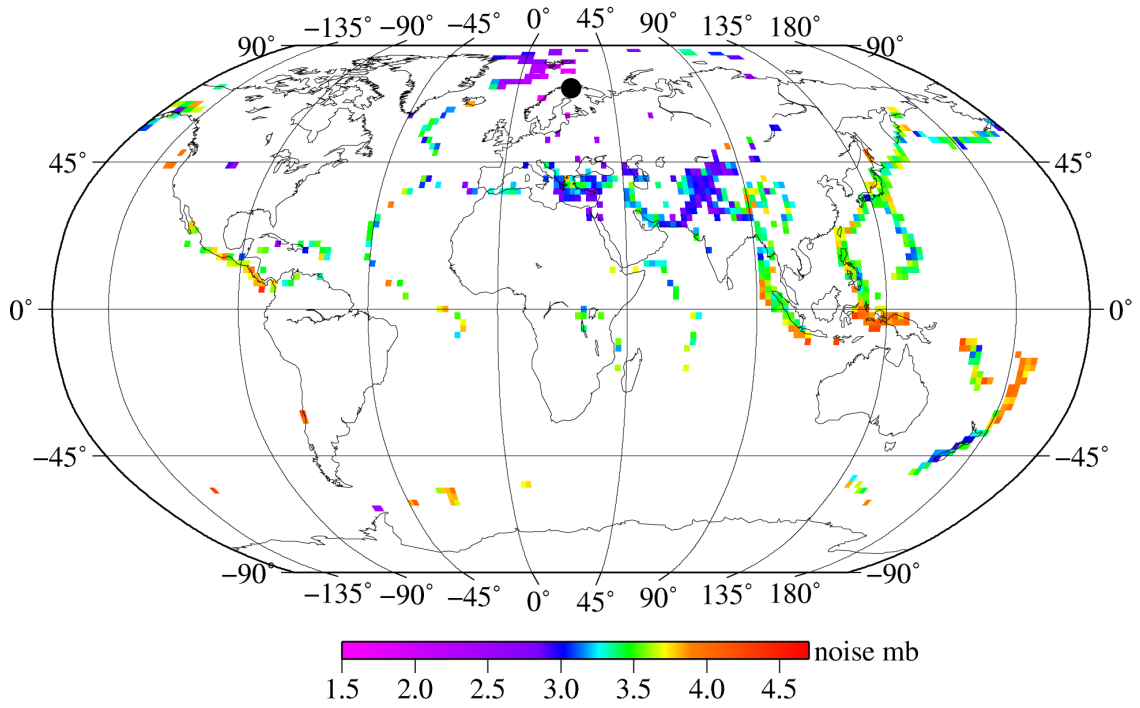

Fig. 6.3.11. Noise thresholds (SNR = 1.0) for the ARCES array in $2^o x 2^o$ bins estimated using the censoring method.

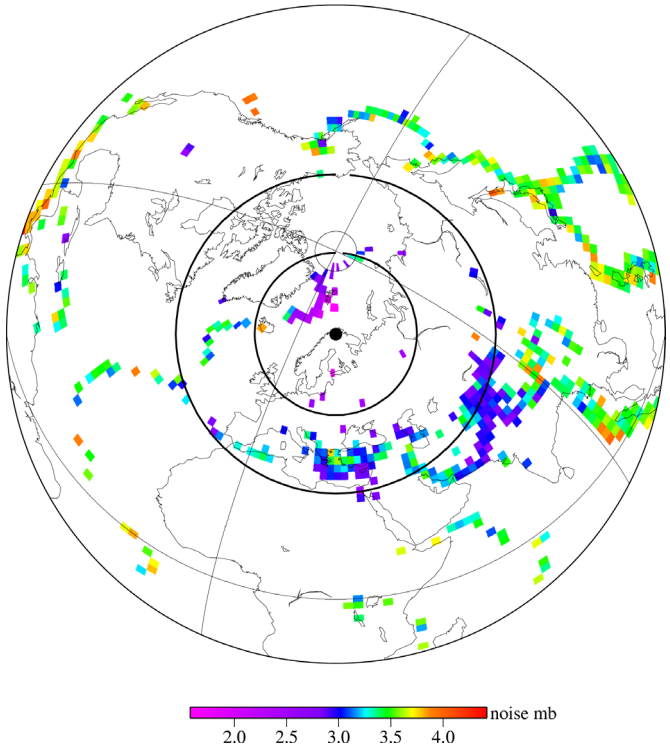

Fig. 6.3.12. Same as Figure 6.3.11, but plotted using an azimuthal projection centered around the location of the ARCES array.

6.3.5 Determining regionalized performance relative to the expected performance

As is illustrated for the ARCES array in Figure 6.3.13, a standard amplitude-distance curve can be well fitted to the estimated noise magnitudes when an average correction is applied. The standard amplitude-distance curve is similar to the curve for zero depth events used by the IDC threshold monitoring subsystem (IDC6.5.14, 2001), which combine the curves of Veith and Clawson (1972), Ringdal and Fyen (1979) and Harjes (1985) to span the full 0-180 degree distance range.

This average correction, which we in the following denote the station noise level, is in fact indicative of the overall station performance. We can use this information to determine regions where the detection performance of a given station is much better (or much worse) than its average detection performance. This is illustrated for ARCES in different map projections in Figures 6.3.14 and 6.3.15.

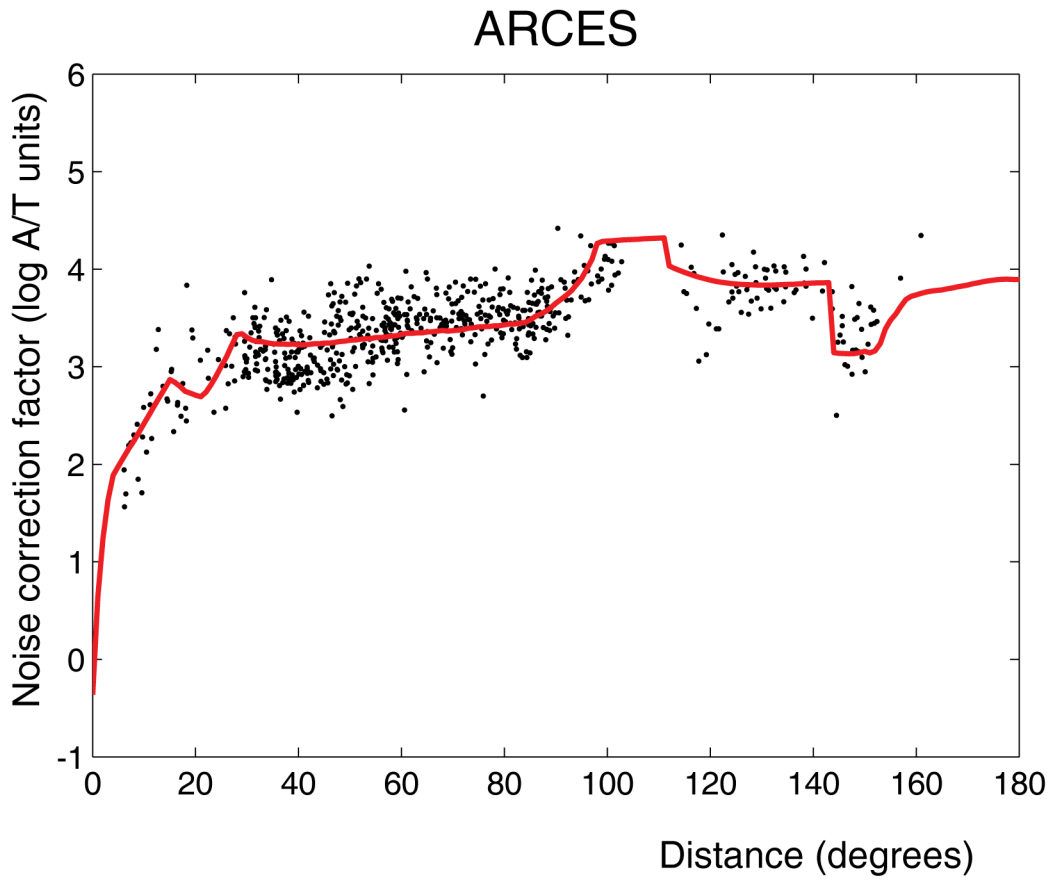

Fig. 6.3.13. The black dots correspond to the estimated noise thresholds shown in Figures 6.3.11 and 6.3.12, now plotted versus epicentral distance from ARCES. The red curve shows the best-fitting standard amplitude-distance curve.

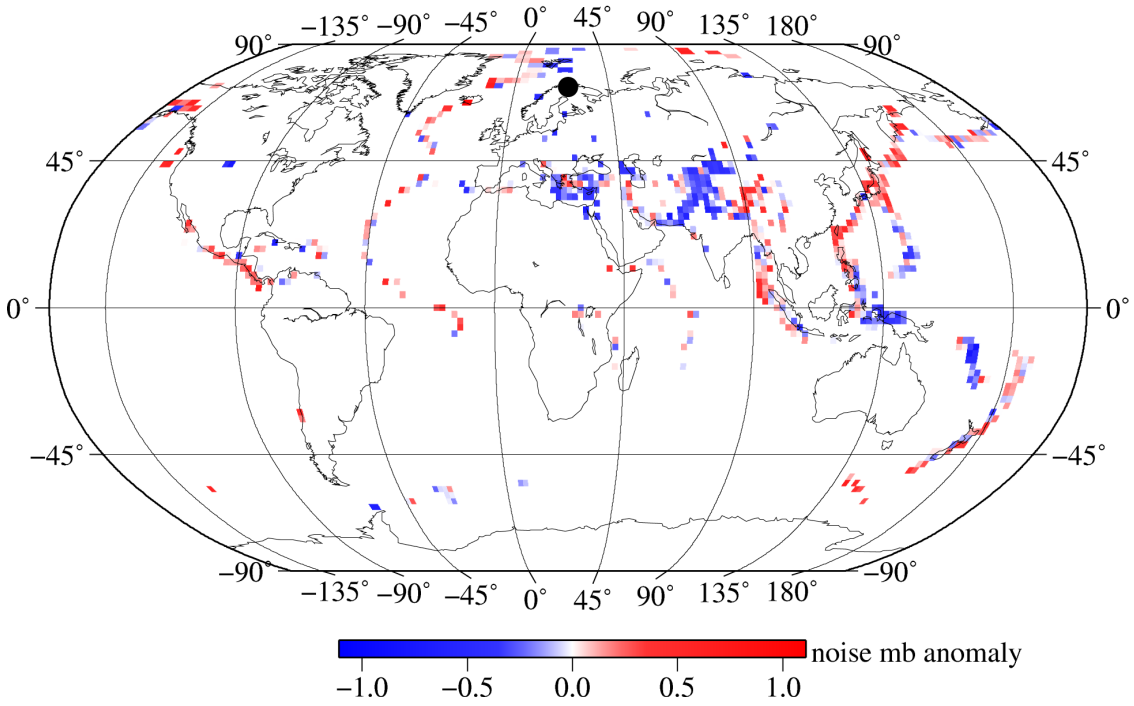

Fig. 6.3.14. Noise magnitude residuals at the ARCES array relative to the average distance dependent amplitude-distance curve shown in Figure 6.3.13. Blue indicate bins with performance better than the average ARCES performance at the corresponding epicentral distance.

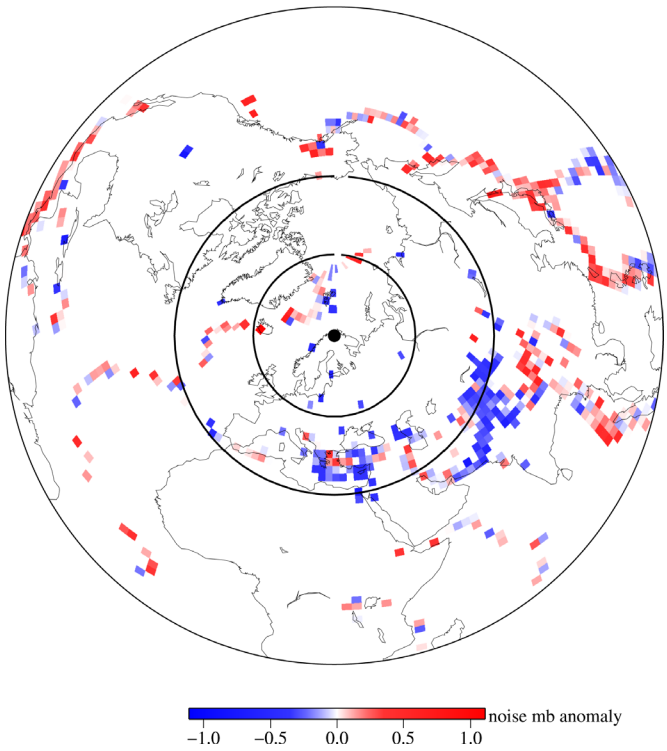

Fig. 6.3.15. Same as Figure 6.3.14, but plotted using an azimuthal projection centered around the location of the ARCES array.

As another example, an analogous picture is shown in Figure 6.3.16 for the Warramunga array in Australia. It might be important to note that in spite of the apparently less than optimum *relative* performance in the seismic belt just north of Australia (relative to the average performance expected at this close distance, given the low WRA noise level), the *absolute* performance of the array in this region is actually quite excellent (see Figure 6.3.17).

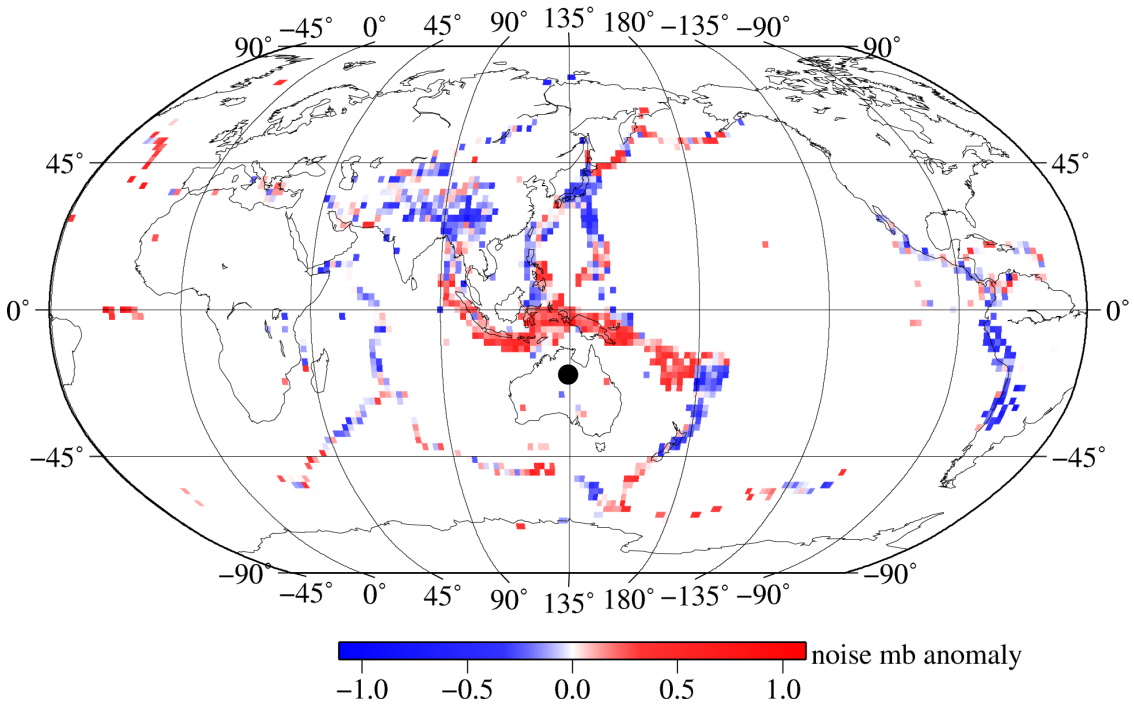

Fig. 6.3.16. Noise magnitude residuals at the WRA array relative to the average distance dependent amplitude-distance curve for the array. Blue indicate bins with performance better than the average WRA performance at the corresponding epicentral distance.

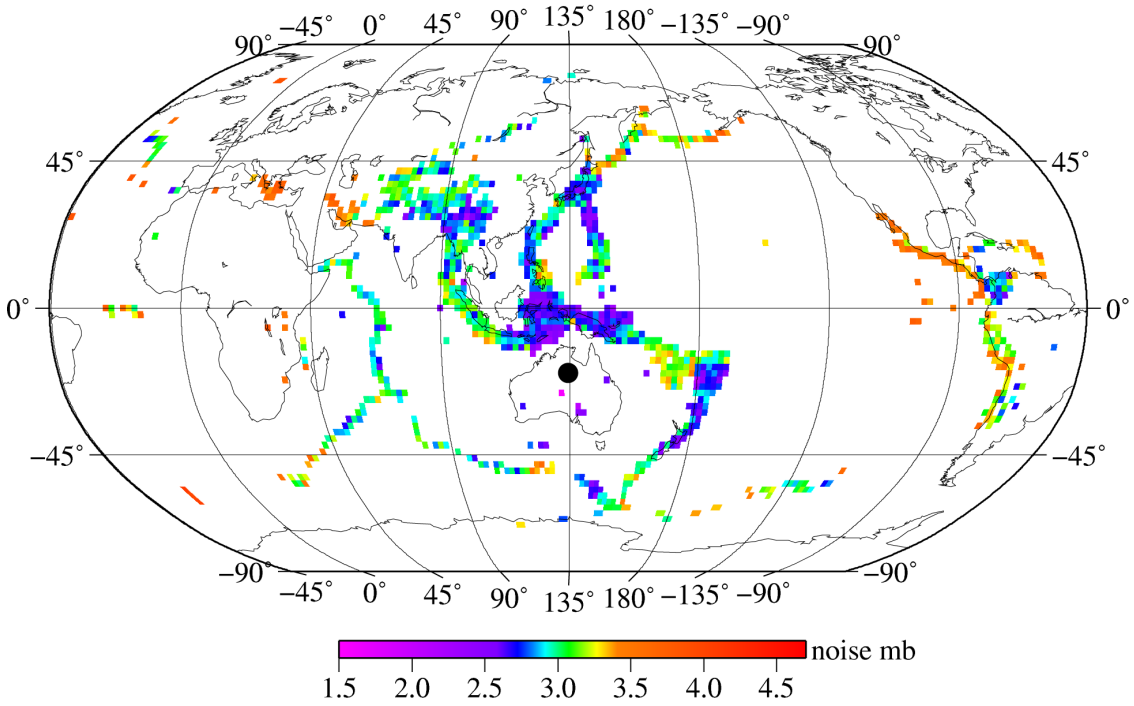

Fig. 6.3.17. Noise thresholds (SNR = 1.0) for the WRA array in $2^o x 2^o$ bins estimated using the censoring method. The blue and violet bins denote "bright spots" where the absolute performance of WRA is especially good.

It should of course be noted that the performance indicators depend on many factors, such as array design, the background noise level, the local station geology, wave propagation characteristics and also on the distance to the most active seismic zones. Furthermore, these overall capabilities are not necessarily representing the value of a given station to the IMS network. For example, some stations are situated in areas where the overall global coverage is poor, and these stations will be important contributors to monitoring events in this region, regardless of their overall performance. Additionally, as has been discussed previously in this paper, all stations have particular bright spots for detection, which may make them especially useful for selected regions.

6.3.6 Overall performance of the IMS primary and auxiliary seismic stations

As shown in Figure 6.3.13, we can for a given station fit a standard amplitude-distance curve to the noise magnitudes estimated in the different bins using an average correction factor, which we denote the station noise level. The lower the station noise level, the better is the expected station performance. Table 6.3.1 gives the estimated station noise levels for the IMS primary seismic stations for events in the teleseismic distance range 20 -95 degrees, sorted by station noise level. A bin size of $5^o x 5^o$ is used for this estimation. In order to account for the variability within each bin, the estimated station noise thresholds were projected onto the bin center using the standard amplitude-distance curve. The results obtained for the $5^o x 5^o$ and $2^o x 2^o$ bins show very good correspondence, but the benefit from using a $5^o x 5^o$ bin is that we can obtain more reliable estimates for regions with sparse seismicity. For the 20-95 degree distance range the

REB database contains information about both the SNR of the detected events as well as the instantaneous station noise magnitude of the non-detected events. This enabled us to apply the maximum likelihood estimation method, as described in section 6.3.2. For each station, Table 6.3.1 also provides the station noise levels estimated using the censoring method, also described in section 6.3.2, as well as the difference between the noise levels estimated by the two methods. Notice the good correspondence. As seen from Table 6.3.1, the arrays ASAR and WRA located in central Australia have the best overall detection performance for events in the teleseismic distance range. This excellent performance is the result of several factors like low background noise levels, efficient wave propagation and the relatively large number of array elements providing high SNR gain by beamforming. Except for the three-component station BGCA, located in the Central African Republic, the 16 best stations are, not surprisingly, all arrays. However, due to difficulties in operating the BGCA station, no data has been available after 7 January 2003. Getting the BGCA station back into operation would be of great benefit to the IMS system, and an upgrade of this station to a seismic array would possibly make it superior to all the arrays in the entire network.

For events in the regional distance range 0-20 degrees, the REB database does not contain information about non-detecting stations. It was therefore not possible to calculate maximum likelihood estimates of the noise thresholds, and we had to rely on the estimates obtained using the censoring method. The results are given in Table 6.3.2. Several of the IMS primary seismic stations are located in regions with low seismicity within regional distances. Consequently, there were for some of these stations, like BGCA and TORD - Niger, a very limited number of events available for assessment of the detection performance at regional distances. In these cases, the results should be interpreted with caution. It can also be seen when comparing Tables 6.3.1 and 6.3.2 that some of the so-called regional arrays, like ARCES and FINES in Norway and Finland, have relatively better performance for detecting events in the regional distance regime. On the other hand, it can also be seen that the performance of several of the so-called teleseismic arrays is significantly reduced. This applies in particular to large-aperture arrays like MJAR, NOA, BRTR, AKASG and CMAR, and is mainly caused by signal incoherency among the array sensors for high-frequency regional seismic signals.

The stated purpose of the IMS auxiliary seismic stations is to improve the locations of the events detected by the primary seismic network. However, several of the auxiliary stations show excellent detection performance, and we show in Table 6.3.3 the station noise levels for events in the regional distance range 0-20 degrees. It is interesting to notice that the three stations with the best performance are all located in the polar regions (SPITS - Spitsbergen, Norway, SNAA - Antarctica, RES - Resolute Bay, Canada). Stations located within the African continent (TSUM - Tsumeb, Namibia, MATP - Matapos, Zimbabwe, LSZ - Lusaka, Zambia) and in Kazakhstan (BVAR array - Borovoye, AKTO - Aktyubinsk, KURK -Kurchatov) all show excellent performance. For some of the stations, the available datasets of regional events were very small, and again, the results should be interpreted with caution. For the three stations MBAR - Uganda, MSKU - Gabon and QSPA - The South Pole, there were no 5^{o}x5^{o} bins that fulfilled the requirement of having 5 or more events for averaging after applying the censoring algorithm.

Table 6.3.1. Overall station noise levels for the IMS primary seismic stations for events in the teleseismic distance range 20-95 degrees.

Station	MLM method		Censoring method			MLM - Censoring
	Noise level	Nbin	Noise level	St. dev.	Nbin	
ASAR	-0.848	191	-0.814	0.375	180	-0.033
WRA	-0.803	207	-0.771	0.399	196	-0.032
MKAR	-0.778	210	-0.715	0.377	200	-0.063
YKA	-0.723	344	-0.689	0.433	317	-0.035
ILAR	-0.714	285	-0.714	0.344	264	0.001
TORD	-0.697	149	-0.678	0.397	126	-0.019
BGCA	-0.657	95	-0.654	0.345	75	-0.002
TXAR	-0.640	201	-0.572	0.360	183	-0.068
SONM	-0.550	325	-0.504	0.359	279	-0.046
PDAR	-0.533	245	-0.497	0.343	205	-0.036
ZALV	-0.484	237	-0.459	0.393	178	-0.025
FINES	-0.478	348	-0.438	0.385	291	-0.040
CMAR	-0.460	341	-0.484	0.361	295	0.024
NVAR	-0.440	291	-0.423	0.338	238	-0.017
AKASG	-0.433	335	-0.470	0.309	276	0.037
BRTR	-0.404	309	-0.425	0.319	237	0.021
ZAL	-0.386	360	-0.366	0.387	275	-0.020
GERES	-0.361	349	-0.389	0.328	272	0.028
ARCES	-0.348	378	-0.309	0.373	311	-0.038
LPAZ	-0.296	162	-0.296	0.337	117	0.000
NOA	-0.291	370	-0.252	0.372	275	-0.040
ESDC	-0.266	373	-0.303	0.319	303	0.037
KBZ	-0.217	90	-0.359	0.409	34	0.143
STKA	-0.162	331	-0.100	0.373	253	-0.062
KSRS	-0.148	265	-0.196	0.365	181	0.049
VNDA	-0.145	214	-0.126	0.397	157	-0.020
DBIC	-0.130	291	-0.135	0.337	184	0.005
ULM	-0.103	314	-0.066	0.333	212	-0.036
CPUP	-0.073	194	-0.069	0.333	113	-0.003
BOSA	-0.062	265	-0.080	0.344	161	0.018
SCHQ	-0.042	337	-0.006	0.348	219	-0.036
BDFB	-0.038	222	-0.035	0.315	132	-0.004
USRK	-0.032	113	-0.161	0.385	58	0.129
THR	-0.026	48	0.063	0.339	10	-0.089
PLCA	-0.011	222	0.007	0.334	109	-0.018

Table 6.3.1. Overall station noise levels for the IMS primary seismic stations for events in the teleseismic distance range 20-95 degrees.

Station	MLM method		Censoring method			MLM - Censoring
	Noise level	Nbin	Noise level	St. dev.	Nbin	
MAW	0.038	294	0.021	0.380	210	0.016
KEST	0.040	226	-0.048	0.359	102	0.088
MJAR	0.041	323	-0.006	0.344	211	0.047
PETK	0.082	181	0.089	0.401	109	-0.007
KMBO	0.179	268	0.109	0.357	128	0.070
ROSC	0.268	183	0.076	0.396	62	0.192
PPT	1.106	85	1.144	0.341	10	-0.038

Table 6.3.2. Overall station noise levels for the IMS primary seismic stations for events in the regional distance range 0-20 degrees.

Station	Censoring method		
	Noise level	St. dev.	Nbin
BGCA	-0.835	0.447	5
TORD	-0.800	0.348	1
ASAR	-0.724	0.477	11
WRA	-0.523	0.438	13
YKA	-0.506	0.501	38
FINES	-0.461	0.375	23
MKAR	-0.433	0.538	43
ARCES	-0.404	0.457	24
VNDA	-0.400	0.485	16
ILAR	-0.392	0.504	43
SCHQ	-0.364	0.496	12
TXAR	-0.295	0.493	31
ZALV	-0.277	0.529	25
PDAR	-0.263	0.505	26
GERES	-0.243	0.474	29
ESDC	-0.228	0.529	31
SONM	-0.212	0.474	38
BOSA	-0.177	0.543	14

Table 6.3.2. Overall station noise levels for the IMS primary seismic stations for events in the regional distance range 0-20 degrees.

Station	Censoring method		
	Noise level	St. dev.	Nbin
ULM	-0.170	0.395	9
ZAL	-0.170	0.499	33
NVAR	-0.043	0.451	24
CMAR	-0.016	0.507	32
KBZ	0.019	0.388	10
PETK	0.049	0.624	26
MAW	0.059	0.317	3
AKASG	0.064	0.380	28
DBIC	0.069	0.593	7
THR	0.070	0.459	9
KMBO	0.075	0.480	18
BRTR	0.076	0.447	34
LPAZ	0.094	0.519	22
STKA	0.139	0.317	5
KEST	0.152	0.550	15
KSRS	0.181	0.397	30
USRK	0.184	0.338	14
NOA	0.187	0.320	22
MJAR	0.277	0.453	31
PLCA	0.289	0.474	20
CPUP	0.354	0.450	14
ROSC	0.450	0.525	25
BDFB	0.501	0.316	2
PPT	1.353	0.404	2

Table 6.3.3. Overall station noise levels for the IMS auxiliary seismic stations for events in the regional distance range 0-20 degrees.

Station	Censoring method		
	Noise level	St.dev.	Nbin
SPITS	-0.716	0.572	32
SNAA	-0.633	0.485	17
RES	-0.568	0.545	8
TSUM	-0.545	0.476	11
BVAR	-0.480	0.373	29
AKTO	-0.368	0.354	25
MATP	-0.332	0.521	11
KURK	-0.301	0.438	29
LSZ	-0.290	0.515	18
SADO	-0.284	0.259	4
SIV	-0.280	0.503	17
FITZ	-0.258	0.616	16
LBTB	-0.238	0.526	12
INK	-0.215	0.506	32
MDT	-0.207	0.715	15
HFS	-0.182	0.491	22
SFJD	-0.152	0.393	7
EKA	-0.072	0.426	32
SDV	-0.065	0.481	27
OPO	-0.051	0.650	16
WSAR	-0.049	0.413	10
RCBR	-0.030	0.405	4
TKL	0.000	0.411	3
AAK	0.039	0.488	32
APG	0.040	0.449	5
CMIG	0.043	0.352	15
KDAK	0.071	0.518	30
SUR	0.075	0.490	14
DAVOX	0.102	0.423	20
DLBC	0.106	0.521	34
ANMO	0.116	0.482	15
ELK	0.124	0.364	20
TEIG	0.126	0.794	17
FRB	0.135	0.544	10

Table 6.3.3. Overall station noise levels for the IMS auxiliary seismic stations for events in the regional distance range 0-20 degrees.

Station	Censoring method		
	Noise level	St.dev.	Nbin
NWAO	0.137	0.503	5
BBTS	0.147	0.475	3
PCRV	0.181	0.485	14
ATTU	0.186	0.581	30
MLR	0.209	0.459	26
CFAA	0.226	0.472	19
MMAI	0.245	0.447	21
BORG	0.253	0.466	8
IDI	0.256	0.422	18
LVC	0.291	0.547	17
YBH	0.300	0.550	17
NEW	0.316	0.437	24
ATAH	0.342	0.523	18
PFO	0.351	0.478	10
DZM	0.398	0.451	24
ASF	0.422	0.406	28
JTS	0.423	0.608	18
ATD	0.425	0.506	8
EIL	0.452	0.504	29
SJG	0.453	0.465	16
JKA	0.500	0.444	33
USHA	0.512	0.539	18
RAR	0.514	0.373	8
GNI	0.524	0.448	29
RPZ	0.528	0.471	24
VRAC	0.535	0.393	23
CTA	0.544	0.379	12
PMSA	0.554	0.542	10
PALK	0.577	0.594	1
URZ	0.590	0.491	26
JNU	0.607	0.534	25
BBB	0.617	0.716	22
KAPI	0.632	0.548	20
BATI	0.640	0.530	18
LPIG	0.692	0.533	4
NNA	0.692	0.579	19

Table 6.3.3. Overall station noise levels for the IMS auxiliary seismic stations for events in the regional distance range 0-20 degrees.

Station	Censoring method		
	Noise level	St.dev.	Nbin
PMG	0.727	0.439	19
PSI	0.754	0.515	14
JMIC	0.760	0.703	12
JOW	0.768	0.499	25
VAE	0.832	0.389	11
AFI	1.011	0.437	14
HNR	1.022	0.507	13
JCJ	1.059	0.434	23
GUMO	1.105	0.476	15
JHJ	1.238	0.470	22
DAV	1.354	0.540	20
RPN	1.370	0.431	4
TGY	1.397	0.424	18
RAO	1.650	0.389	11
MBAR	-	-	-
MSKU	-	-	-
QSPA	-	-	-

Tormod Kværna
Frode Ringdal
Ulf Baadshaug

References

Dahlman, O., S. Mykkeltveit and H. Haak (2009). Nuclear Test Ban - Converting Political Visions to Reality, Springer, ISBN 978-1-4020-6883-6

Hannon, W. (1985): Seismic verification of a comprehensive test ban, Science, 227, 251-257.

Harjes. H.-P. (1985): Global seismic network assessment for teleseismic detection of underground nuclear explosions, J. Geophys., 57, 1-13.

IDC6.5.14 (2001): IDC Documentation, Threshold Monitoring Subsystem Software User Manual, SAIC-01/3004

Kværna, T. and F. Ringdal (1999): Seismic Threshold Monitoring for Continuous Assessment of Global Detection Capability, Bull. Seism. Soc. Am., 89, 946-959.

Kværna, T., F. Ringdal and U. Baadshaug (2007): North Korea's nuclear test: the capability for seismic monitoring of the North Korean test site. Seism. Res. Lett., 78/5, 487-496.

Ringdal, F. (1976): Maximum likelihood estimation of seismic magnitude, Bull. Seism. Soc. Am., 66, 789-802.

Ringdal, F. (1986): Study of magnitudes, seismicity and earthquake detectability using a global network, Bull. Seism. Soc. Am., 76, 1641-1659.

Ringdal, F. and J. Fyen (1979): Analysis of global P-wave attenuation characteristics using ISC data files. Semiann. Tech. Summ., 1 Apr - 30 Sep 1979, NORSAR Sci. Rep. 1-79/80, NORSAR, Kjeller, Norway

Ringdal, F. and T. Kværna (1989): A multichannel processing approach to real time network detection, phase association and threshold monitoring, Bull. Seism. Soc. Am., 79, 1927-1940.

Ringdal, F. (1990): Teleseismic event detection using the NORESS array, with special reference to low-yield Semipalatinsk explosions, Bull. Seism. Soc. Am., 80 Part B, 2127-2142.

Ringdal, F. and T. Kværna (1992): Continuous seismic threshold monitoring, Geophys. J. Int., 111, 505-514.

Sereno, T.J. and S.R. Bratt (1989): Seismic detection capability at NORESS and implications for the detection threshold of a hypothetical network in the Soviet Union, J. Geophys. Res., 94, 10397-10414.

Sykes, L. and J. Evernden (1982): The verification of a comprehensive nuclear test ban, Sci. Am., 247, 47-55.

Veith, K.F and G.E. Clawson (1972). Magnitude from short-period P-wave data. Bull. Seism. Soc. Am., 62, 47-55.

Appendix

A similar procedure to the one presented here for estimating station detection capability can be applied to estimating station bias β. In this case, let m_i denote the station magnitude if the *i'th* event has been detected and the station noise magnitude (upper bound) if the *i'th* event has not been detected, and define the quantity b_i by:

$$b_i = m_i - \mathrm{mbmx}_i \tag{3}$$

Denoting as before by D the ensemble of REB events in this region detected by the station, we obtain the following likelihood function:

$$L(\beta) = \prod_{i \in D} \left(\frac{1}{\sigma}\right) \phi \left[\frac{b_i - \beta}{\sigma}\right] \prod_{i \notin D} \Phi \left[\frac{b_i - \beta}{\sigma}\right] \tag{4}$$

Again, the station bias is defined as the value of β that maximizes the likelihood function. It would also here probably be appropriate to keep σ constant (at a value of e.g. 0.35) in order to increase the stability of the estimate when there are few data points, but it is clear that this parameter could be estimated directly from the data simultaneously with estimating station bias β.